HIGHER ACCURACY METHODS FOR FLUID FLOWS IN VARIOUS APPLICATIONS: THEORY AND IMPLEMENTATION

By

Dilek Erkmen

A DISSERTATION

Submitted in partial fulfillment of the requirements for the degree of

DOCTOR OF PHILOSOPHY

In Mathematical Sciences

MICHIGAN TECHNOLOGICAL UNIVERSITY

2020

This dissertation has been approved in partial fulfillment of the requirements for the Degree of DOCTOR OF PHILOSOPHY in Mathematical Sciences.

Department of Mathematical Sciences

Dissertation Advisor:	*Dr. Alexander E. Labovsky*
Committee Member:	*Dr. Allan Struthers*
Committee Member:	*Dr. Cécile M. Piret*
Committee Member::	*Dr. Aleksandr Sergeyev*
Department Chair:	*Dr. Mark S. Gockenbach*

Contents

List of Figures

List of Tables

Preface

The results, obtained in this dissertation, have been published by the author and collaborators as research articles in various research journals. The work contained in this dissertation is spread over four chapters.

In the first and third chapter, the author has collaborated with Alexander E. Labovsky[1]. The work in chapter 1 has been published in the Journal of Mathematical Analysis and Applications (JMAA), and the one in chapter 3 has been published in the journal of Applied Mathematics and Computation (AMC).

In the second chapter, the author has collaborated with Mustafa Aggul[2], Jeffrey M. Connors[3] and Alexander E. Labovsky[1], and the report has been published in SIAM Journal on Numerical Analysis (SINUM).

In the fourth chapter, the author has collaborated with Songul Kaya[4] and Aytekin Çıbık[5], and this work has been published in the Journal of Computational and Applied Mathematics (CAM).

---

[1]Department of Mathematical Sciences, Michigan Technological University, Houghton, MI, 49931, USA.

[2]Department of Mathematics, Hacettepe University, Ankara, 6800, TURKEY.

[3]Department of Mathematics, University of Connecticut, Storrs, CT 06269, USA.

[4]Department of Mathematics, Middle East Technical University, Ankara, 06531, TURKEY.

[5]Department of Mathematics, Gazi University, Ankara, 06550, TURKEY.

Acknowledgments

I would like to express my special appreciation and thanks to my advisor, Dr. Alexander Labovsky, for his guidance through each stage of the process and his endless support. His advice on both research as well as on my career have been invaluable.

I would also like to thank Dr. Aleksandr Sergeyev, Dr. Cécile Piret and Dr. Allan Struthers for taking time out of their busy schedules in order to serve as my committee members.

I would like to thank to Turkish Government and Ministry of National Education in Turkey for providing financial and spiritual support to me with a full scholarship during my master and PhD educations.

Finally, the warmest gratitude goes to my family for their unconditional encouragement, patience and emotional support.

Abstract

This dissertation contains research on several topics related to Defect-deferred correction (DDC) method applying to CFD problems. First, we want to improve the error due to temporal discretization for the problem of two convection dominated convection-diffusion problems, coupled across a joint interface. This serves as a step towards investigating an atmosphere-ocean coupling problem with the interface condition that allows for the exchange of energies between the domains.

The main diffuculty is to decouple the problem in an unconditionally stable way for using legacy code for subdomains. To overcome the issue, we apply the Deferred Correction (DC) method. The DC method computes two successive approximations and we will exploit this extra flexibility by also introducing the artificial viscosity to resolve the low viscosity issue. The low viscosity issue is to lose an accuracy and a way of finding a approximate solution as a diffusion coeffiscient gets low. Even though that reduces the accuracy of the first approximation, we recover the second order accuracy in the correction step. Overall, we construct a defect and deferred correction (DDC) method. So that not only the second order accuracy in time and space is obtained but the method is also applicable to flows with low viscosity.

Upon successfully completing the project in Chapter 1, we move on to implementing similar ideas for a fluid-fluid interaction problem with nonlinear interface condition; the results of this endeavor are reported in Chapter 2.

In the third chapter, we represent a way of using an algorithm of an existing penalty-projection for MagnetoHydroDynamics, which allows for the usage of

the less sophisticated and more computationally attractive Taylor-Hood pair of finite element spaces. We numerically show that the new modification of the method allows to get first order accuracy in time on the Taylor-Hood finite elements while the existing method would fail on it.

In the fourth chapter, we apply the DC method to the magnetohydrodynamic (MHD) system written in Elsässer variables to get second order accuracy in time. We propose and analyze an algorithm based on the penalty projection with grad-div stabilized Taylor Hood solutions of Elsässer formulations.

Chapter 1

Defect-deferred correction method for the two-domain convection-dominated convection-diffusion problem

1.1 Introduction

When attempting to solve a two-domain fluid-fluid interaction problem in a large domain with complex geometries, several key issues immediately appear. The more complicated the setting is, the more we are inclined to use the legacy codes - highly optimized black box subdomain solvers. This is often the only available option, because the monolithic, coupled problem can be difficult to efficiently discretize and solve. Thus, an attractive approach to some problems (as an am-

bitious underlying goal, consider the hurricane prediction, an atmosphere-ocean application on a huge domain with very complex boundaries and turbulent atmosphere flow) is the partitioned time stepping method which would decouple the problem and allow for the easy implementation of subdomain solvers. Additionally, these subdomain equations can be solved in parallel, if the data is explicitly passed across the shared interface at each time step.

Keeping with the goal of modelling the turbulent atmosphere-ocean flows using the preexisting codes for the atmosphere (separately) and the ocean, we seek, as a starting point of our project, an unconditionally stable partitioned time stepping method for fluid-fluid problems. Two of these methods, the IMEX method and the data-passing scheme, were proposed and thoroughly investigated in [7]; the data-passing scheme, introduced in this chapter, was proven to be unconditionally stable for the two-domain heat-heat coupled problem. The same group of authors then successfully applied this method to the atmosphere-ocean coupled problem, proving that there exists a modification of the interface condition that allows for the unconditional stability of the data-passing scheme.

In this chapter we aim at improving two existing flaws of this method: it is only first order accurate in space and time, and it is not designed for the turbulent (or convection-dominated) flows. The defect correction methods (discussed in more detail later in this section) start with a stable, low-order accurate, computationally inexpensive method. Once the choice of such a method is made, the defect correction proceeds by computing a sequence of approximations to the solution; each successive approximation is of higher accuracy than the previous one. The approximations are sought on the same mesh (no mesh refinement

necessary for the improvement in accuracy!) and the only change in the setup of the discretized problems is the modified right-hand side. The matrix of the system doesn't change, thus maintaining the computational attractiveness and the ease of implementation. Finally, the defect correction procedure is easy to parallelize.

When one is required to use the legacy codes for the convection-dominated (or turbulent) flow, the choice of a stable method is not obvious. The Galerkin finite element method cannot be used in a turbulent regime (iterative solver fails to converge within the time frame of the problem), but the only changes one is allowed to make, while using the legacy codes, concern the problem data. Many turbulence models are available for the Navier-Stokes equations at high Reynolds numbers, but most of them introduce either statistical (long-time) averages, requiring multiple solves of the very complicated system, or local spatial averages (LES approach) which modifies the structure of the PDE by usually requiring more derivatives to be taken; these do not allow for the usage of legacy codes. A step in the direction of using deferred correction (which is the defect correction idea, applied to increase the accuracy with respect to time) with a turbulence model was taken in [19]. In order to be able to use the legacy codes, we resort to the simple but efficient artificial viscosity approximation, which increases the flow's viscosity coefficient. The combination of artificial viscosity (in space) and Backward Euler (in time) discretization is the stable and first order accurate method upon which we will build the DDC procedure. We will use the data-passing idea of [7] to decouple the problem in a stable way.

The idea of using a stabilization as simple as the artifical viscosity, for the

real-life fluid-fluid coupling in turbulence regime, might seem naïve. Yet, as shown in [22], the defect-deferred procedure, based on this stabilization, produces a sequence of approximations that captures more and more features of the true, turbulent solution.To quote [22], "even on a very coarse mesh the effect of doing the correction is the same as if the flow at a higher Reynolds number was considered."

As a step towards the turbulent atmosphere-ocean coupling, we consider the two-domain convection-diffusion problem at high convection-to-diffusion ratio (in the computational tests we take the ratio of convection to diffusion coefficients to be 10^5). The interface condition is the linearized version of the rigid-lid condition used in meteorology, see [21] for a more detailed discussion on the rigid-lid condition and the references therein. In order to create an unconditionally stable, second order accurate in both space and time, partitioned time stepping method, we apply the combined DDC techniques to the data-passing scheme of [7]. The combination of the DDC was introduced and successfully tested in [22] in application to the one-domain Navier-Stokes equations.

Consider the d-dimensional domain (in this chapter we consider $d = 2$) Ω that consists of two subdomains Ω_1 and Ω_2 coupled across an interface I (example in Figure 1.1 below).

The problem is: *given* $b_i \in \mathbb{R}^d$, $\nu_i > 0, f_i : [0,T] \to H^1(\Omega_i)^d, u_i(0) \in H^1(\Omega_i)^d$ *and* $\kappa \in \mathbb{R}$, *find (for* $i = 1, 2$*)* $u_i : \Omega_i \times [0,T] \to \mathbb{R}^d$ *satisfying*

$$
\begin{aligned}
u_{i,t} - \nu_i \Delta u_i + b_i \cdot \nabla u_i &= f_i, \quad \text{in } \Omega_i, && (1.1.1)\\
-\nu_i \nabla u_i \cdot \hat{n}_i &= \kappa(u_i - u_j), \quad \text{on } I,\ i,j = 1,2\,,\ i \neq j\,, && (1.1.2)\\
u_i(x,0) &= u_i^0(x), \quad \text{in } \Omega_i, && (1.1.3)\\
u_i &= g_i, \quad \text{on } \Gamma_i = \partial\Omega_i \setminus I. && (1.1.4)
\end{aligned}
$$

Let

$$X_i := \{v_i \in H^1(\Omega_i)^d : v_i = 0 \text{ on } \Gamma_i\}.$$

For $u_i \in X_i$ we denote $\mathbf{u} = (u_1, u_2)$, $\mathbf{f} = (f_1, f_2)$ and $X := \{\mathbf{v} = (v_1, v_2) : v_i \in H^1(\Omega_i)^d : v_i = 0 \text{ on } \Gamma_i, i = 1,2\}$. A natural subdomain variational formulation for (1.1.1)-(1.1.4), obtained by multiplying (1.1.1) by v_i, integrating and applying the divergence theorem, is to find (for $i,j = 1,2, i \neq j$) $u_i : [0,T] \to X_i$ satisfying

$$
(u_{i,t}, v_i)_{\Omega_i} + \nu_i(\nabla u_i, \nabla v_i)_{\Omega_i} + \int_I \kappa(u_i - u_j) v_i ds + (b_i \cdot \nabla u_i, v_i)_{\Omega_i} = (f_i, v_i)_{\Omega_i},
$$

$$
\text{for all } v_i \in X_i. \quad (1.1.5)
$$

The natural monolithic variational formulation for (1.1.1)-(1.1.4) is found by summing (1.1.5) over $i,j = 1,2$ and $i \neq j$ and is to find $\mathbf{u} : [0,T] \to X$ satisfying

$$
(\mathbf{u}_t, \mathbf{v}) + \nu(\nabla \mathbf{u}, \nabla \mathbf{v}) + \int_I \kappa[\mathbf{u}][\mathbf{v}] ds + (b \cdot \nabla \mathbf{u}, \mathbf{v}) = (\mathbf{f}, \mathbf{v}), \forall v \in X, \qquad (1.1.6)
$$

where $[\cdot]$ denotes the jump of the indicated quantity across the interface I , $(\cdot,\cdot)$ is the $L^2(\Omega_1 \cup \Omega_2)$ inner product and $\nu = \nu_i$ in Ω_i.

Figure 1.1 illustrates the subdomains considered here, representative of commonly studied models in fluid-fluid and fluid-structure interaction, [5, 6, 7].

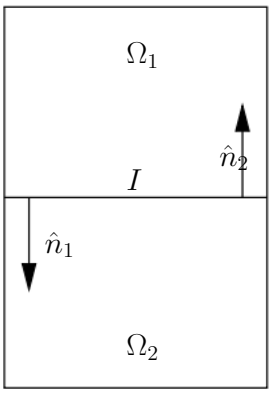

Figure 1.1: Example subdomains, coupled across an interface I.

Comparing (1.1.6) and (1.1.5) we see that the monolithic problem (1.1.6) has a global energy that is exactly conserved, (in the appropriate sense), (set $\mathbf{v} = \mathbf{u}$ in (1.1.6)). The subdomain sub-problems (1.1.5) do not possess a subdomain energy which behaves similarly due to energy transfer back and forth across the interface I. It is possible for decoupling strategies to become unstable due to the input of non-physical energy as a numerical artifact.

Fluid-structure interaction problems, in particular blood flow models, are another typical application of partitioned methods. In these models the equations of elastic deformation of an arterial wall are coupled to equations of fluid flow through the vessel. Recently, it has been shown partitioned methods may be employed for this problem with the addition of a stabilization term on the fluid-structure interface. A defect correction step is implemented to recover optimal time accuracy, (see [6]).

In this chapter, a second order in space and time, non-overlapping uncoupling method for (1.1.1)-(1.1.4) is presented: the two-step DDC method. At each step of the method the interface term in (1.1.5) is advanced in time to give one step

black box decoupling of the subdomain problems in Ω_1 and Ω_2. Additionally, the deferred correction technique allows for the different time scales to be used in different domains, and even for the different terms within the same equation (see the work of Minion et al, [16, 18, 17] and the references for more details). This is important in the atmosphere-ocean coupling, where one flow (air) changes at a much higher pace than the other (sea); also, the diffusion and the convection terms sometimes need to be modelled at different time scales.

The general idea of any Defect Correction Method (DCM) can be formulated as follows (see, e.g., [20, 4]):

Find a unique solution of $Fx = 0$, by

DCM: Use an approximation $\tilde{F}$ to build an iterative procedure:

$$\tilde{F}x_1 = 0, \tag{1.1.7}$$

$$x_{i+1} = (I - \tilde{F}^{-1}F)x_i, i \geq 1.$$

The choice of a particular approximation $\tilde{F}$ determines the defect correction method in use. The general idea of defect correction and deferred correction methods for solving partial differential equations has been known for a long time, see the survey article [4]. Defect correction was proven computationally attractive in fluid applications. See, e.g., [14, 9, 13, 22, 1, 2] and references therein for other defect correction work relevant to fluids.

The main advantage of the deferred correction approach is that a simple low-order method can be employed, and the recovered solution is of high-order accuracy, due to a sequence of deferred correction equations.

The classical deferred correction approach could be seen, e.g., in [10]. However, in 2000 a modification of the classical deferred correction approach was

introduced by Dutt, Greengard and Rokhlin, [8]. This allowed the construction of stable and high-order accurate *spectral deferred correction* methods. In [15] M.L. Minion discusses these spectral deferred correction (SDC) methods in application to an initial value ODE

$$\begin{aligned} \phi'(t) &= F(t, \phi(t)),\ t \in [a, b] \\ \phi(a) &= \phi_a. \end{aligned} \tag{1.1.8}$$

The solution is written in terms of the Picard integral equation; a polynomial is used to interpolate the subintegrand function and the obtained integral term is replaced by its quadrature approximation. In the case when the right hand side of the ODE can be decomposed into a sum of the stiff and non-stiff terms, a semi-implicit spectral deferred correction method (SISDC) is introduced, which allows to treat the non-stiff terms explicitly and the stiff terms implicitly. These SISDC methods for solving ordinary differential equations are further discussed in [15].

The remainder of this work is organized as follows: in Section 1.2, notation and mathematical preliminaries are given and the two-step DDC method is introduced (Algorithm 1.2.1). The unconditional stability of the proposed method is proven in Section 1.3. Convergence results are presented in Section 1.4, and computations are performed to investigate stability and accuracy of a two-step DDC algorithm in Section 1.5.

1.2 Method Description, Notation and Preliminaries

This section presents the numerical schemes for (1.1.1)-(1.1.4), and provides the necessary definitions and lemmas for the stability and convergence analysis. For $D \subset \Omega$, the Sobolev space $H^k(D) = W^{k,2}(D)$ is equipped with the usual norm $\|\cdot\|_{H^k(D)}$, and semi-norm $|\cdot|_{H^k(D)}$, for $1 \leq k < \infty$, e.g. Adams [3]. The L^2 norm is denoted by $\|\cdot\|_D$. For functions $v(x,t)$ defined for almost every $t \in (0,T)$ on a function space $V(D)$, we define the norms $(1 \leq p \leq \infty)$

$$\|v\|_{L^\infty(0,T;V)} = \operatorname*{ess\,sup}_{0<t<T} \|v(\cdot,t)\|_V \quad \text{and} \quad \|v\|_{L^p(0,T;V)} = \left(\int_0^T \|v\|_V^p dt \right)^{1/p} .$$

The dual space of the Banach space V is denoted V'.

Let the domain $\Omega \subset \mathbb{R}^d$ (typically $d = 2, 3$) have convex, polygonal subdomains Ω_i for $i = 1, 2$ with $\partial\Omega_1 \cap \partial\Omega_2 = \Omega_1 \cap \Omega_2 = I$. Let Γ_i denote the portion of $\partial\Omega_i$ that is not on I, i.e. $\Gamma_i = \partial\Omega_i \setminus I$. For $i = 1, 2$, let $X_i = \left\{ v \in H^1(\Omega_i)^d \mid v|_{\Gamma_i} = g_i \right\}$, let $(\cdot,\cdot)_{\Omega_i}$ denote the standard L^2 inner product on Ω_i, and let $(\cdot,\cdot)_{X_i}$ denote the standard H^1 inner product on Ω_i. Define $X = X_1 \times X_2$ and $L^2(\Omega) = L^2(\Omega_1) \times L^2(\Omega_2)$. For $\mathbf{u}, \mathbf{v} \in X$ with $\mathbf{u} = [u_1, u_2]^T$ and $\mathbf{v} = [v_1, v_2]^T$, define the L^2 inner product

$$(\mathbf{u}, \mathbf{v}) = \sum_{i=1,2} \int_{\Omega_i} u_i v_i \, dx \,,$$

and H^1 inner product

$$(\mathbf{u}, \mathbf{v})_X = \sum_{i=1,2} \left(\int_{\Omega_i} u_i v_i \, dx + \int_{\Omega_i} \nabla u_i \cdot \nabla v_i \, dx \right) ,$$

and the induced norms $\|\mathbf{v}\| = (\mathbf{v},\mathbf{v})^{1/2}$ and $\|\mathbf{v}\|_X = (\mathbf{v},\mathbf{v})_X{}^{1/2}$, respectively. The case where $g_i = 0, i = 1,2$ will be considered here, and can be easily extended to the case of nonhomogeneous Dirichlet conditions on $\partial\Omega_i \setminus I$.

Lemma 1.2.1. *$(X, \|\cdot\|_X)$ is a Hilbert space.*

Proof. The choice of boundary conditions for X_1 and X_2 will ensure $X_i \subset H^1(\Omega_i)$, $i = 1,2$ are closed subspaces. Hence by the definitions of $(\cdot,\cdot)_X$ and $\|\cdot\|_X$, $(X, \|\cdot\|_X)$ is a Hilbert space. □

The following discrete Gronwall's lemma and its modified version from [12] will be utilized in the subsequent analysis.

Lemma 1.2.2. *(Gronwall's lemma) Let k, M, and $a_\mu, b_\mu, c_\mu, \gamma_\mu$, for integers $\mu > 0$, be nonnegative numbers such that*

$$a_n + k\sum_{\mu=0}^{n} b_\mu \le k\sum_{\mu=0}^{n} \gamma_\mu a_\mu + k\sum_{\mu=0}^{n} c_\mu + M \text{ for } n \ge 0. \tag{1.2.1}$$

Suppose that $k\gamma_\mu < 1$, for all μ, and set $\sigma_\mu \equiv (1 - k\gamma_\mu)^{-1}$. Then,

$$a_n + k\sum_{\mu=0}^{n} b_\mu \le exp\left(k\sum_{\mu=0}^{n} \sigma_\mu\gamma_\mu\right)\left\{k\sum_{\mu=0}^{n} c_\mu + M\right\} \text{ for } n \ge 0. \tag{1.2.2}$$

The restriction on the time step can be waived if $\gamma_n = 0$.

Lemma 1.2.3. *(Modified Gronwall's lemma) Let k, M, and $a_\mu, b_\mu, c_\mu, \gamma_\mu$, for integers $\mu > 0$, be nonnegative numbers such that*

$$a_n + k\sum_{\mu=0}^{n} b_\mu \le k\sum_{\mu=0}^{n-1} \gamma_\mu a_\mu + k\sum_{\mu=0}^{n} c_\mu + M \text{ for } n \ge 0. \tag{1.2.3}$$

Then, with $\sigma_\mu \equiv (1 - k\gamma_\mu)^{-1}$,

$$a_n + k\sum_{\mu=0}^{n} b_\mu \le exp\left(k\sum_{\mu=0}^{n-1} \sigma_\mu\gamma_\mu\right)\left\{k\sum_{\mu=0}^{n} c_\mu + M\right\} \text{ for } n \ge 0. \tag{1.2.4}$$

1.2.1 Discrete Formulation

Let $\mathcal{T}_i$ be a triangulation of Ω_i and $\mathcal{T}_h = \mathcal{T}_1 \cup \mathcal{T}_2$. Take $X_i^h \subset X_i$ to be conforming finite element spaces for $i = 1, 2$, and define $X^h = X_1^h \times X_2^h \subset X$. It follows that $X^h \subset X$ is a Hilbert space with corresponding inner product and induced norm. We shall consider X_i^h to be spaces of continuous piecewise polynomials of degree $m \geq 2$.

For $t_k \in [0, T]$, $\mathbf{u}^k$ will denote the discrete approximation to $\mathbf{u}(t_k)$.

A partitioned time stepping approach for the heat-heat equations in the same setting as (1.1.1)-(1.1.4) was introduced by Connors, Howell, Layton in [7]. The analogue of this data-passing scheme for our problem is presented below.

1.2.2 First-order Data-Passing Scheme

Let $\Delta t > 0$, $f_i \in L^2(\Omega_i)$. For each $M \in \mathbb{N}, M \leq \frac{T}{\Delta t}$, given $u_i^n \in X_{i,h}$, $n = 0, 1, 2, \cdots, M-1$, solve on each subdomain (for $i, j = 1, 2, i \neq j$) to find $u_i^{n+1} \in X_{i,h}$ satisfying

$$\left(\frac{u_i^{n+1} - u_i^n}{\Delta t}, v_i\right) + \nu_i(\nabla u_i^{n+1}, \nabla v_i) + \kappa \int_I (u_i^{n+1} - u_j^n) v_i \, ds + (b_i \cdot \nabla u_i^n, v_i) = (f_i(t^{n+1}), v_i), \ \forall v_i \in X_{i,h} \,. \quad (1.2.5)$$

This scheme was extensively studied in [7] and was proven to be unconditionally stable and first order accurate. Moreover, in [21] the authors were able to extend this scheme to the atmosphere-ocean problem and prove (using a subtle modification of the jump condition) that the unconditional stability stands.

Based on this scheme, we now introduce the defect-deferred algorithm to increase the method's accuracy and expand the set of applications to include the flows at very high convection-to-diffusion ratio. The artificial viscosity is chosen to be the first order accurate spatial approximation to stabilize the convection-dominated flows; the defect correction algorithm (1.1.7) is then combined with the spectral deferred correction approach of [16].

Throughout the remainder of this chapter we will use tu, u, cu to denote, respectively, the true solution, the defect step approximation and the correction step approximation.

The defect correction method, based on the artificial viscosity approximation of (1.2.5), would lead to the following system of equations.

$$\begin{aligned}
\left(\frac{u_i^{n+1}-u_i^n}{\Delta t}, v_i\right) + (\nu_i + h)(\nabla u_i^{n+1}, \nabla v_i) \qquad (1.2.6)\\
+(1+\frac{h}{\nu_i})\kappa \int_I (u_i^{n+1} - u_j^n) v_i \, ds + (b_i \cdot \nabla u_i^n, v_i)\\
= (f_i(t^{n+1}), v_i), \ \forall v_i \in X_{i,h}\\
\left(\frac{cu_i^{n+1}-cu_i^n}{\Delta t}, v_i\right) + (\nu_i + h)(\nabla cu_i^{n+1}, \nabla v_i)\\
+(1+\frac{h}{\nu_i})\kappa \int_I (cu_i^{n+1} - cu_j^n) v_i \, ds + (b_i \cdot \nabla cu_i^n, v_i)\\
= (f_i(t^{n+1}), v_i) + h(\nabla u_i^{n+1}, \nabla v_i) + \frac{h}{\nu_i}\kappa \int_I (u_i^{n+1} - u_j^n) v_i \, ds,\\
\forall v_i \in X_{i,h}.
\end{aligned}$$

However, if the interface condition (1.1.2) is modified to replace ν_i with $\nu_i + h$, this results in

$$\left(\frac{u_i^{n+1}-u_i^n}{\Delta t},v_i\right)+(\nu_i+h)(\nabla u_i^{n+1},\nabla v_i)+\kappa\int_I(u_i^{n+1}-u_j^n)v_i\,ds \quad (1.2.7)$$
$$+(b_i\cdot\nabla u_i^n,v_i)=(f_i(t^{n+1}),v_i),\ \forall v_i\in X_{i,h}$$
$$\left(\frac{cu_i^{n+1}-cu_i^n}{\Delta t},v_i\right)+(\nu_i+h)(\nabla cu_i^{n+1},\nabla v_i)+\kappa\int_I(cu_i^{n+1}-cu_j^n)v_i\,ds$$
$$+(b_i\cdot\nabla cu_i^n,v_i)=(f_i(t^{n+1}),v_i)+h(\nabla u_i^{n+1},\nabla v_i),\ \forall v_i\in X_{i,h}.$$

Both the modified and non-modified jump conditions were compared numerically, in favor of (1.2.7) (see Section 1.5). Therefore, only the theory for this approach will be considered below.

The deferred correction algorithm applied to the model problem (1.2.5) is as follows.

$$\left(\frac{u_i^{n+1}-u_i^n}{\Delta t},v_i\right)+\nu_i(\nabla u_i^{n+1},\nabla v_i)+\kappa\int_I(u_i^{n+1}-u_j^n)v_i\,ds+(b_i\cdot\nabla u_i^n,v_i) \quad (1.2.8a)$$
$$=(f_i(t^{n+1}),v_i),\ \forall v_i\in X_i^h$$
$$\left(\frac{cu_i^{n+1}-cu_i^n}{\Delta t},v_i\right)+\nu_i(\nabla r_i^{n+1},\nabla v_i)+\kappa\int_I(r_i^{n+1}-r_j^n)v_i\,ds \quad (1.2.8b)$$
$$+(b_i\cdot\nabla r_i^n,v_i)=\frac{1}{\Delta t}I_n^{n+1}(u_i).$$

Here $r_i^k=cu_i^k-u_i^k$, $k=0,1,...,N$.

$I_n^{n+1}(u_i)$ is a numerical quadrature approximation to $\int_{t_n}^{t_{n+1}}F(\tau,u_i(\tau))d\tau$, where $F(t,u_i)=(f_i(t),v_i)-\nu_i(\nabla u_i(t),v_i)+\kappa\int_I(u_i(t)-u_j(t))v_i ds+(b_i\cdot\nabla u_i(t),v_i)$.

Remark 1.2.1. *Provided the integral terms $I_n^{n+1}(u_i)$ are computed with the accuracy of order $O((\Delta t)^2)$, after 1 correction iteration the above procedure will*

produce an approximate solution with global accuracy $O((\Delta t)^2)$. If the points $t_m \in [t_n, t_{n+1}]$ are chosen to be Gaussian quadrature nodes, then the integral is being computed with a spectral integration rule, which is the reason for the name ***spectral*** *deferred corrections. For the two-step method the spectral integration simplifies to the trapezoid rule.*

The variational formulation of the two-step DDC method is obtained by combining the DDC techniques (1.2.7)-(1.2.8) into the following

Algorithm 1.2.1 (Two Step DDC)**.** *Let $\Delta t > 0$, $M = \frac{T}{\Delta t}$, $f_i \in L^2(\Omega_i)$. Given u_i^n, find $u_i^{n+1} \in X_i^h$, $i, j = 1, 2, i \neq j$, $n = 0, 1, 2, \cdots, M-1$, satisfying*

$$\left(\frac{u_i^{n+1} - u_i^n}{\Delta t}, v_i\right) + (\nu_i + h)\left(\nabla u_i^{n+1}, \nabla v_i\right) + \kappa \int_I (u_i^{n+1} - u_j^n) v_i ds + (b_i \cdot \nabla u_i^n, v_i) = \left(f_i^{n+1}, v_i\right), \ \forall v_i \in X_{i,h} \quad (1.2.9)$$

Also, given cu_i^n, find $cu_i^{n+1} \in X_i^h$ satisfying

$$\begin{aligned}\left(\frac{cu_i^{n+1} - cu_i^n}{\Delta t}, v_i\right) + (\nu_i + h)\left(\nabla cu_i^{n+1}, \nabla v_i\right) + \kappa \int_I (cu_i^{n+1} - cu_j^n) v_i ds + \\ (b \cdot \nabla cu_i^n, v_i) = \left(\frac{f_i^{n+1} + f_i^n}{2}, v_i\right) - \frac{\Delta t}{2}\left(b_i \cdot \nabla(\frac{u_i^{n+1} - u_i^n}{\Delta t}), v_i\right) \\ + \Delta t \frac{(\nu_i + h)}{2}(\nabla(\frac{u_i^{n+1} - u_i^n}{\Delta t}), \nabla v_i) + \frac{\kappa}{2}\Delta t \int_I (\frac{u_i^{n+1} - u_i^n}{\Delta t}) v_i ds \\ + \frac{\kappa}{2}\Delta t \int_I (\frac{u_j^{n+1} - u_j^n}{\Delta t}) v_i ds + h\left(\nabla(\frac{u_i^{n+1} + u_i^n}{2}), \nabla v_i\right), \ \forall v_i \in X_{i,h}. \quad (1.2.10)\end{aligned}$$

The terms in the right hand side of (1.2.10) are written in a form that hints at the reason for the increased accuracy of the correction step solution. Note also that the structure of the left hand side (and therefore the matrix of the system) is identical for (1.2.9) and (1.2.10); thus, a simple and computationally cheap ar-

tificial viscosity data-passing approximation is computed twice to achieve higher accuracy while maintaining the unconditional stability.

1.3 Stability

In this section we prove the unconditional stability of both the defect step and the correction step approximations.

Lemma 1.3.1. *(Stability of Defect approximation) Let* $\mathbf{u}^{n+1} \in X^h$ *satisfy (1.2.9) for each* $n \in \left\{0, 1, 2, \cdots, \frac{T}{\Delta t} - 1\right\}$. *Then* $\exists C > 0$ *independent of* h, Δt *such that* $\mathbf{u}^{n+1}$ *satisfies:*

$$\left\|\mathbf{u}^{n+1}\right\|^2 + (\nu + h)\Delta t \sum_{k=1}^{n+1} \left\|\nabla \mathbf{u}^k\right\|^2 + \kappa \Delta t (\|u_1^{n+1}\|_I^2 + \|u_2^{n+1}\|_I^2)$$
$$\leq C \left\{ \|\mathbf{u}^0\|^2 + \kappa \Delta t (\|u_1^0\|_I^2 + \|u_2^0\|_I^2) + \frac{2}{\nu + h} \Delta t \sum_{k=1}^{n+1} \|\mathbf{f}^k\|_{-1}^2 \right\}.$$

Proof. Choose $v_i = u_i^{n+1}$ in (1.2.9), $i \neq j$ to obtain

$$\left(\frac{u_i^{n+1} - u_i^n}{\Delta t}, u_i^{n+1}\right) + (\nu + h)\left\|\nabla u_i^{n+1}\right\|^2 + \left(b \cdot \nabla u_i^n, u_i^{n+1}\right)$$
$$+ \int_I \kappa (u_i^{n+1} - u_j^n) u_i^{n+1} ds = \left(f_i^{n+1}, u_i^{n+1}\right).$$

Applying the Cauchy-Schwarz inequality and summing over i,j=1,2 , $i \neq j$, yields

$$\frac{\|\mathbf{u}^{n+1}\|^2 - \|\mathbf{u}^n\|^2}{2\Delta t} + (\nu + h)\left\|\nabla \mathbf{u}^{n+1}\right\|^2 + \left(b \cdot \nabla \mathbf{u}^n, \mathbf{u}^{n+1}\right) + \kappa \left\|u_1^{n+1}\right\|_I^2 + \kappa \left\|u_2^{n+1}\right\|_I^2$$
$$-\kappa \|u_1^n\|_I \left\|u_2^{n+1}\right\|_I - \kappa \|u_2^n\|_I \left\|u_1^{n+1}\right\|_I \leq \left\|\nabla \mathbf{u}^{n+1}\right\| \left\|\mathbf{f}^{n+1}\right\|_{-1}.$$

Young's inequality allows to "hide" all the **u**-terms, leading to the telescoping

series in the left hand side (LHS)

$$\frac{\|\mathbf{u}^{n+1}\|^2 - \|\mathbf{u}^n\|^2}{2\Delta t} + (\nu+h)\left\|\nabla \mathbf{u}^{n+1}\right\|^2 + \frac{\kappa}{2}(\left\|u_1^{n+1}\right\|_I^2 - \|u_1^n\|_I^2)$$
$$+\frac{\kappa}{2}(\left\|u_2^{n+1}\right\|_I^2 - \|u_2^n\|_I^2) \leq \frac{\nu+h}{4}\left\|\nabla \mathbf{u}^{n+1}\right\|^2 + \frac{1}{\nu+h}\left\|\mathbf{f}^{n+1}\right\|_{-1}^2$$
$$+\frac{\nu+h}{4}\left\|\nabla \mathbf{u}^{n+1}\right\|^2 + \frac{|b|^2}{\nu+h}\|\mathbf{u}^n\|^2$$

Summing over the time levels and multiplying by $2\Delta t$, we obtain

$$\left\|\mathbf{u}^{n+1}\right\|^2 + (\nu+h)\Delta t\sum_{k=1}^{n+1}\left\|\nabla \mathbf{u}^k\right\|^2 + \kappa\Delta t(\left\|u_1^{n+1}\right\|_I^2 + \left\|u_2^{n+1}\right\|_I^2)$$
$$\leq \left\|\mathbf{u}^0\right\|^2 + \kappa\Delta t(\left\|u_1^0\right\|_I^2 + \left\|u_2^0\right\|_I^2) + \frac{2}{\nu+h}\Delta t\sum_{k=1}^{n+1}\left\|\mathbf{f}^k\right\|_{-1}^2 + \frac{2|b|^2}{\nu+h}\Delta t\sum_{k=0}^{n}\left\|\mathbf{u}^k\right\|^2$$

The summation in the last term on the right hand side does not include the time level $(n+1)$. Therefore, using the modified Gronwall's Lemma, we obtain

$$\left\|\mathbf{u}^{n+1}\right\|^2 + (\nu+h)\Delta t\sum_{k=1}^{n+1}\left\|\nabla \mathbf{u}^k\right\|^2 + \kappa\Delta t(\left\|u_1^{n+1}\right\|_I^2 + \left\|u_2^{n+1}\right\|_I^2)$$
$$\leq C\left\{\|\mathbf{u}^0\|^2 + \kappa\Delta t(\|u_1^0\|_I^2 + \|u_2^0\|_I^2) + \frac{2}{\nu+h}\Delta t\sum_{k=1}^{n+1}\|\mathbf{f}^k\|_{-1}^2\right\}$$

□

Hence, the initial approximation $\mathbf{u}$ is unconditionally stable. We conclude the proof of stability of the DDC approximations by considering the second step approximation $\mathbf{cu}$.

Theorem 1.3.2 (Stability of Correction Step of DDC)**.** *Let* $\mathbf{cu^{n+1}} \in \mathbf{X^h}$ *satisfy (1.2.10) for each* $n \in \left\{0, 1, 2, \cdots, \frac{T}{\Delta t} - 1\right\}$*. Then* $\exists\, C > 0$ *independent of* h, Δt

such that $\mathbf{cu}^{n+1}$ *satisfies:*

$$\left\|\mathbf{cu}^{n+1}\right\|^2 + (\nu+h)\Delta t\sum_{k=1}^{n+1}\left\|\nabla\mathbf{cu}^k\right\|^2 + \kappa\,\Delta t(\left\|cu_1^{n+1}\right\|_I^2 + \left\|cu_2^{n+1}\right\|_I^2)$$
$$\leq C\Bigg[\|\mathbf{cu}^0\|^2 + \kappa\,\Delta t(\|cu_1^0\|_I^2 + \|cu_2^0\|_I^2)$$
$$+\frac{1}{\nu+h}\left\{\|\mathbf{u}^0\|^2 + \kappa\Delta t(\|u_1^0\|_I^2 + \|u_2^0\|_I^2) + \frac{1}{\nu+h}\Delta t\sum_{k=1}^{n+1}\|\mathbf{f}^k\|_{-1}^2\right\}\Bigg].$$

Proof. Choosing $v_i = cu_i^{n+1}$ in (1.2.10) gives

$$\left(\frac{cu_i^{n+1}-cu_i^n}{\Delta t}, cu_i^{n+1}\right) + (\nu_i+h)\left\|\nabla cu_i^{n+1}\right\|^2 + \left(b_i\cdot\nabla cu_i^n, cu_i^{n+1}\right)$$
$$+\int_I \kappa(cu_i^{n+1}-cu_j^n)cu^{n+1}ds = \left(\frac{f_i^{n+1}+f_i^n}{2}, cu_i^{n+1}\right)$$
$$-\frac{\Delta t}{2}\left(b\cdot\nabla(\frac{u_i^{n+1}-u_i^n}{\Delta t}), cu_i^{n+1}\right) + \frac{\Delta t(\nu_i+h)}{2}\left(\nabla(\frac{u_i^{n+1}-u_i^n}{\Delta t}), \nabla cu_i^{n+1}\right)$$
$$+\frac{1}{2}\kappa\int_I(u_j^{n+1}-u_j^n+u_i^{n+1}-u_i^n)cu_i^{n+1}ds + h\left(\nabla(\frac{u_i^{n+1}+u_i^n}{2}), \nabla cu_i^{n+1}\right).$$

Compared to the proof of stability of the defect solution $\mathbf{u}$, there are four extra terms in the RHS. They are bounded as follows. After the summation over $i=1,2$ we obtain

$$\left|\frac{\Delta t}{2}\left(b\cdot\nabla(\frac{\mathbf{u}^{n+1}-\mathbf{u}^n}{\Delta t}), \mathbf{cu}^{n+1}\right)\right| \leq \frac{1}{2}\left|(b\cdot\nabla\mathbf{cu}^{n+1}, \mathbf{u}^{n+1})\right| + \frac{1}{2}\left|(b\cdot\nabla\mathbf{cu}^{n+1}, \mathbf{u}^n)\right|$$
$$\leq 2\epsilon(\nu+h)\|\nabla\mathbf{cu}^{n+1}\|^2 + \frac{|b|^2}{16\epsilon(\nu+h)}(\|\mathbf{u}^{n+1}\|^2 + \|\mathbf{u}^n\|^2).$$

Similarly

$$\left|\frac{\nu+h}{2}(\nabla\mathbf{u}^{n+1}, \nabla\mathbf{cu}^{n+1}) - \frac{\nu+h}{2}(\nabla u^n, \nabla\mathbf{cu}^{n+1})\right| \leq 2\epsilon\,(\nu+h)\|\nabla\mathbf{cu}^{n+1}\|^2$$
$$+\frac{\nu+h}{16\,\epsilon}\,(\|\nabla\mathbf{u}^{n+1}\|^2 + \|\nabla\mathbf{u}^n\|^2).$$

Using again the Cauchy-Swcharz and Young's inequalities, we find a bound on the h-term as follows

$$\left| h\left(\nabla(\frac{\mathbf{u}^{n+1}+\mathbf{u}^n}{2}), \nabla\mathbf{cu}^{n+1}\right)\right| \leq 2\epsilon(\nu+h)\|\nabla\mathbf{cu}^{n+1}\|^2 + \frac{h^2}{16\epsilon(\nu+h)}(\|\nabla\mathbf{u}^{n+1}\|^2 + \|\nabla\mathbf{u}^n\|^2)\,.$$

Summing over the time levels, choosing $\epsilon = \frac{1}{28}$ allows us to hide the $\nabla\mathbf{cu}$-terms in the LHS. There are also eight boundary terms

$$\frac{\kappa}{2}\int_I (u_2^{n+1} - u_2^n + u_1^{n+1} - u_1^n)cu_1^{n+1}ds + \frac{\kappa}{2}\int_I (u_1^{n+1} - u_1^n + u_2^{n+1} - u_2^n)cu_2^{n+1}ds.$$

For each of the eight terms, use the Cauchy-Schwarz inequality, followed by the Young's inequality and use the trace theorem to obtain the bounds

$$\|cu_i^{n+1}\|_I^2 \leq \|cu_i^{n+1}\|_{\partial\Omega_i}^2 \leq C_{Trace}\|\nabla cu_i^{n+1}\|_{\Omega_i}^2$$
$$\|u_i^{n+1}\|_I^2 \leq \|u_i^{n+1}\|_{\partial\Omega_i}^2 \leq C_{Trace}\|\nabla u_i^{n+1}\|_{\Omega_i}^2\,.$$

Utilizing the stability bound on the defect solution $\mathbf{u}$ completes the proof. □

1.4 Convergence analysis

We start by proving the accuracy estimate of the defect solution.

Theorem 1.4.1. *(Accuracy of Defect Solution) Let $tu_i(t;x) \in L^2(0,T;X)$ solve (1.1.1)–(1.1.4) for all $t \in (0,T)$. Let also $tu_{i,t}(t;x) \in L^2(0,T;X)$ and $tu_{i,tt}(t;x) \in L^2(0,T;L^2(\Omega_i))$, $i = 1,2$. Then $\exists C > 0$ independent of h, Δt such that for any*

$n \in \{0, 1, 2, \cdots, M-1 = \frac{T}{\Delta t} - 1\}$, *the solution* u_i^{n+1} *of (1.2.9) satisfies*

$$\|\mathbf{tu}^{n+1} - \mathbf{u}^{n+1}\|^2 + (\nu + h)\Delta t \sum_{j=1}^{n+1} \|\nabla(\mathbf{tu}^j - \mathbf{u}^j)\|^2 + \kappa \Delta t \sum_{i=1}^{2} \|tu_i^{n+1} - u_i^{n+1}\|_I^2 \leq C(h^2 + \Delta t^2) \tag{1.4.1}$$

Proof. Restricting the test functions to X_h, write (1.1.5) at time t_{n+1} as

$$\begin{aligned} \left(\frac{tu_i^{n+1} - tu_i^n}{\Delta t}, v_i\right)_{\Omega_i} + (\nu_i + h)(\nabla tu_i^{n+1}, \nabla v_i)_{\Omega_i} + \kappa \int_I (tu_i^{n+1} - tu_j^n) v_i ds \\ + (b_i \cdot \nabla tu_i^n, v_i)_{\Omega_i} = (f_i^{n+1}, v_i)_{\Omega_i} + h(\nabla tu_i^{n+1}, \nabla v_i)_{\Omega_i} \\ + \left(\frac{tu_i^{n+1} - tu_i^n}{\Delta t} - tu_{i,t}^{n+1}, v_i\right)_{\Omega_i} - \Delta t \left(b_i \cdot \nabla(\frac{tu_i^{n+1} - tu_i^n}{\Delta t}), v_i\right)_{\Omega_i} \\ + \kappa \int_I (tu_j^{n+1} - tu_j^n) v_i ds \end{aligned} \tag{1.4.2}$$

Denote $\frac{tu_i^{n+1} - tu_i^n}{\Delta t} - tu_{i,t}^{n+1} \equiv \rho_i^{n+1}$. Subtract (1.2.9) from (1.4.2) to obtain the equation for the error, $e_i^{n+1} = tu_i^{n+1} - u_i^{n+1}$, $i = 1, 2$. For any $v_i \in X_i^h$

$$\begin{aligned} \left(\frac{e_i^{n+1} - e_i^n}{\Delta t}, v_i\right)_{\Omega_i} + (\nu_i + h)(\nabla e_i^{n+1}, \nabla v_i)_{\Omega_i} + \kappa \int_I (e_i^{n+1} - e_j^n) v_i ds \\ + (b_i \cdot \nabla e_i^n, v_i)_{\Omega_i} = h(\nabla tu_i^{n+1}, \nabla v_i)_{\Omega_i} + (\rho_i^{n+1}, v_i)_{\Omega_i} \\ -\Delta t \left(b_i \cdot \nabla(\frac{tu_i^{n+1} - tu_i^n}{\Delta t}), v_i\right) + \Delta t \kappa \int_I \left(\frac{tu_j^{n+1} - tu_j^n}{\Delta t}\right) v_i ds, \ \ i \neq j. \end{aligned} \tag{1.4.3}$$

Do the summation over $i = 1, 2$; decompose the error $\mathbf{e}^{n+1} = (\tilde{\mathbf{u}}^{n+1} - \mathbf{u}^{n+1}) - (\tilde{\mathbf{u}}^{n+1} - \mathbf{tu}^{n+1}) = \boldsymbol{\phi}^{n+1} - \boldsymbol{\eta}^{n+1}$, for some $\tilde{\mathbf{u}}^{n+1} \in X_h$ and take $\mathbf{v} = \boldsymbol{\phi}^{n+1} \in X^h$.

Then $\forall n \geq 0$

$$\begin{aligned}
&\left(\frac{\boldsymbol{\phi}^{n+1}-\boldsymbol{\phi}^{n}}{\Delta t}, \boldsymbol{\phi}^{n+1}\right) + (\nu+h)(\nabla\boldsymbol{\phi}^{n+1}, \nabla\boldsymbol{\phi}^{n+1}) + \kappa \sum_{i=1,2}\int_I (\boldsymbol{\phi}_i^{n+1})^2 ds \\
&\quad = h(\nabla t u^{n+1}, \nabla\boldsymbol{\phi}^{n+1}) + (\rho^{n+1}, \boldsymbol{\phi}^{n+1}) + \Delta t\kappa \int_I \left(\frac{tu^{n+1}-tu^{n}}{\Delta t}\right)\boldsymbol{\phi}^{n+1} ds \\
&\qquad + \left(\frac{\boldsymbol{\eta}^{n+1}-\boldsymbol{\eta}^{n}}{\Delta t}, \boldsymbol{\phi}^{n+1}\right) + (\nu+h)(\nabla\boldsymbol{\eta}^{n+1}, \nabla\boldsymbol{\phi}^{n+1}) \\
&\qquad - \Delta t\left(b_i\cdot\nabla(\frac{tu_i^{n+1}-tu_i^{n}}{\Delta t}), \boldsymbol{\phi}^{n+1}\right) + \kappa\int_I \boldsymbol{\phi}^{n+1}\boldsymbol{\eta}^{n+1} ds \\
&\qquad + \kappa\sum_{i\neq j}\int_I \mathbf{e}_j^n \boldsymbol{\phi}_i^{n+1} ds + (b\cdot\nabla\boldsymbol{\eta}^{n}, \boldsymbol{\phi}^{n+1}) - (b\cdot\nabla\boldsymbol{\phi}^{n}, \boldsymbol{\phi}^{n+1}) \quad (1.4.4)
\end{aligned}$$

Using the Cauchy-Schwarz and Young's inequalities followed by the Trace theorem gives

$$\begin{aligned}
&\frac{\|\boldsymbol{\phi}^{n+1}\|^2 - \|\boldsymbol{\phi}^{n}\|^2}{2\Delta t} + (\nu+h)(\|\nabla\boldsymbol{\phi}^{n+1}\|^2 + \kappa\|\boldsymbol{\phi}_1^{n+1}\|_I^2 + \kappa\|\boldsymbol{\phi}_2^{n+1}\|_I^2 \\
&\qquad \leq \epsilon(\nu+h)\|\nabla\boldsymbol{\phi}^{n+1}\|^2 + \frac{h^2}{4\epsilon(\nu+h)}\|\nabla\mathbf{tu}^{n+1}\|^2 \\
&\qquad + \epsilon(\nu+h)\|\nabla\boldsymbol{\phi}^{n+1}\|^2 + \frac{C_{PF}^2}{4\epsilon(\nu+h)}\|\rho^{n+1}\|^2 + \epsilon(\nu+h)\|\nabla\boldsymbol{\phi}^{n+1}\|^2 \\
&\qquad + \frac{C_{Trace}^4\Delta t^2\kappa^2}{4\epsilon(\nu+h)}\|\nabla\left(\frac{\mathbf{tu}^{n+1}-\mathbf{tu}^{n}}{\Delta t}\right)\|^2 + \epsilon(\nu+h)\|\nabla\boldsymbol{\phi}^{n+1}\|^2 \\
&\qquad + \frac{C_{PF}^2}{4\epsilon(\nu+h)}\|\frac{\boldsymbol{\eta}^{n+1}-\boldsymbol{\eta}^{n}}{\Delta t}\|^2 + \epsilon(\nu+h)\|\nabla\boldsymbol{\phi}^{n+1}\|^2 + \frac{(\nu+h)}{4\epsilon}\|\nabla\boldsymbol{\eta}^{n+1}\|^2 \\
&\qquad + \epsilon(\nu+h)\|\nabla\boldsymbol{\phi}^{n+1}\|^2 + \frac{C_{Trace}^4\kappa^2}{4\epsilon(\nu+h)}\|\nabla\boldsymbol{\eta}^{n+1}\|^2 + \frac{\kappa}{2}\|\boldsymbol{\phi}_1^{n+1}\|_I^2 + \frac{\kappa}{2}\|\boldsymbol{\phi}_2^{n+1}\|_I^2 \\
&\qquad + \frac{\kappa}{2}\|\boldsymbol{\phi}_1^{n}\|_I^2 + \frac{\kappa}{2}\|\boldsymbol{\phi}_2^{n}\|_I^2 + \epsilon(\nu+h)\|\nabla\boldsymbol{\phi}^{n+1}\|^2 \\
&\qquad + \frac{C_{Trace}^4\kappa^2}{4\epsilon(\nu+h)}\|\nabla\boldsymbol{\eta}^{n}\|^2 + 3\epsilon(\nu+h)\|\nabla\boldsymbol{\phi}^{n+1}\|^2 + \frac{|b|^2}{4\epsilon(\nu+h)}\|\boldsymbol{\eta}^{n}\|^2 \\
&\qquad + \frac{|b|^2}{4\epsilon(\nu+h)}\|\boldsymbol{\phi}^{n}\|^2 + \frac{|b|^2}{4\epsilon(\nu+h)}(\Delta t)^2\|\nabla\left(\frac{\mathbf{tu}^{n+1}-\mathbf{tu}^{n}}{\Delta t}\right)\|^2 \quad (1.4.5)
\end{aligned}$$

Moving the four boundary integrals from the RHS to the LHS, choosing $\epsilon = \frac{1}{20}$, summing over the time levels, using the modified Gronwall's lemma and the triangle inequality (to pass from $\boldsymbol{\phi}^{n+1}$ to $\mathbf{e}^{n+1}$) completes the proof. □

In order to prove the accuracy estimate for the correction approximation, we will need the following

Theorem 1.4.2. *(Accuracy of Time Derivative of the Error in the Defect Step) Let the assumptions of Theorem* 1.4.1 *be satisfied. Also, let* $\Delta\mathbf{tu} \in L^2(0,T;L^2(\Omega))$ *and* $\mathbf{tu}_{ttt} \in L^2(0,T;L^2(\Omega))$. *Then* $\exists C > 0$ *independent of* h, Δt *such that for any* $n \in \{0,1,2,\cdots,M-1=\frac{T}{\Delta t}-1\}$ *, the discrete time derivative of the error* $\frac{e_i^{n+1}-e_n^i}{\Delta t}$ *satisfies*

$$\|\frac{\mathbf{e}^{n+1}-\mathbf{e}^n}{\Delta t}\|^2 + (\nu+h)\Delta t\sum_{j=1}^{n}\|\nabla\left(\frac{\mathbf{e}^{j+1}-\mathbf{e}^j}{\Delta t}\right)\|^2 + \frac{\kappa\Delta t}{2}\sum_{j=1}^{n}\sum_{i=1}^{2}\|\frac{e_i^{j+1}-e_i^j}{\Delta t}\|_I^2 \leq C\left(h^2+(\Delta t)^2\right). \quad (1.4.6)$$

Proof. Taking $v_i = \frac{\phi_i^{n+1}-\phi_i^n}{\Delta t} \in X_{i,h}$ in (1.4.3) leads to

$$\begin{aligned}\left(\frac{e_i^{n+1}-e_i^n}{\Delta t},\frac{\phi_i^{n+1}-\phi_i^n}{\Delta t}\right)_{\Omega_i} &+ (\nu_i+h)(\nabla e_i^{n+1},\nabla(\frac{\phi_i^{n+1}-\phi_i^n}{\Delta t}))_{\Omega_i}\\ +\kappa\int_I(e_i^{n+1}-e_j^n)\frac{\phi_i^{n+1}-\phi_i^n}{\Delta t}ds &+ (b_i\cdot\nabla e_i^n,\frac{\phi_i^{n+1}-\phi_i^n}{\Delta t})_{\Omega_i}\\ = h(\nabla tu_i^{n+1},\nabla(\frac{\phi_i^{n+1}-\phi_i^n}{\Delta t}))_{\Omega_i} &+ (\rho_i^{n+1},\frac{\phi_i^{n+1}-\phi_i^n}{\Delta t})_{\Omega_i} \qquad (1.4.7)\\ -\Delta t\left(b_i\cdot\nabla(\frac{tu_i^{n+1}-tu_i^n}{\Delta t}),\frac{\phi_i^{n+1}-\phi_i^n}{\Delta t}\right)&\\ +\Delta t\kappa\int_I\left(\frac{tu_j^{n+1}-tu_j^n}{\Delta t}\right)\frac{\phi_i^{n+1}-\phi_i^n}{\Delta t}ds,\ \ i\neq j.&\end{aligned}$$

Also, take $v_i = \frac{\phi_i^{n+1}-\phi_i^n}{\Delta t}$ in (1.4.3) at the previous time level, and subtract the resulting equation from (1.4.7). Denoting $s_i^{n+1} \equiv \frac{\phi_i^{n+1}-\phi_i^n}{\Delta t}$, summing over $i = 1, 2$ we obtain for $n \geq 1$

$$
\begin{aligned}
\|\mathbf{s}^{n+1}\|^2 - (\mathbf{s}^{n+1}, \mathbf{s}^n) + (\nu + h)\Delta t \|\nabla \mathbf{s}^{n+1}\|^2 + \Delta t (b \cdot \nabla \mathbf{s}^n, \mathbf{s}^{n+1}) \\
+ \sum_{i,j=1,2, i\neq j} \Delta t \int_I \kappa (s_i^{n+1} - s_j^n) s_i^{n+1} ds \\
= \Delta t \left(\frac{\boldsymbol{\eta}^{n+1} - 2\boldsymbol{\eta}^n + \boldsymbol{\eta}^{n-1}}{(\Delta t)^2}, \mathbf{s}^{n+1} \right) \\
+ (\nu + h)\Delta t \left(\nabla \left(\frac{\boldsymbol{\eta}^{n+1} - \boldsymbol{\eta}^n}{\Delta t} \right), \nabla \mathbf{s}^{n+1} \right) \\
+ \Delta t \left(b \cdot \nabla \left(\frac{\boldsymbol{\eta}^n - \boldsymbol{\eta}^{n-1}}{\Delta t} \right), \mathbf{s}^{n+1} \right) \\
+ \sum_{i,j=1,2, i\neq j} \Delta t \int_I \kappa \left(\frac{\eta_i^{n+1} - \eta_i^n}{\Delta t} - \frac{\eta_j^n - \eta_j^{n-1}}{\Delta t} \right) s_i^{n+1} ds \\
+ h\Delta t \left(\nabla \left(\frac{\mathbf{tu}^{n+1} - \mathbf{tu}^n}{\Delta t} \right), \nabla \mathbf{s}^{n+1} \right) \\
+ \Delta t \left(\frac{\rho^{n+1} - \rho^n}{\Delta t}, \mathbf{s}^{n+1} \right) \\
+ \sum_{i,j=1,2, i\neq j} (\Delta t)^2 \int_I \kappa \left(\frac{\mathbf{tu}_j^{n+1} - 2\mathbf{tu}_j^n + \mathbf{tu}_j^{n-1}}{(\Delta t)^2} \right) \mathbf{s}^{n+1} ds
\end{aligned}
\tag{1.4.8}
$$

Using the Cauchy-Schwarz and Young's inequalities leads to

$$\begin{aligned}
\frac{1}{2}\|\mathbf{s}^{n+1}\|^2 - \frac{1}{2}\|\mathbf{s}^{n}\|^2 + (\nu+h)\Delta t\|\nabla\mathbf{s}^{n+1}\|^2 + \frac{\Delta t\kappa}{2}\|s_1^{n+1}\|_I^2 + \frac{\Delta t\kappa}{2}\|s_2^{n+1}\|_I^2 \\
\leq \epsilon(\nu+h)\Delta t\|\nabla\mathbf{s}^{n+1}\|^2 + \frac{C_{PF}^2\Delta t}{4\epsilon(\nu+h)}\|\frac{\boldsymbol{\eta}^{n+1}-2\boldsymbol{\eta}^{n}+\boldsymbol{\eta}^{n-1}}{(\Delta t)^2}\|^2 \\
+\epsilon(\nu+h)\Delta t\|\nabla\mathbf{s}^{n+1}\|^2 + \frac{1}{4\epsilon(\nu+h)}\Delta t\|b\|^2\|\mathbf{s}^{n}\|^2 \\
+\epsilon(\nu+h)\Delta t\|\nabla\mathbf{s}^{n+1}\|^2 + \frac{(\nu+h)\Delta t}{4\epsilon}\|\nabla(\frac{\boldsymbol{\eta}^{n+1}-\boldsymbol{\eta}^{n}}{\Delta t})\|^2 \\
+\epsilon(\nu+h)\Delta t\|\nabla\mathbf{s}^{n+1}\|^2 + \frac{\|b\|^2\Delta t}{4\epsilon(\nu+h)}\|\frac{\boldsymbol{\eta}^{n+1}-\boldsymbol{\eta}^{n}}{\Delta t}\|^2 + 2\epsilon(\nu+h)\Delta t\|\nabla\mathbf{s}^{n+1}\|^2 \\
+\frac{C_{Trace}^4\kappa\Delta t}{4\epsilon(\nu+h)}\left(\|\nabla(\frac{\boldsymbol{\eta}^{n+1}-\boldsymbol{\eta}^{n}}{\Delta t})\|^2 + \|\nabla(\frac{\boldsymbol{\eta}^{n}-\boldsymbol{\eta}^{n-1}}{\Delta t})\|^2\right) \\
+\epsilon(\nu+h)\Delta t\|\nabla\mathbf{s}^{n+1}\|^2 + \frac{h^2\Delta t}{4\epsilon(\nu+h)}\|\nabla(\frac{\mathbf{tu}^{n+1}-\mathbf{tu}^{n}}{\Delta t})\|^2 \\
+\epsilon(\nu+h)\Delta t\|\nabla\mathbf{s}^{n+1}\|^2 + \frac{C_{PF}^2\Delta t}{4\epsilon(\nu+h)}\|\frac{\rho^{n+1}-\rho^{n}}{\Delta t}\|^2 + \frac{\Delta t\kappa}{4}\|s_1^{n+1}\|_I^2 \\
+\frac{\Delta t\kappa}{4}\|s_2^{n+1}\|_I^2 + (\Delta t)^2\Delta t\kappa\sum_{i=1,2}\|\frac{tu_i^{n+1}-2tu_i^{n}+tu_i^{n-1}}{(\Delta t)^2}\|_I^2.
\end{aligned} \tag{1.4.9}$$

Summing over the time levels, multiplying both sides by 2, letting $\epsilon = \frac{1}{16}$ and using the modified Gronwall's lemma gives

$$\|\mathbf{s}^{n+1}\|^2 + (\nu+h)\Delta t\sum_{i=2}^{n+1}\|\nabla\mathbf{s}^{i}\|^2 + \frac{\kappa\Delta t}{2}\sum_{i=2}^{n+1}\sum_{j=1}^{2}\|s_j^i\|_I^2 \leq C\left(\|\mathbf{s}^1\|^2 + O(h^2+(\Delta t)^2)\right) \tag{1.4.10}$$

In order to get a bound on $\|\mathbf{s}^1\|^2$, consider (1.4.3) at $n=0$. Note also that we choose u_i^0 so that $(tu_i^0 - u_i^0, v_i) = 0, \forall v_i \in X_i^h, i = 1,2$. Thus, $\mathbf{e^0} = -\boldsymbol{\eta^0}$ and

$\boldsymbol{\phi}^0 = 0$. We let $\mathbf{v} = \mathbf{s}^1 = \frac{\boldsymbol{\phi}^1 - \boldsymbol{\phi}^0}{\Delta t} = \frac{\boldsymbol{\phi}^1}{\Delta t}$ to obtain

$$\begin{aligned}\|\mathbf{s}^1\|^2 + \frac{(\nu+h)}{\Delta t}\|\nabla\boldsymbol{\phi}^1\|^2 + \kappa\|\boldsymbol{\phi}_1^1\|_I^2 + \kappa\|\boldsymbol{\phi}_2^1\|_I^2 &= \left(\frac{\boldsymbol{\eta}^1 - \boldsymbol{\eta}^0}{\Delta t}, \mathbf{s}^1\right) \\ &+ (\nu+h)(\nabla\boldsymbol{\eta}^1, \nabla\mathbf{s}^1) + (b\cdot\nabla\boldsymbol{\eta}^0, \mathbf{s}^1) + \sum_{i,j=1,2,i\neq j}\int_I \kappa(\eta_i^1 - \eta_j^0)s_i^1 ds \\ &+ h(\nabla\mathbf{tu}^1, \nabla\mathbf{s}^1) + (\rho^1, \mathbf{s}^1) + \sum_{i,j=1,2,i\neq j}\Delta t\int_I \kappa\left(\frac{tu_j^1 - tu_j^0}{\Delta t}\right)s_i^1 ds \quad (1.4.11)\end{aligned}$$

Using the Cauchy-Schwarz and Young's inequalities, we show the following

$$\begin{aligned}&\|\mathbf{s}^1\|^2 + \frac{(\nu+h)}{\Delta t}\|\nabla\boldsymbol{\phi}^1\|^2 + \frac{\kappa}{2}\|\boldsymbol{\phi}_1^1\|_I^2 + \frac{\kappa}{2}\|\boldsymbol{\phi}_2^1\|_I^2 \\ &\leq C\Bigg[\|\frac{\boldsymbol{\eta}^1 - \boldsymbol{\eta}^0}{\Delta t}\|^2 + (\nu+h)\|\Delta\boldsymbol{\eta}^1\|^2 + \|b\|^2\|\nabla\boldsymbol{\eta}^0\|^2 \quad (1.4.12) \\ &+ \sum_{i=0,1,j=1,2}\kappa\|\nabla\eta_j^i\|^2 + h^2\|\Delta\mathbf{tu}^1\|^2 + \|\rho^1\|^2 + (\Delta t)^2\kappa\sum_{j=1,2}\|\frac{tu_j^1 - tu_j^0}{\Delta t}\|_I^2\Bigg]\end{aligned}$$

Inserting (1.4.12) into (1.4.10) completes the proof. □

We now have all the intermediate results that are needed for proving the accuracy of the correction step solution **cu**.

Theorem 1.4.3. *(Accuracy of Correction Step) Let the assumptions of Theorem 1.4.2 be satisfied. Then $\exists C > 0$ independent of h, Δt such that for any $n \in \{0, 1, 2, \cdots, M-1 = \frac{T}{\Delta t} - 1\}$, the solution cu_i^{n+1} of (1.2.10) satisfies*

$$\begin{aligned}\|\mathbf{tu}^{n+1} - \mathbf{cu}^{n+1}\|^2 + (\nu+h)\Delta t\sum_{j=1}^{n+1}\|\nabla(\mathbf{tu}^j - \mathbf{cu}^j)\|^2 + \kappa\Delta t\sum_{i=1}^{2}\|tu_i^{n+1} - cu_i^{n+1}\|_I^2 \\ \leq C\left(h^4 + (\Delta t)^4\right) \quad (1.4.13)\end{aligned}$$

Proof. First, sum (1.4.2) at time levels t_n and t_{n+1} and divide by 2, to obtain in

$\Omega_i\,, i = 1, 2$:

$$\left(\frac{tu_i^{n+1} - tu_i^n}{\Delta}, v_i\right) + (\nu_i + h)(\nabla tu_i^{n+1}, \nabla v_i) + \int_I \kappa(tu_i^{n+1} - tu_j^n)v_i ds$$
$$+ (b_i \cdot \nabla tu_i^n, v_i) = \left(\frac{f_i(t_{n+1}) + f_i(t_n)}{2}, v_i\right)$$
$$+ \frac{\Delta t(\nu_i + h)}{2}\left(\nabla(\frac{tu_i^{n+1} - tu_i^n}{\Delta t}), \nabla v_i\right)$$
$$+ h\left(\nabla(\frac{tu_i^{n+1} + tu_i^n}{2}), \nabla v_i\right) + \frac{\kappa\Delta t}{2}\int_I \left(\frac{tu_i^{n+1} - tu_i^n}{\Delta t}\right) v_i ds$$
$$+ \frac{\kappa\Delta t}{2}\int_I \left(\frac{tu_j^{n+1} - tu_j^n}{\Delta t}\right) v_i ds - \frac{\Delta t}{2}\left(b_i \cdot \nabla(\frac{tu_i^{n+1} - tu_i^n}{\Delta t}), v_i\right)$$
$$+ \left(\frac{tu_i^{n+1} - tu_i^n}{\Delta t} - \frac{tu_{i,t}^{n+1} + tu_{i,t}^n}{2}, v_i\right) \quad (1.4.14)$$

For the $O(\Delta t^2)$-term introduce the notation $\frac{tu_i^{n+1} - tu_i^n}{\Delta t} - \frac{tu_{i,t}^{n+1} + tu_{i,t}^n}{2} \equiv \gamma_i^{n+1}$. Subtract the correction step equation (1.2.10) from (1.4.14). We obtain for $i, j = 1, 2, i \neq j$

$$\left(\frac{ce_i^{n+1} - ce_i^n}{\Delta t}, v_i\right) + (\nu_i + h)(\nabla ce_i^{n+1}, \nabla v_i) + \int_I \kappa(ce_i^{n+1} - ce_j^n)v_i ds + (b \cdot \nabla ce_i^n, v_i)$$
$$= \frac{\Delta t(\nu_i + h)}{2}\left(\nabla(\frac{e_i^{n+1} - e_i^n}{\Delta t}), \nabla v_i\right) + h\left(\nabla(\frac{e_i^{n+1} + e_i^n}{2}), \nabla v_i\right) + (\gamma_i^{n+1}, v_i)$$
$$+ \frac{\kappa\Delta t}{2}\int_I \left(\frac{e_i^{n+1} - e_i^n}{\Delta t}\right) v_i ds + \frac{\kappa\Delta t}{2}\int_I \left(\frac{e_j^{n+1} - e_j^n}{\Delta t}\right) v_i ds$$
$$- \frac{\Delta t}{2}\left(b_i \cdot \nabla(\frac{e_i^{n+1} - e_i^n}{\Delta t}), v_i\right). \quad (1.4.15)$$

Similarly to the error decomposition in the case of the defect approximation, decompose $ce_i^{n+1} = tu_i^{n+1} - cu_i^{n+1} = \phi_i^{n+1} - \eta_i^{n+1}, \phi_i \in X_{i,h}$. We now choose $v_i = \phi_i^{n+1} \in X_{i,h}$ in (1.4.15), sum over $i = 1, 2$ and use the Cauchy-Schwarz and Young's inequalities to obtain bounds on the terms in (1.4.15), similar to what

we did for equation (1.4.4). The bounds on $\mathbf{e^{n+1}}$ and $\frac{\mathbf{e^{n+1}}-\mathbf{e^n}}{\Delta t}$ from Theorem 1.4.1 and Theorem 1.4.2 complete the proof. □

1.5 Computational Testing

The convergence properties of the two-step DDC method (Algorithm 1.2.1) are investigated quantitatively in the case of a test problem with the known solution (see [7]).

Assume $\Omega_1 = [0,1] \times [0,1]$ and $\Omega_2 = [0,1] \times [-1,0]$, so I is the portion of the x-axis from 0 to 1. Then $\mathbf{n}_1 = [0,\ -1]^T$ and $\mathbf{n}_2 = [0,\ 1]^T$. For ν_1, ν_2, and κ all arbitrary positive constants, the right hand side function $\mathbf{f}$ from (1.1.1) is calculated so that the true solution is given by $u_i = (u_{i1}, u_{i2}), i = 1, 2$

$$\begin{aligned}
u_{11}(t,x,y) &= x(1-x)(1-y)e^{-t} \\
u_{12}(t,x,y) &= -x(1-x)(1-y)e^{-t} \\
u_{21}(t,x,y) &= x(1-x)(1+\frac{\nu_1}{\kappa}-\frac{\nu_1}{\nu_2}y-(1+\frac{\nu_1}{\nu_2}+\frac{\nu_1}{\kappa})y^2)e^{-t} \\
u_{22}(t,x,y) &= -x(1-x)(1+\frac{\nu_1}{\kappa}-\frac{\nu_1}{\nu_2}y-(1+\frac{\nu_1}{\nu_2}+\frac{\nu_1}{\kappa})y^2)e^{-t}\,.
\end{aligned}$$

This choice of $\mathbf{u}$ satisfies the interface conditions (1.1.2) and the boundary conditions (1.1.4) with $g_1 = g_2 = 0$. The computations were performed using finite element spaces consisting of continuous piecewise polynomials of degree 2. The code was implemented using the software package `FreeFEM++` [11].

1.5.1 Convergence rate study

Computational results are provided for $\kappa = 1$ and for the moderate ($\nu_1 = \nu_2 = 1$) and small ($\nu_1 = \nu_2 = 0.00001$) values of the diffusion coefficients. In the following tables, the norm $\|\mathbf{u}\|$ is the discrete $L^2(0,T;L^2(\Omega))$ norm, given by

$$\|\mathbf{u}\| = \left(\sum_{n=1}^{N} \Delta t |\mathbf{u}(t_n)|^2_{L^2(\Omega_i)} \right)^{1/2}, \tag{1.5.1}$$

and $|\mathbf{u}|_{H^1}$ is the discrete $L^2(0,T;H^1(\Omega))$ seminorm, given by

$$|\mathbf{u}|_{H^1} = \left(\sum_{n=1}^{N} \Delta t |\nabla \mathbf{u}(t_n)|_{L^2(\Omega)} \right)^{1/2}, \tag{1.5.2}$$

where $N = T/\Delta t$. Tables 1.1 and 1.2 compare the cases of modified vs. non-modified jump condition in Algorithm 1.2.1 for $\nu_i = 1$. Tables 1.3 and 1.4 perform the same comparison for the case of convection-dominated flows at $\nu_i = 0.00001$. The errors are calculated in the norms (1.5.1) and (1.5.2).

For the case $\nu_i = 1, i = 1, 2$ the method with the modified jump condition performs as predicted by the theory (with the accuracy improving from $O(h+\Delta t)$ to $O(h^2 + (\Delta t)^2)$ in the correction step). With the jump condition unchanged, the accuracy does not climb beyond first order accuracy, even in the correction step. The results for using different jump conditions at $\nu_i = 10^{-5}$ are even further apart.

DEFECT	**SUBSTEP**				
h	Δt	$\|\mathbf{u}(t)-\mathbf{u}\|_{L^2}$	rate	$\|\mathbf{u}(t)-\mathbf{u}\|_{H^1}$	rate
1/4	1/4	4.09893e-2		1.53394e-1	
1/8	1/8	2.4502e-2	0.74	8.99462e-2	0.77
1/16	1/16	1.34949e-2	0.86	4.91759e-2	0.87
1/32	1/32	710272e-3	0.92	2.57988e-2	0.93
1/64	1/64	364762e-3	0.96	1.32293e-2	0.96
CORRECTION	**SUBSTEP**				
h	Δt	$\|\mathbf{u}(t)-\mathbf{cu}\|_{L^2}$	rate	$\|\mathbf{u}(t)-\mathbf{cu}\|_{H^1}$	rate
1/4	1/4	1.50131e-2		5.94415e-2	
1/8	1/8	5.37793e-3	1.48	2.0774e-2	1.51
1/16	1/16	1.85568e-3	1.53	7.34807e-3	1.49
1/32	1/32	7.06498e-4	1.39	2.9411e-3	1.32
1/64	1/64	3.08825e-4	1.19	1.34023e-3	1.13

Table 1.1: Errors for computed approximations, $\boldsymbol{\nu} = 1$, non-modified jump condition

Clearly, the correct way of implementing the proposed method is to modify the interface condition so that the diffusion coefficient is treated consistently throughout the problem. Also, when the convection-to-diffusion ratio is moderate ($\nu_i = 1$) the observed convergence rates are in full agreement with the theoretical findings. When the diffusion coefficient is very small compared to the spatial mesh diameter, convergence rates in the $L^2(0,T;L^2(\Omega))$-norm start to deteriorate, but the correction step still gives a clear advantage over the first order accurate defect approximation. However, the accuracy in the $L^2(0,T;H^1(\Omega))$-seminorm has decayed drastically; this is due to the fact that for the chosen values of ν the mesh is much too coarse; the term $\nu + h$, appearing in the error

DEFECT	**SUBSTEP**				
h	Δt	$\|\mathbf{u}(t)-\mathbf{u}\|_{L^2}$	rate	$\|\mathbf{u}(t)-\mathbf{u}\|_{H^1}$	rate
1/4	1/4	4.10392e-2		1.5309e-1	
1/8	1/8	2.42801e-2	0.75	8.9456e-2	0.77
1/16	1/16	1.33056e-2	0.86	4.87916e-2	0.87
1/32	1/32	6.98608e-3	0.92	2.55628e-2	0.93
1/64	1/64	358342e-3	0.96	1.3099e-2	0.96
CORRECTION	**SUBSTEP**				
h	Δt	$\|\mathbf{u}(t)-\mathbf{cu}\|_{L^2}$	rate	$\|\mathbf{u}(t)-\mathbf{cu}\|_{H^1}$	rate
1/4	1/4	1.36326e-2		5.50424e-2	
1/8	1/8	4.61153e-3	1.56	1.80651e-2	1.60
1/16	1/16	1.36977e-3	1.75	5.36588e-3	1.75
1/32	1/32	3.78436e-4	1.85	1.49775e-3	1.84
1/64	1/64	1.00268e-4	1.91	4.02327e-4	1.89

Table 1.2: Errors for computed approximations, $\boldsymbol{\nu} = 1$, modified jump condition

estimates of the method, is now almost equal to h, which immediately affects both the a priori error estimates and the computational results. This suggests, that if the legacy codes are to be used for the coupled convection-dominated convection-diffusion problem in the manner of Algorithm 1.2.1, then one has to refine the mesh substantially in order to capture the gradient of the solution. Notice, however, that the solution itself is well modelled (in the $L^2(0,T;L^2(\Omega))$-norm) even on a coarse mesh. If one does not wish to refine the mesh, then taking one or two more correction steps could produce a solution that is qualitatively and quantitatively closer to the true, turbulent solution. The latter statement is partially supported by the qualitative tests in [22], but many more tests would need to be performed to make this conclusive.

DEFECT	**SUBSTEP**				
h	Δt	$\|\mathbf{u}(t)-\mathbf{u}\|_{L^2}$	rate	$\|\mathbf{u}(t)-\mathbf{u}\|_{H^1}$	rate
1/4	1/4	7.91115e-2		5.3402e-1	
1/8	1/8	7.08314e-2	0.15	5.44157e-1	-0.02
1/16	1/16	5.9474e-2	0.25	5.6404e-1	-0.05
1/32	1/32	5.31807e-2	0.16	6.32873e-1	-0.16
1/64	1/64	5.11973e-2	0.05	7.7229e-1	-0.28
CORRECTION	**SUBSTEP**				
h	Δt	$\|\mathbf{u}(t)-\mathbf{cu}\|_{L^2}$	rate	$\|\mathbf{u}(t)-\mathbf{cu}\|_{H^1}$	rate
1/4	1/4	7.3621e-2		5.61272e-1	
1/8	1/8	6.06277e-2	0.28	5.98215e-1	-0.09
1/16	1/16	5.45552e-2	0.15	6.79845e-1	-0.18
1/32	1/32	5.32717e-2	0.03	8.45552e-1	-0.31
1/64	1/64	5.23807e-2	0.02	1.10753	-0.38

Table 1.3: Errors for computed approximations, $\boldsymbol{\nu} = 10^{-5}$, non-modified jump condition

1.6 Summary and future work

A method was presented that aims at resolving an atmosphere-ocean coupling problem in a turbulent regime, with high accuracy in both space and time, and with the usage of legacy codes. With this, seemingly impossible, goal in mind, we considered a simplified problem here: create a stable and high-accuracy (second order accurate in both space and time) method for solving a coupled two-domain convection dominated convection-diffusion problem in legacy codes. The coupling condition is a linearized version of the rigid lid condition, often used atmosphere-ocean models.

To that end, the combined approach of DDC was implemented, based on

DEFECT	**SUBSTEP**				
h	Δt	$\|\mathbf{u}(t)-\mathbf{u}\|_{L^2}$	rate	$\|\mathbf{u}(t)-\mathbf{u}\|_{H^1}$	rate
1/4	1/4	9.23371e-2		3.64616e-1	
1/8	1/8	7.30489e-2	0.33	3.06128e-1	0.25
1/16	1/16	4.72726e-2	0.62	2.27403e-1	0.42
1/32	1/32	2.71885e-2	0.79	1.62003e-1	0.48
1/64	1/64	1.46477e-2	0.89	1.14559e-1	0.49
CORRECTION	**SUBSTEP**				
h	Δt	$\|\mathbf{u}(t)-\mathbf{cu}\|_{L^2}$	rate	$\|\mathbf{u}(t)-\mathbf{cu}\|_{H^1}$	rate
1/4	1/4	6.75345e-2		2.89442e-1	
1/8	1/8	3.59619e-2	0.90	2.15663e-1	0.42
1/16	1/16	1.47159e-2	1.28	1.55311e-1	0.47
1/32	1/32	5.43386e-3	1.44	1.12958e-1	0.45
1/64	1/64	1.87323e-3	1.54	8.05629e-2	0.48

Table 1.4: Errors for computed approximations, $\boldsymbol{\nu} = 10^{-5}$, modified jump condition

the clever (and stable, although only first order accurate) decoupling procedure of [7]. The presented method was investigated both theoretically (proving the unconditional stability and second order accuracy in both space and time) and numerically (where a comparison was made between a non-modified and a modified coefficient in the jump condition, the latter clearly being the right way of implementing the method). Since this is a difficult problem, and an even more difficult application is still ahead, more numerical tests are needed to get a clearer picture of the method's capabilities (and, more importantly, limitations!) in modelling the convection dominated or turbulent flows. However, the numerical results demonstrate that the method is computationally attractive, as even a coarse mesh would suffice to get fast, yet accurate approximations of a laminar

flow. As the convection-to-diffusion ratio increases, either more correction steps might be needed, or a finer mesh, or both. Nevertheless, even in the convection dominated regime the numerical test shows that the accuracy of the correction step solution (in the $L^2(0,T;L^2(\Omega))$-norm) increased beyond first order accuracy even on a relatively coarse mesh.

Chapter 2

A Defect-Deferred Correction Method for Fluid-Fluid Interaction

2.1 Introduction

Global climate and regional weather simulations often require the resolution of phenomena related to atmosphere-ocean interaction (AOI), such as hurricanes, monsoons, and climate variability like El Niño-Southern Oscillation and the Madden-Julian Oscillation [26, 43, 44, 45]. The most common numerical approach is to pass fluxes (across the fluid interface) of conserved quantities between an ocean code and an atmosphere code with some prescribed frequency, such as every simulated day. The ocean and atmosphere codes otherwise view each other as black boxes. Each code is optimized to resolve the dynamics of the respective physical system. For example, energy in the atmosphere remains significant at smaller time scales and larger spatial scales than in the ocean, so

different time steps and grids are often used for each system. This intuitive approach is now well-established, with numerous codes in existence. Some examples are the so-called *global circulation models* (GCMs) used to assess climate change by the IPCC [34], as well as coupled Weather Research and Forecasting (WRF) and Regional Oceanic Models (ROMS) [33, 31, 39, 40].

We consider an approach to improve two numerical aspects of typical AOI simulations: artificial diffusion (or viscosity) processes, and the coupling across the fluid interface. Viscosity and diffusion parameterizations are included in simulations to control numerical noise and to model subscale mixing processes; we provide some details in Section 2.1.2. But the net effect can be to overdiffuse (formally) and impact model resolution. For example, reduction of viscosity parameters in the ocean alone have been shown to improve some simulation outputs for both the ocean and atmosphere [35], but the model viscosity should remain larger than physical parameter values in order to control numerical noise. Meanwhile, typical coupling methods induce time-consistency errors (with rare exceptions; coupling details are discussed below). Some studies indicate sensitivity with respect to this error, demonstrating that improved coupling methods could translate to better simulation results in many cases [27, 33].

There is an abundance of literature regarding the physics behind surface fluxes and the preservation of flux conservation properties when mapping between different computational grids. In contrast, the literature that addresses the temporal aspects of flux calculations in the context of AOI is somewhat sparse. The method in [28] exemplifies the approach used for climate models, while approaches for regional coupled models may be found in [25, 41]. The

common feature we point out is that the time consistency is always formally first-order with respect to the size of time interval between coupling air and sea components. An exception is the recent method in [32, 33], which employs iteration to achieve second-order consistency; further details are discussed below. Generally, the development of flux-passing algorithms is complicated by technical issues of numerical stability and consistency. Numerical analysis of algorithms can illustrate the challenges and provide insight for future developments, but few examples of this sort of analysis exist that address time-dependent issues. To our knowledge, the papers are [5, 21, 30, 32, 46]. Our approach is investigated for a simple model of two viscous fluids that retains the key aspect of their coupling; the ensuing algorithms are amenable to a rigorous mathematical analysis.

Consider the d-dimensional domain Ω in space that consists of two subdomains Ω_1 and Ω_2, coupled across an interface I, for times $t \in [0,T]$. The problem is: *given* $\nu_i > 0$, $f_i : [0,T] \to H^1(\Omega_i)^d, u_i(0) \in H^1(\Omega_i)^d$ *and* $\kappa \in \mathbb{R}$, *find (for* $i = 1,2$*)* $u_i : \Omega_i \times [0,T] \to \mathbb{R}^d$ *and* $p_i : \Omega_i \times [0,T] \to \mathbb{R}$ *satisfying (for* $0 < t \leq T$*)*

$$u_{i,t} = \nu_i \Delta u_i - u_i \cdot \nabla u_i - \nabla p_i + f_i, \quad \text{in } \Omega_i, \tag{2.1.1}$$

$$-\nu_i \hat{n}_i \cdot \nabla u_i \cdot \tau = \kappa |u_i - u_j|(u_i - u_j) \cdot \tau, \quad \text{on } I,\ i,j = 1,2\,,\ i \neq j \tag{2.1.2}$$

$$u_i \cdot \hat{n}_i = 0 \quad \text{on } I, i = 1,2 \tag{2.1.3}$$

$$\nabla \cdot u_i = 0, \quad \text{in } \Omega_i \tag{2.1.4}$$

$$u_i(x,0) = u_i^0(x), \quad \text{in } \Omega_i, \tag{2.1.5}$$

$$u_i = 0, \quad \text{on } \Gamma_i = \partial\Omega_i \setminus I. \tag{2.1.6}$$

The vectors $\hat{n}_i$ are the unit normals on $\partial\Omega_i$, and τ is any vector such that $\tau \cdot \hat{n}_i = 0$. The parameters ν_i represent kinematic viscosities. We include generic body forces f_i, for generality. This model for fluid velocities, u_i, and pressures, p_i, was studied in [21], initially.

The coupling condition (2.1.2) represents the flux of momentum across a boundary layer region near the fluid interface. The interface is modelled as being flat (just a line segment for $d = 2$). The bulk fluids slide past each other across the boundary layers. The action of the fluid in the layer region is modelled as imparting a horizontal frictional drag force that scales quadratically with the jump in velocities across the layers. The constant $\kappa > 0$ is a friction parameter. A discussion of the full equations of the atmosphere and ocean and their mathematical analysis is provided in the work of Lions, Temam and Wang [37]. Our condition (2.1.2) is analogous to the coupling equations in [37],

up to scaling constants.

In application, momentum flux is not calculated using simultaneous values of the ocean and air velocities, as would be required to satisfy (2.1.2). Fluxes are averaged locally in time to remove aliasing effects and computed using explicit or semi-implicit methods, so that the ocean and atmosphere codes may be run independently; sequentially, or even in parallel. This introduces a consistency error in time. A review of numerical coupling strategies is provided in the work of Lemarié, Blayo and Debreu [32], where an alternative coupling method is proposed and analyzed that is second-order consistent in time, and could be extended to higher order. In contrast, the methods in most codes, and in [5, 21, 30, 46], are only first-order time accurate. The approaches in [5, 32] advocate iterating between the fluid solvers until convergence. These methods are flux-conservative and stable. In particular, the method of [32] applies to a general class of flux computations encountered in application codes.

In this chapter, we develop a method that is unconditionally stable and second-order time accurate, with exactly two solves per time step; further iterations are not required for stability or (formal) consistency. It is desirable to minimize iterations as much as possible, since in practice these require the execution of expensive physics subroutines and additional parallel communication. However, further iterations (in the manner of [32]) might still be justified for accuracy when fluxes become large. We also provide a correction for the use of viscosity parameterizations. Our goal is to outline a broad methodology, but also provide a specific algorithm with a full mathematical analysis, and computational examples to illustrate the theory. The coupling method we focus on is

not flux-conservative or time-averaged, as one encounters in application codes. More general flux calculations will be handled in future work.

2.1.1 Improvement of time consistency via spectral deferred correction

The main advantage of the deferred correction approach is that a simple low-order method can be employed, and the recovered solution is of high-order accuracy, due to a sequence of deferred correction equations. The classical deferred correction approach could be seen, e.g., in [10]. However, in 2000 a modification of the classical deferred correction approach was introduced by Dutt, Greengard and Rokhlin, [8]. This allowed the construction of stable and high-order accurate *spectral deferred correction* (SDC) methods.

In [15], M.L. Minion discusses these SDC methods in application to an initial value ODE. For clarity, that discussion is adapted here to explain the application to our problem. Assume a method-of-lines approach in each fluid domain; application of a given discrete method in space for (2.1.1)-(2.1.6) generates a semi-discrete problem of the form

$$\begin{aligned} \phi_i'(t) &= F_i(t, \phi_1(t), \phi_2(t)), \ t \in (0, T] \\ \phi_i(0) &= \phi_i^0, \end{aligned} \tag{2.1.7}$$

for $i = 1, 2$. Here, $\phi_i \in \mathbb{R}^{N_i}$ is a vector of unknowns to approximate, for example, all fluid variables at grid points in space, and $F_i : (0, T] \times \mathbb{R}^{N_1} \times \mathbb{R}^{N_2} \to \mathbb{R}^{N_i}$. Boundary conditions are already included in the operator F_i. The simultaneous flux conditions (2.1.2) are applied on I, which is the reason that both ϕ_1 and ϕ_2

are required as inputs for F_i. The above formulation does not assume that the same methods are applied to the equations in both fluid domains.

Let $\mathbf{u} = (u_1, u_2)$ and define $[\mathbf{u}] \equiv u_1 - u_2$. Our base (low-order) numerical method is derived by applying a backward-Euler method to approximate (2.1.7), but with the following semi-implicit modification to the coupling conditions:

$$\begin{aligned} -\nu_i \hat{n}_i \cdot \nabla u_i(t^{n+1}) \cdot \tau \approx{}& \kappa |[\mathbf{u}](t^n)| u_i(t^{n+1}) \cdot \tau \\ & - \kappa \sqrt{|[\mathbf{u}](t^n)|} \sqrt{|[\mathbf{u}](t^{n-1})|} u_j(t^n) \cdot \tau, \quad \text{on } I,\ i,j = 1,2\,,\ i \neq j. \end{aligned} \tag{2.1.8}$$

When using a finite element formulation in space, this treatment of the coupling was shown to be unconditionally stable in [21]. Without the geometric averaging in (2.1.8), the coupling is known to exhibit less stable behavior for large enough time steps; see [46]. Since the data $u_j(t^{n+1})$ is not used in the coupling, the result is a system of fully-discrete equations of the form

$$\begin{aligned} \frac{\phi_i^{n+1} - \phi_i^n}{\Delta t} &= \tilde{F}_i(\phi_i^{n+1}, \phi_i^n, \phi_i^{n-1}, \phi_j^n, \phi_j^{n-1}) \\ &= F_i(t^{n+1}, \phi_1(t^{n+1}), \phi_2(t^{n+1})) + \mathcal{O}(\Delta t), \end{aligned} \tag{2.1.9}$$

where $\phi_i^n \approx \phi_i(t^n)$, for $i = 1, 2$ and $i \neq j$. The variables ϕ_1^{n+1} and ϕ_2^{n+1} are thus "decoupled", enabling solvers for each to run in parallel. We note that other coupling methods and time discretizations could be represented in an analogous form in order to explore extensions to applications. The time step size Δt represents the length of time between coupling of the fluid models. Typically, subcycling of the atmosphere is performed due to the faster dynamics compared to the ocean. In mathematical terminology, this is known as *multirate time stepping*, which will be addressed in a future paper.

In the deferred correction approach, the formal accuracy of (2.1.9) is increased to order Δt^k through a series of $k-1$ additional correction steps. We focus on the case of $k=2$, so we define one correction step. In the derivation of the correction equations, one introduces an abstract continuum reconstruction in time of the data ϕ_i^n, say $\tilde{\phi}_i : [0,T] \to \mathbb{R}^{N_i}$, such that $\tilde{\phi}_i(t^n) = \phi_i^n$ for $i = 1, 2$ and all n. Corrections are found by approximating the error function $\delta_i(t) \equiv \phi_i(t) - \tilde{\phi}_i(t)$. One notes first that we may eliminate ϕ_i by inserting $\phi_i = \tilde{\phi}_i + \delta_i$ in (2.1.7) and integrating to yield

$$\tilde{\phi}_i(t) + \delta_i(t) = \phi_i^0 + \int_0^t F_i(\tau, \tilde{\phi}_1 + \delta_1, \tilde{\phi}_2 + \delta_2)\, d\tau.$$

The following functions are one measure of error in $\tilde{\phi}_i$:

$$E_i(t, \tilde{\phi}_1(t), \tilde{\phi}_2(t)) \equiv \phi_i^0 + \int_0^t F_i(\tau, \tilde{\phi}_1, \tilde{\phi}_2)\, d\tau - \tilde{\phi}_i(t).$$

An equation for the error is then

$$\delta_i(t) = \int_0^t \left\{ F_i(\tau, \tilde{\phi}_1 + \delta_1, \tilde{\phi}_2 + \delta_2) - F_i(\tau, \tilde{\phi}_1, \tilde{\phi}_2) \right\} d\tau + E_i(t, \tilde{\phi}_1(t), \tilde{\phi}_2(t)),$$

from which one sees that

$$\begin{aligned} \frac{\delta_i(t^{n+1}) - \delta_i(t^n)}{\Delta t} = \frac{1}{\Delta t} \int_{t^n}^{t^{n+1}} \left\{ F_i(\tau, \tilde{\phi}_1 + \delta_1, \tilde{\phi}_2 + \delta_2) - F_i(\tau, \tilde{\phi}_1, \tilde{\phi}_2) \right\} d\tau \\ + \frac{E_i(t^{n+1}, \tilde{\phi}_1^{n+1}, \tilde{\phi}_2^{n+1}) - E_i(t^n, \tilde{\phi}_1^n, \tilde{\phi}_2^n)}{\Delta t}. \end{aligned} \tag{2.1.10}$$

The E_i-terms satisfy

$$\frac{E_i(t^{n+1}, \tilde{\phi}_1^{n+1}, \tilde{\phi}_2^{n+1}) - E_i(t^n, \tilde{\phi}_1^n, \tilde{\phi}_2^n)}{\Delta t} = \frac{1}{\Delta t} \int_{t^n}^{t^{n+1}} F_i(\tau, \tilde{\phi}_1, \tilde{\phi}_2)\, d\tau - \frac{\tilde{\phi}_i^{n+1} - \tilde{\phi}_i^n}{\Delta t}.$$

In order to achieve the desired (second-order) accuracy, the deferred correction method requires this latter integral to be evaluated using a second-order quadrature rule. We apply the trapezoidal rule in this chapter.

A benefit of the deferred correction approach is that the same base discretization method may be applied to the remaining terms in (2.1.10), so we apply our semi-discrete method and approximate F_i by $\tilde{F}_i$. The error approximations are denoted by $\delta_i^n \approx \delta_i(t^n)$, which are added to ϕ_i^n to get the corrected approximations, say

$$\eta_i^n \equiv \phi_i^n + \delta_i^n = \phi_i(t^n) + \mathcal{O}(\Delta t^2).$$

After applying the discretization method to (2.1.10) and eliminating the values δ_i^n, the method for the corrected approximation is

$$\begin{aligned}\frac{\eta_i^{n+1} - \eta_i^n}{\Delta t} = &\left\{\tilde{F}_i(\eta_i^{n+1}, \eta_i^n, \eta_i^{n-1}, \eta_j^n, \eta_j^{n-1}) - \tilde{F}_i(\phi_i^{n+1}, \phi_i^n, \phi_i^{n-1}, \phi_j^n, \phi_j^{n-1})\right\} \\ &+ \frac{1}{2}\left\{F_i(t^{n+1}, \phi_1^{n+1}, \phi_2^{n+1}) + F_i(t^n, \phi_1^n, \phi_2^n)\right\}.\end{aligned} \tag{2.1.11}$$

Note that η_j^{n+1} is not needed to compute η_i^{n+1} for $i \neq j$. The data ϕ_i^{n+1} and some terms in (2.1.11) are already computed in the predictor step. The correction step is equivalent to performing the predictor step with some extra source terms and an algebraic change to the approximation of the momentum flux. This property of the deferred correction approach makes it potentially viable for application codes, since the existing code structure (the implementation of the predictor step) could be leveraged quite heavily to implement the corrector step.

2.1.2 Reduction of numerical diffusion effects via defect correction

The general idea of defect correction and deferred correction methods for solving partial differential equations has been known for a long time. For a survey,

see [4]. Defect correction has been proven computationally attractive in fluid applications; see, e.g., [14, 9, 13, 1, 2] and references therein. Initial approaches to using the DDC ideas for AOI were tested in [22, 69], where the method was successfully applied to the Navier-Stokes equations in one domain ([22]) and convection-diffusion equations in the two-domain setting (with the coupling condition introduced as a linearized version of rigid lid) in [69]. The general idea of any *defect correction method* (DCM) can be formulated as follows (see, e.g., [20, 4]). Given an operator $\tilde{G}$ to approximate $Gx = 0$, build an iterative procedure:

$$\begin{aligned} \tilde{G}x_1 &= 0, \\ \tilde{G}x_{i+1} &= \tilde{G}x_i - Gx_i, i \geq 1. \end{aligned} \tag{2.1.12}$$

The choice of a particular approximation $\tilde{G}$ determines the defect correction method in use. In this chapter, the "defect" will represent numerical viscosity, which we represent using the additional (constant) parameters $H_i > 0$ to obtain an effective viscosity coefficient of $\nu_i + H_i$, $i = 1, 2$. The operator $\tilde{G}$ in (2.1.12) may be interpreted as using the effective viscosity in the construction of the operator $\tilde{F}_i$. Then G represents a corresponding operator that does not use numerical viscosity. In the deferred correction step (2.1.11), this translates to using the viscosity coefficient ν_i alone in the construction of the operator F_i.

In summary, the combined DDC method is equivalent to using the following

viscous terms when constructing the operators in (2.1.9) and (2.1.11):

$$(\nu_i + H_i)\Delta\eta_i^{n+1} \Leftrightarrow \tilde{F}_i(\eta_i^{n+1}, \eta_i^n, \eta_i^{n-1}, \eta_j^n, \eta_j^{n-1})$$
$$(\nu_i + H_i)\Delta\phi_i^{n+1} \Leftrightarrow \tilde{F}_i(\phi_i^{n+1}, \phi_i^n, \phi_i^{n-1}, \phi_j^n, \phi_j^{n-1})$$
$$\nu_i\Delta\phi_i^j \Leftrightarrow F_i(t^j, \phi_1^j, \phi_2^j),\ j = n, n+1.$$

The DDC method constitutes an easy way to enhance the deferred correction algorithm by reducing the impact of artificial viscosity. This approach preserves an important attribute of deferred correction: that the code structure used to implement the predictor step may be leveraged to implement the corrector step.

Constant-coefficient mixing-length models are used to some extent in codes, but a number of more sophisticated parameterizations also exist. For sake of brevity, we refer to the atmosphere and ocean components of the Community Earth Systems Model (see [29, 42]) and focus on the dissipation of momentum. In the atmosphere code, divergent modes in horizontal transport may be controlled with different options. Harmonic mixing $\nabla\cdot\alpha\nabla$ is one; another is to use the more scale-selective biharmonic mixing like $\nabla\cdot\nu\nabla\Delta$, again with constant coefficient in lower model layers for all cases. In upper model layers, the constants are allowed monotonically-increasing values (up to about four times the bulk value) due to the different dynamics near the top of the atmosphere.

Vertical dynamics are time-split from the horizontal, and vertical viscosity is handled using implicit, backward-Euler time stepping with a moist turbulence scheme. One calculates an eddy-diffusivity parameter $K = l \cdot \sqrt{e} \cdot S$, with l a mixing length, e a diagnostic turbulent kinetic energy, and S a stability parameter. The calculations of these quantities are semi-implicit during the iteration required for the implicit-Euler step, and dependent on many state variables.

The ocean model also provides a range of options for horizontal and vertical viscosity. For horizontal dynamics, both harmonic and biharmonic damping operators may be used, with spatially-varying coefficients. There is an option for anisotropic horizontal viscosity, which is represented as the divergence of a viscous stress tensor that depends linearly on the velocity gradient. The tensor coefficients may vary in space and time in some prescribed way, or may be computed in terms of the strain-rates, nonlinearly, in the manner of Smagorinsky. Vertical viscosity $\partial_z \mu \partial_z$ can be implemented either explicitly or implicitly, with a constant-coefficient option. Another option allows a computation for μ as a function of the local Richardson number. Finally, μ can be computed using the so-called K-profile parameterization (KPP); this is complex and we refer the reader to [36] for details. The Richardson and KPP methods let μ depend on various state variables.

In this chapter, only constant-coefficient harmonic diffusion is used to prevent the numerical analysis from being too technical and complicated. More sophisticated operators could be explored by changing the definitions of the functions F_i, and various time-stepping approaches, including operator-splitting. These extensions are left for future investigation.

The remainder of this work is organized as follows: in Section 2.2, notation and mathematical preliminaries are given and the two-step DDC method is introduced (Algorithm 2.2.1) using a finite element discretization in space. The unconditional stability of the proposed method and convergence results are proven in Section 2.3. Computations are performed to illustrate the stability and accuracy predictions of the theory in Section 2.4. In our computations we

also observe that the corrector step provides a significant improvement to accuracy at the largest tested scales of time step and artificial viscosity parameters. This indicates a potential benefit in application, where time step sizes and artificial viscosity (or diffusion) values are restricted by computational resources. In Section 2.5 we conclude with a summary and discussion of future work.

2.2 Method Description, Notation and Preliminaries

This section presents the numerical schemes for (2.1.1)-(2.1.6), and provides the necessary definitions and lemmas for the stability and convergence analysis. For $D \subset \Omega$, the Sobolev space $H^k(D) = W^{k,2}(D)$ is equipped with the usual norm $\|\cdot\|_{H^k(D)}$, and semi-norm $|\cdot|_{H^k(D)}$, for $1 \leq k < \infty$, e.g. Adams [3]. The L^2 norm is denoted by $\|\cdot\|_D$. For functions $v(x,t)$ defined for almost every $t \in (0,T)$ on a function space $V(D)$, we define the norms $(1 \leq p \leq \infty)$

$$\|v\|_{L^\infty(0,T;V)} = \operatorname*{ess\,sup}_{0<t<T} \|v(\cdot,t)\|_V \quad \text{and} \quad \|v\|_{L^p(0,T;V)} = \left(\int_0^T \|v\|_V^p dt\right)^{1/p}.$$

The dual space of the Banach space V is denoted V'.

For $i = 1, 2$, let

$$X_i := \{v_i \in H^1(\Omega_i)^d : v_i = 0 \, on \, \Gamma_i, i = 1, 2, v_i \cdot \hat{n}_i = 0 \, on \, I\}$$

be velocity spaces, with associated pressure spaces

$$Q_i = \{q_i \in L^2(\Omega_i)^d : \int_{\Omega_i} q_i d\Omega_i = 0\}.$$

We denote $\mathbf{u} = (u_1, u_2)$, $\mathbf{f} = (f_1, f_2)$ and $X := \{\mathbf{v} = (v_1, v_2) : v_i \in X_i, i = 1, 2\}$. Similarly, we denote $\mathbf{q} = (q_1, q_2)$ and $Q := \{\mathbf{q} = (q_1, q_2) : q_i \in Q_i, i = 1, 2\}$.

A natural subdomain variational formulation for (2.1.1)-(2.1.6), obtained by multiplying (2.1.1) by v_i, integrating and applying the divergence theorem, is to find (for $i, j = 1, 2, i \neq j$) $u_i : [0, T] \to X_i$ and $p_i : [0, T] \to Q_i$ satisfying

$$\begin{aligned}(u_{i,t}, v_i)_{\Omega_i} + \nu_i(\nabla u_i, \nabla v_i)_{\Omega_i} + (u_i \cdot \nabla u_i, v_i)_{\Omega_i} - (p_i, \nabla v_i) \\ + \int_I \kappa(u_i - u_j)|u_i - u_j|v_i ds = (f_i, v_i)_{\Omega_i},\ \forall\, v_i \in X_i, \\ (\nabla \cdot u_i, q_i) = 0,\ \forall\, q_i \in Q_i.\end{aligned} \tag{2.2.1}$$

The natural monolithic variational formulation for (2.1.1)-(2.1.6) is found by summing (2.2.1) over $i, j = 1, 2$ and $i \neq j$ and is to find $\mathbf{u} : [0, T] \to X$ and $\mathbf{p} : [0, T] \to Q$ satisfying

$$\begin{aligned}(\mathbf{u}_t, \mathbf{v}) + \nu(\nabla \mathbf{u}, \nabla \mathbf{v}) + (\mathbf{u} \cdot \nabla \mathbf{u}, \mathbf{v}) - (\mathbf{p}, \nabla \cdot \mathbf{v}) + \int_I \kappa|[\mathbf{u}]|[\mathbf{u}][\mathbf{v}]ds = (\mathbf{f}, \mathbf{v}), \forall v \in X, \\ (\nabla \cdot \mathbf{u}, \mathbf{q}) = 0,\ \forall\, q \in Q\end{aligned} \tag{2.2.2}$$

where $[\cdot]$ denotes the jump of the indicated quantity across the interface I , $(\cdot, \cdot)$ is the $L^2(\Omega_1 \cup \Omega_2)$ inner product and $\nu = \nu_i$ in Ω_i.

Comparing (2.2.2) and (2.2.1) we see that the monolithic problem (2.2.2) has a global energy that is exactly conserved, (in the appropriate sense), (set $\mathbf{v} = \mathbf{u}$ and $\mathbf{q} = \mathbf{p}$ in (2.2.2)). The subdomain sub-problems (2.2.1) do not possess a subdomain energy which behaves similarly due to energy transfer back and forth across the interface I. It is possible for decoupling strategies to become unstable due to the input of non-physical energy as a numerical artifact; see [7, 21].

Let the domain $\Omega \subset \mathbb{R}^d$ (typically $d = 2, 3$) have convex, polygonal subdomains Ω_i for $i = 1, 2$ with $\partial\Omega_1 \cap \partial\Omega_2 = \Omega_1 \cap \Omega_2 = I$. Let Γ_i denote the portion of $\partial\Omega_i$ that is not on I, i.e. $\Gamma_i = \partial\Omega_i \setminus I$. For $i = 1, 2$, let $X_i = \left\{v \in H^1(\Omega_i)^d \mid v|_{\Gamma_i} = g_i\right\}$, let $(\cdot,\cdot)_{\Omega_i}$ denote the standard L^2 inner product on Ω_i, and let $(\cdot,\cdot)_{X_i}$ denote the standard H^1 inner product on Ω_i. Define $X = X_1 \times X_2$ and $L^2(\Omega) = L^2(\Omega_1) \times L^2(\Omega_2)$. For $\mathbf{u}, \mathbf{v} \in X$ with $\mathbf{u} = [u_1, u_2]^T$ and $\mathbf{v} = [v_1, v_2]^T$, define the L^2 inner product

$$(\mathbf{u}, \mathbf{v}) = \sum_{i=1,2} \int_{\Omega_i} u_i \cdot v_i \, dx \,,$$

and H^1 inner product

$$(\mathbf{u}, \mathbf{v})_X = \sum_{i=1,2} \left(\int_{\Omega_i} u_i \cdot v_i \, dx + \int_{\Omega_i} \nabla u_i : \nabla v_i \, dx \right) ,$$

and the induced norms $\|\mathbf{v}\| = (\mathbf{v}, \mathbf{v})^{1/2}$ and $\|\mathbf{v}\|_X = (\mathbf{v}, \mathbf{v})_X{}^{1/2}$, respectively. The case where $g_i = 0, i = 1, 2$ will be considered here, and can be easily extended to the case of nonhomogeneous Dirichlet conditions on $\partial\Omega_i \setminus I$.

The inf-sup stable pair of velocity-pressure spaces (P_m, P_{m-1}) will be chosen with $m \geq 2$.

For functions $u, v, w \in X_i$, $i = 1, 2$ we define the expilicitly skew-symmetrized nonlinear form on Ω_i by

$$c_i(u; v, w) = \frac{1}{2}(u \cdot \nabla v, w)_{\Omega_i} - \frac{1}{2}(u \cdot \nabla w, v)_{\Omega_i} \tag{2.2.3}$$

Lemma 2.2.1. *$(X, \|\cdot\|_X)$ is a Hilbert space.*

Proof. The choice of boundary conditions for X_1 and X_2 will ensure $X_i \subset H^1(\Omega_i)$, $i = 1, 2$ are closed subspaces. Hence by the definitions of $(\cdot,\cdot)_X$ and $\|\cdot\|_X$, $(X, \|\cdot\|_X)$ is a Hilbert space. ■ □

The following discrete Gronwall's lemma and its modified version from [12] will be utilized in the subsequent analysis.

Lemma 2.2.2. *(Gronwall's lemma) Let k, M, and $a_\mu, b_\mu, c_\mu, \gamma_\mu$, for integers $\mu > 0$, be nonnegative numbers such that*

$$a_n + k\sum_{\mu=0}^{n} b_\mu \leq k\sum_{\mu=0}^{n} \gamma_\mu a_\mu + k\sum_{\mu=0}^{n} c_\mu + M \text{ for } n \geq 0. \tag{2.2.4}$$

Suppose that $k\gamma_\mu < 1$, for all μ, and set $\sigma_\mu \equiv (1 - k\gamma_\mu)^{-1}$. Then,

$$a_n + k\sum_{\mu=0}^{n} b_\mu \leq exp\left(k\sum_{\mu=0}^{n} \sigma_\mu\gamma_\mu\right)\left\{k\sum_{\mu=0}^{n} c_\mu + M\right\} \text{ for } n \geq 0. \tag{2.2.5}$$

Lemma 2.2.3. *(Modified Gronwall's lemma) Let k, M, and $a_\mu, b_\mu, c_\mu, \gamma_\mu$, for integers $\mu > 0$, be nonnegative numbers such that*

$$a_n + k\sum_{\mu=0}^{n} b_\mu \leq k\sum_{\mu=0}^{n-1} \gamma_\mu a_\mu + k\sum_{\mu=0}^{n} c_\mu + M \text{ for } n \geq 0. \tag{2.2.6}$$

Then, with $\sigma_\mu \equiv (1 - k\gamma_\mu)^{-1}$,

$$a_n + k\sum_{\mu=0}^{n} b_\mu \leq exp\left(k\sum_{\mu=0}^{n-1} \sigma_\mu\gamma_\mu\right)\left\{k\sum_{\mu=0}^{n} c_\mu + M\right\} \text{ for } n \geq 0. \tag{2.2.7}$$

Lemma 2.2.4. *Let $v \in H^1_\Omega$. Then there exists $C = C(\Omega) > 0$, a finite constant such that*

$$\|v\|_{L^3(\partial\Omega)} \leq C(\|v\|^{1/4}_{L^2(\Omega)}\|\nabla v\|^{3/4}_{L^2(\Omega)} + \|v\|^{1/6}_{L^2(\Omega)}\|\nabla v\|^{5/6}_{L^2(\Omega)}) \tag{2.2.8}$$

$$\|v\|_{L^2(\partial\Omega)} \leq C\|v\|^{1/2}_{L^2(\Omega)}\|\nabla v\|^{1/2}_{L^2(\Omega)} \tag{2.2.9}$$

$$\|v\|_{L^4(\partial\Omega)} \leq C\|\nabla v\|_{L^2(\Omega)} \tag{2.2.10}$$

Proof. See [24], Theorem II.4.1, pg. 63. ■ □

Lemma 2.2.5. *Let $u, v, w \in H^1(\Omega_i)$ for $i = 1, 2$. Then there exists $C = C(\Omega_i) > 0$, a finite constant such that*

$$c_i(u; v, w) \leq C\|u\|_{\Omega_i}^{1/2}\|\nabla u\|_{\Omega_i}^{1/2}\|\nabla v\|_{\Omega_i}\|\nabla w\|_{\Omega_i} \tag{2.2.11}$$

Proof. The proof can be found in [21]. ■ □

The following constants and assumptions on the problem data (written here as assumptions on the true solution $\mathbf{u}$) will be used in the proofs below.

Definition 2.2.1. *Let $i = 1, 2$.*

$$C_u := \|\mathbf{u}(x,t)\|_{L^\infty(0,T;L^\infty(\Omega))}, C_{u_{i,t}} := \|\mathbf{u}_{i,t}(x,t)\|_{L^\infty(0,T;L^\infty(\Omega))}, C_{\nabla u_{i,t}} := \|\nabla \mathbf{u}_{i,t}(x,t)\|_{L^\infty(0,T;L^\infty(\Omega))}$$

Assumption 2.2.1. *$\exists \alpha > 0$, such that $\alpha \leq |[\mathbf{u}(\vec{x}, t)]|$, $\forall \vec{x} \in I$, $\forall t \in (0, T]$.*

Assumption 2.2.2. *Let the true solution u satisfy*

$$\left|\frac{\partial}{\partial t}(|\mathbf{u}_i(t)|)\right| \leq C\Delta t^{1/4}, \text{for } i = 1, 2, 0 < t \leq \Delta t, \forall \vec{x} \in I. \tag{2.2.12}$$

2.2.1 Discrete Formulation

Let $\mathcal{T}_i$ be a triangulation of Ω_i and $\mathcal{T}_h = \mathcal{T}_1 \cup \mathcal{T}_2$. Take $X_i^h \subset X_i$ to be conforming finite element spaces for $i = 1, 2$, and define $X^h = X_1^h \times X_2^h \subset X$. It follows that $X^h \subset X$ is a Hilbert space with corresponding inner product and induced norm. We shall consider X_i^h to be spaces of continuous piecewise polynomials of degree $m \geq 2$.

For $t_k \in [0, T]$, $\hat{\mathbf{u}}^\mathbf{k}$, $\tilde{\mathbf{u}}^\mathbf{k}$ will denote the discrete approximations (defect step and correction step, respectively) to $\mathbf{u}(t_k)$.

Every DDC method is based on a lower-order accurate method, which still possesses some desirable characteristics. In our case, it is the geometric averaging-based data passing scheme from [21].

Let $\Delta t > 0$, $f_i \in L^2(\Omega_i)$. For each $M \in \mathbb{N}, M \leq \frac{T}{\Delta t}$, given $u_i^n \in X_{i,h}$ and $p_i^n \in Q_{i,h}$, $n = 0, 1, 2, \cdots, M-1$, solve on each subdomain (for $i, j = 1, 2, i \neq j$) to find $u_i^{n+1} \in X_{i,h}$ satisfying

$$\begin{aligned}\left(\frac{u_i^{n+1} - u_i^n}{\Delta t}, v_i\right) + \nu_i(\nabla u_i^{n+1}, \nabla v_i) + \kappa \int_I u_i^{n+1}|u_i^n - u_j^n| v_i \, ds \\ - \kappa \int_I u_j^n |u_i^n - u_j^n|^{1/2} |u_i^{n-1} - u_j^{n-1}|^{1/2} v_i \, ds \\ + c_i(u_i^{n+1}; u_i^{n+1}, v_i) - (p_i^{n+1}, \nabla \cdot v_i) = (f_i(t^{n+1}), v_i), \ \forall v_i \in X_{i,h} \, . \\ (\nabla \cdot u_i^{n+1}, q_i) = 0, \ \forall \, q_i \in Q_{i,h}. \quad (2.2.13)\end{aligned}$$

This scheme was extensively studied in [21] and was proven to be unconditionally stable and first order accurate. The variational formulation of the two-step DDC method is obtained by combining the DDC techniques, as described in Sections 2.1.1-2.1.2.

Algorithm 2.2.1 (Two Step DDC). *Let $\Delta t > 0$, $M = \frac{T}{\Delta t}$, $f_i \in L^2(\Omega_i)$. Given $\hat{u}_i^n$, find $\hat{u}_i^{n+1} \in X_i^h$, $i, j = 1, 2, i \neq j$, $n = 0, 1, 2, \cdots, M-1$, satisfying*

$$\begin{aligned}\left(\frac{\hat{u}_i^{n+1} - \hat{u}_i^n}{\Delta t}, v_i\right) + (\nu_i + H_i)\left(\nabla \hat{u}_i^{n+1}, \nabla v_i\right) + \kappa \int_I |[\hat{u}^n]| \hat{u}_i^{n+1} v_i ds \\ - \kappa \int_I \hat{u}_j^n |[\hat{u}^n]|^{1/2} |[\hat{u}^{n-1}]|^{1/2} v_i ds \\ - (\hat{p}_i^{n+1}, \nabla \cdot v_i) + c_i\left(\hat{u}_i^{n+1}; \hat{u}_i^{n+1}, v_i\right) = \left(f_i^{n+1}, v_i\right), \ \forall v_i \in X_{i,h} \quad (2.2.14)\end{aligned}$$

Then, given $\hat{u}_i^{n+1}$ *and* $\tilde{u}_i^n$*, find* $\tilde{u}_i^{n+1} \in X_i^h$ *satisfying*

$$\left(\frac{\tilde{u}_i^{n+1}-\tilde{u}_i^n}{\Delta t}, v_i\right) + (\nu_i + H_i)\left(\nabla\tilde{u}_i^{n+1}, \nabla v_i\right) - \kappa\int_I \tilde{u}_j^n|[\tilde{u}^n]|^{1/2}|[\tilde{u}^{n-1}]|^{1/2}v_i ds$$
$$- (\tilde{p}_i^{n+1}, \nabla\cdot v_i) + \kappa\int_I |[\tilde{u}^n]|\tilde{u}_i^{n+1}v_i ds + c_i\left(\tilde{u}_i^{n+1}; \tilde{u}_i^{n+1}, v_i\right) = \left(\frac{f_i^{n+1}+f_i^n}{2}, v_i\right)$$
$$+ \frac{\Delta t(\nu_i+H_i)}{2}\left(\nabla(\frac{\hat{u}_i^{n+1}-\hat{u}_i^n}{\Delta t}), \nabla v_i\right) + \frac{\kappa}{2}\Delta t\int_I |[\hat{u}^n]|(\frac{\hat{u}_i^{n+1}-\hat{u}_i^n}{\Delta t})v_i ds$$
$$- \frac{\kappa}{2}\Delta t\int_I \hat{u}_i^{n+1}(\frac{|[\hat{u}^{n+1}]|-|[\hat{u}^n]|}{\Delta t})v_i ds + H_i\left(\nabla(\frac{\hat{u}_i^{n+1}+\hat{u}_i^n}{2}), \nabla v_i\right)$$
$$- \kappa\int_I \hat{u}_j^n|[\hat{u}^n]|^{1/2}|[\hat{u}^{n-1}]|^{1/2}v_i ds + \frac{\kappa}{2}\int_I |[\hat{u}^{n+1}]|\hat{u}_j^{n+1}v_i ds$$
$$+ \frac{\kappa}{2}\int_I |[\hat{u}^n]|\hat{u}_j^n v_i ds + \frac{1}{2}c_i(\hat{u}_i^{n+1}; \hat{u}_i^{n+1}, v_i)$$
$$- \frac{1}{2}c_i(\hat{u}_i^n; \hat{u}_i^n, v_i) - \left(\frac{\hat{p}_i^{n+1}-\hat{p}_i^n}{2}, \nabla\cdot v_i\right), \ \forall v_i \in X_{i,h}. \quad (2.2.15)$$

The structure of the left hand side (and therefore the matrix of the system) is identical for (2.2.14) and (2.2.15); thus, a simple and computationally cheap artificial viscosity data-passing approximation is computed twice to achieve higher accuracy while maintaining the unconditional stability.

2.3 Proof of Stability and Convergence analysis

In this section we prove the unconditional stability of both the defect step and the correction step approximations. Also we show the accuracy of defect, correction and time derivative steps.

Lemma 2.3.1. *(Stability of Defect approximation) Let* $\hat{u}_i^j \in X_{i,h}$ *satisfy (2.2.14) for each* $j \in \left\{0, 1, 2, \cdots, \frac{T}{\Delta t} - 1\right\}$, $i = 1, 2$. *Then* $\exists C > 0$ *independent of* h, Δt

such that $\hat{\mathbf{u}}^{n+1}$ *satisfies:*

$$\left\|\hat{\mathbf{u}}^{n+1}\right\|^2+\sum_{j=1}^{n}\left\|\hat{\mathbf{u}}^{j+1}-\hat{\mathbf{u}}^{j}\right\|^2+\Delta t\sum_{j=1}^{n}\left[(\nu_1+H_1)\|\nabla u_1^{j+1}\|_{\Omega_1}^2+(\nu_2+H_2)\|\nabla u_2^{j+1}\|_{\Omega_2}^2\right]$$
$$+\kappa\Delta t\int_I|[\hat{\mathbf{u}}^n]|(|u_1^{n+1}|^2+|u_2^{n+1}|^2)ds\ +\kappa\Delta t\sum_{j=1}^{n}\int_I|u_1^{j+1}|[\hat{\mathbf{u}}^j]|^{1/2}-u_2^j|[\hat{\mathbf{u}}^{j-1}]|^{1/2}|^2ds$$
$$+\kappa\Delta t\sum_{j=1}^{n}\int_I|u_2^{j+1}|[\hat{\mathbf{u}}^j]|^{1/2}-u_1^j|\hat{\mathbf{u}}^{j-1}|^{1/2}|^2ds\le\|\mathbf{u}^1\|^2+\kappa\Delta t\int_I|[\mathbf{u}^0]|(|u_1^1|^2+|u_2^1|^2)ds$$
$$+\sum_{j=1}^{n}\left[\frac{\Delta t}{\nu_1+H_1}\|f_1^{j+1}\|_{-1}^2+\frac{\Delta t}{\nu_2+H_2}\|f_2^{j+1}\|_{-1}^2\right]. \quad (2.3.1)$$

Proof. Replace ν_1 and ν_2 with ν_1+H_1 and ν_2+H_2, respectively, in the proof of Lemma 3.1 in [21]. ■ □

The accuracy result for the defect solution u is obtained in a manner very similar to Theorem 3.2 in [21].

Theorem 2.3.2. *(Accuracy of Defect Solution) Let* $\hat{u}_i^k\in X_{i,h}$ *satisfy (2.2.14) for each* $k\in 2,\cdots,n\le N-1$. *Let* $\tilde{\nu}=max\{\nu_1^{-1},\nu_2^{-1}\}$, $\hat{\nu}=max\{\nu_1,\nu_2\}$, *and let* $D^{n+1}=\tilde{\nu}^3(1+\kappa^4E^{n+1}+\|\nabla\mathbf{u}^{n+1}\|^4)$, *where* $E^{n+1}=max_{j=0,1,\cdots,n+1}\{\|\mathbf{u}^j\|_I^4\}$. *Assume* $\Delta t\le\frac{1}{D^{n+1}}$, *and that* $(\mathbf{u},\mathbf{p})$ *is a strong solution of the coupled NSE system (2.1.1)–(2.1.6) with* $\mathbf{u}_t\in L^2(0,T;X)$ *and* $\mathbf{u}_{tt}\in L^2(0,T;L^2(\Omega))$. *Then the solution* $\hat{\mathbf{u}}^{n+1}$ *of (2.2.14) satisfies:*

$$\|\mathbf{u}^{n+1}-\hat{\mathbf{u}}^{n+1}\|^2+\frac{\Delta t}{2}\Bigg[(\nu_1+H_1)\sum_{k=1}^{n}\|\nabla(u_1^{k+1}-\hat{u}_1^{k+1})\|_{\Omega_1}^2$$
$$+(\nu_2+H_2)\sum_{k=1}^{n}\|\nabla(u_2^{k+1}-\hat{u}_2^{k+1})\|_{\Omega_2}^2\Bigg]\leq Cexp\left\{\Delta t\sum_{n=1}^{j}\frac{D^{n+1}}{1-\Delta tD^{n+1}}\right\}\Bigg[\|\mathbf{u}^1-\hat{\mathbf{u}}^1\|^2$$
$$+\inf_{\mathbf{v}^1\in V_h}\|\mathbf{u}^1-\mathbf{v}^1\|^2+\Delta t(\nu_1+H_1)(\|\nabla(u_1^1-\hat{u}_1^1)\|_{\Omega_1}^2$$
$$+\frac{1}{2}\|\nabla(u_1^0-\hat{u}_1^0)\|_{\Omega_1}^2+\inf_{v_1^1\in V_{1,h}}\|\nabla(u_1^1-v_1^1)\|_{\Omega_1}^2+\frac{1}{2}\inf_{v_1^0\in V_{1,h}}\|\nabla(u_1^0-v_1^0)\|_{\Omega_1}^2)$$
$$+\Delta t(\nu_2+H_2)(\|\nabla(u_2^1-\hat{u}_2^1)\|_{\Omega_2}^2+\frac{1}{2}\|\nabla(u_2^0-\hat{u}_2^0)\|_{\Omega_2}^2$$
$$+\inf_{v_2^1\in V_{2,h}}\|\nabla(u_2^1-v_2^1)\|_{\Omega_2}^2+\frac{1}{2}\inf_{v_2^0\in V_{2,h}}\|\nabla(u_2^0-v_2^0)\|_{\Omega_2}^2)$$
$$+\Delta t^2\|\mathbf{u}_{tt}\|_{L^2(0,T;L^2(\Omega))}^2+\inf_{\mathbf{v}\in V_h}\|(\mathbf{u}-\mathbf{v})_t\|_{L^2(0,T;L^2(\Omega))}^2$$
$$+\inf_{\mathbf{q}\in Q_h}\|\mathbf{p}-\mathbf{q}\|_{L^2(0,T;L^2(\Omega))}^2+\kappa^2\Delta t^2\|\mathbf{u}_t\|_{L^2(0,T;X)}^2$$
$$+T\max_{k=2,\cdots,n+1}(\inf_{\mathbf{v}^k\in V_h}\|\nabla(\mathbf{u}^k-\mathbf{v}^k)\|^2)+\frac{H_1^2}{\nu_1+H_1}C_{\nabla u_1}^2+\frac{H_2^2}{\nu_2+H_2}C_{\nabla u_2}^2\Bigg] \quad (2.3.2)$$

where C has the following dependence on κ , ν_1 and ν_2: $C=O(max\{\tilde{\nu},\hat{\nu},(1+\Delta t\kappa^4)\tilde{\nu}^3,\kappa^2\})$.

Proof. The proof can be found in [21], replacing ν_1 and ν_2 with ν_1+H_1 and ν_2+H_2, respectively. The extra term $H_i(\nabla u_i^{n+1},\nabla v_i)$ is treated by applying the Cauchy-Schwarz and Young's inequalities to obtain the accuracy of $O(H_1^2+H_2^2)$. ■ □

Corollary 2.3.1. *Let the problem data be smooth enough; let the discrete velocity-pressure spaces consist of continuous piecewise polynomials of degrees m and $m-1$, respectively ($m\geq 2$). Then there exists a constant C independent of*

$h, H, \Delta t,$ *s.t.*

$$\|\mathbf{u}^{n+1} - \hat{\mathbf{u}}^{n+1}\|^2 + \frac{\Delta t}{2}\Bigg[(\nu_1 + H_1)\sum_{k=1}^{n}\|\nabla(u_1^{k+1} - \hat{u}_1^{k+1})\|_{\Omega_1}^2 + (\nu_2 + H_2)\sum_{k=1}^{n}\|\nabla(u_2^{k+1} - \hat{u}_2^{k+1})\|_{\Omega_2}^2\Bigg] \leq C(h^{2m} + \Delta t^2 + H_1^2 + H_2^2). \tag{2.3.3}$$

In order to show the improved accuracy for the correction approximation, we will need the following result. In order to keep this chapter from being prohibitively long, the proof is given in full detail in [23]. Consider $e_i^j = u_i^j - \hat{u}_i^j$, $i = 1, 2$, $j = 0, 1, 2, \cdots, M$.

Theorem 2.3.3. *(Accuracy of Time Derivative of the Error in the Defect Step) Let* $u_i(\Delta t) \in H^2(\Omega_i)$, $\Delta\mathbf{u} \in L^2(0, T; L^2(\Omega))$ *and* $\mathbf{u}_{tt}, \mathbf{u}_t, \mathbf{u} \in L^2(0, T; L^2(\Omega))$. *Let* $min(h, \Delta t) < C(\frac{\nu_i + h_i}{\kappa})$.

Let also $max(h, \Delta t, H_1, H_2) \leq \frac{\alpha}{4\sqrt{C_f}}$, *where* α *is the constant introduced in Assumption 2.2.1, and* C_f *is the constant from* (2.3.3).

Then $\exists C > 0$ *independent of* h, H_i, Δt *such that for any* $n \in \{0, 1, 2, \cdots, M - 1 = \frac{T}{\Delta t} - 1\}$, *the discrete time derivative of the error* $\frac{e_i^{n+1} - e_i^n}{\Delta t}$ *satisfies*

$$\|\frac{\mathbf{e}^{n+1} - \mathbf{e}^n}{\Delta t}\|^2 + (\nu_1 + H_1)\Delta t\sum_{j=1}^{n}\|\nabla\left(\frac{e_1^{j+1} - e_1^j}{\Delta t}\right)\|^2 + (\nu_2 + H_2)\Delta t\sum_{j=1}^{n}\|\nabla\left(\frac{e_2^{j+1} - e_2^j}{\Delta t}\right)\|^2 \leq C\left(h^{2m} + (\Delta t)^2 + H^2\right). \tag{2.3.4}$$

Proof. Focusing on Ω_1 first, write (2.2.1) at time t_{n+1} to obtain

$$\begin{aligned}\left(\frac{u_1^{n+1}-u_1^n}{\Delta t},v_1\right)+(\nu_1+H_1)(\nabla u_1^{n+1},\nabla v_1)+c_1(u_1^{n+1};u_1^{n+1},v_1)\\ -(p_1^{n+1},\nabla\cdot v_1)+\kappa\int_I u_1^{n+1}|[u^{n+1}]|v_1ds-\kappa\int_I u_2^{n+1}|[u^{n+1}]|^{1/2}|[u^{n+1}]|^{1/2}v_1ds\\ =(f_1^{n+1},v_1)+H_1(\nabla u_1^{n+1},\nabla v_1)+\left(\frac{u_1^{n+1}-u_1^n}{\Delta t}-u_{1,t}^{n+1},v_1\right)\end{aligned}\tag{2.3.5}$$

Denote $\frac{u_1^{n+1}-u_1^n}{\Delta t}-u_{1,t}^{n+1}\equiv\rho_1^{n+1}$. Subtract (2.2.14) from (2.3.5) to obtain the equation for the error, $e_i^{n+1}=u_i^{n+1}-\hat{u}_i^{n+1}, i=1,2$. For any $v_1\in X_1^h$

$$\begin{aligned}\left(\frac{e_1^{n+1}-e_1^n}{\Delta t},v_1\right)+(\nu_1+H_1)(\nabla e_1^{n+1},\nabla v_1)+c_1(u_1^{n+1};u_1^{n+1},v_1)\\ -c_1(\hat{u}_1^{n+1};\hat{u}_1^{n+1},v_1)\\ -(p_1^{n+1}-\hat{p}_1^{n+1},\nabla\cdot v_1)+\kappa\int_I u_1^{n+1}|[u^{n+1}]|v_1ds\\ -\kappa\int_I\hat{u}_1^{n+1}|[\hat{u}^n]|v_1ds-\kappa\int_I u_2^{n+1}|[u^{n+1}]|v_1ds\\ +\kappa\int_I\hat{u}_2^n|[\hat{u}^n]|^{1/2}|[\hat{u}^{n-1}]|^{1/2}v_1ds=H_1(\nabla u_1^{n+1},\nabla v_1)+(\rho_1^{n+1},v_1)\end{aligned}\tag{2.3.6}$$

Decompose $e_1^i=u_1^i-\hat{u}_1^i=(\breve{u}_1^i-\hat{u}_1^i)-(\breve{u}_1^i-u_1^i)=\phi_1^i-\eta_1^i$, for some $\breve{u}_1^i\in X_1^h$. Taking $v_1=\frac{\phi_1^{n+1}-\phi_1^n}{\Delta t}\in X_{1,h}$ in (2.3.6) leads to

$$\begin{aligned}\left(\frac{e_1^{n+1}-e_1^n}{\Delta t},\frac{\phi_1^{n+1}-\phi_1^n}{\Delta t}\right)+(\nu_1+H_1)(\nabla e_1^{n+1},\nabla\frac{\phi_1^{n+1}-\phi_1^n}{\Delta t})\\ +c_1(u_1^{n+1};u_1^{n+1},\frac{\phi_1^{n+1}-\phi_1^n}{\Delta t})-c_1(u_1^{n+1};u_1^{n+1},\frac{\phi_1^{n+1}-\phi_1^n}{\Delta t})\\ -(p_1^{n+1}-\hat{p}_1^{n+1},\nabla\cdot\frac{\phi_1^{n+1}-\phi_1^n}{\Delta t})+\kappa\int_I u_1^{n+1}|[u^{n+1}]|\frac{\phi_1^{n+1}-\phi_1^n}{\Delta t}ds\\ -\kappa\int_I\hat{u}_1^{n+1}|[\hat{u}^n]|\frac{\phi_1^{n+1}-\phi_1^n}{\Delta t}ds-\kappa\int_I u_2^{n+1}|[u^{n+1}]|\frac{\phi_1^{n+1}-\phi_1^n}{\Delta t}ds\\ +\kappa\int_I\hat{u}_2^n|[\hat{u}^n]|^{1/2}|[\hat{u}^{n-1}]|^{1/2}\frac{\phi_1^{n+1}-\phi_1^n}{\Delta t}ds=H_1(\nabla u_1^{n+1},\nabla\frac{\phi_1^{n+1}-\phi_1^n}{\Delta t})\\ +(\rho_1^{n+1},\frac{\phi_1^{n+1}-\phi_1^n}{\Delta t})\end{aligned}\tag{2.3.7}$$

Also, take $v_1 = \frac{\phi_1^{n+1}-\phi_1^n}{\Delta t}$ in (2.3.6) at the previous time level, and subtract the resulting equation from (2.3.7). Denoting $s_1^{n+1} \equiv \frac{\phi_1^{n+1}-\phi_1^n}{\Delta t}$,we obtain for $n \geq 1$

$$
\begin{aligned}
\|s_1^{n+1}\|^2 - (s_1^{n+1}, s_1^n) + (\nu_1 + H_1)\Delta t \|\nabla s_1^{n+1}\|^2 + c_1(u_1^{n+1}; u_1^{n+1}, s_1^{n+1}) \\
-c_1(u_1^n; u_1^n, s_1^{n+1}) - c_1(\hat{u}_1^{n+1}; \hat{u}_1^{n+1}, s_1^{n+1}) + c_1(\hat{u}_1^n; \hat{u}_1^n, s_1^{n+1}) \\
+\Delta t \left(\frac{p_1^{n+1} - p_1^n}{\Delta t} - \frac{\hat{p}_1^{n+1} - \hat{p}_1^n}{\Delta t}, \nabla \cdot s_1^{n+1} \right) + \kappa \int_I u_1^{n+1} |[u^{n+1}]| s_1^{n+1} ds \\
-\kappa \int_I u_1^n |[u^n]| s_1^{n+1} ds - \kappa \int_I \hat{u}_1^{n+1} |[\hat{u}^n]| s_1^{n+1} ds + \kappa \int_I \hat{u}_1^n |[\hat{u}^{n-1}]| s_1^{n+1} ds \\
-\kappa \int_I u_2^{n+1} |[u^{n+1}]| s_1^{n+1} ds + \kappa \int_I u_2^n |[u^n]| s_1^{n+1} ds \\
+\kappa \int_I \hat{u}_2^n |[\hat{u}^n]|^{1/2} |[\hat{u}^{n-1}]|^{1/2} s_1^{n+1} ds - \kappa \int_I \hat{u}_2^{n-1} |[\hat{u}^{n-1}]|^{1/2} |[\hat{u}^{n-2}]|^{1/2} s_1^{n+1} ds \\
= H_1 \Delta t \left(\nabla(\frac{u_1^{n+1} - u_1^n}{\Delta t}), \nabla s_1^{n+1} \right) + \Delta t \left(\frac{\rho_1^{n+1} - \rho_1^n}{\Delta t}, s_1^{n+1} \right) \\
+\Delta t \left(\frac{\eta_1^{n+1} - 2\eta_1^n + \eta_1^{n-1}}{(\Delta t)^2}, s_1^{n+1} \right) \\
+(\nu_1 + H_1)\Delta t \left(\nabla(\frac{\eta_1^{n+1} - \eta_1^n}{\Delta t}), \nabla s_1^{n+1} \right)
\end{aligned}
\tag{2.3.8}
$$

The nonlinear terms are bounded in a manner, typical for the deferred correction methods for NSE (see, e.g., [22, 19]). This part of the proof is also available in [23].

Consider the first 4 interface terms

$$
\begin{aligned}
\kappa \int_I u_1^{n+1} |[u^{n+1}]| s_1^{n+1} ds - \kappa \int_I \hat{u}_1^{n+1} |[\hat{u}^n]| s_1^{n+1} ds \\
-(\kappa \int_I u_1^n |[u^n]| s_1^{n+1} ds - \kappa \int_I \hat{u}_1^n |[\hat{u}^{n-1}]| s_1^{n+1} ds) = F_1 - F_2.
\end{aligned}
$$

Write F_1 as

$$\begin{aligned}
F_1 &= \kappa \int_I u_1^{n+1}|[u^{n+1}]|s_1^{n+1}ds - \kappa \int_I \hat{u}_1^{n+1}|[u^{n+1}]|s_1^{n+1}ds \\
&\quad +\kappa \int_I \hat{u}_1^{n+1}|[u^{n+1}]|s_1^{n+1}ds - \kappa \int_I \hat{u}_1^{n+1}|[u^{n}]|s_1^{n+1}ds \\
&\quad +\kappa \int_I \hat{u}_1^{n+1}|[u^{n}]|s_1^{n+1}ds - \kappa \int_I \hat{u}_1^{n+1}|[\hat{u}^{n}]|s_1^{n+1}ds \\
&= \kappa \int_I e_1^{n+1}|[u^{n+1}]|s_1^{n+1}ds + \kappa \int_I \hat{u}_1^{n+1}(|[u^{n+1}]| - |[u^{n}]|)s_1^{n+1}ds \\
&\quad +\kappa \int_I \hat{u}_1^{n+1}|[e^{n}]|s_1^{n+1}ds \\
&= \kappa \int_I e_1^{n+1}|[u^{n+1}]|s_1^{n+1}ds + \kappa \int_I u_1^{n+1}(|[u^{n+1}]| - |[u^{n}]|)s_1^{n+1}ds \\
&\quad -\kappa \int_I e_1^{n+1}(|[u^{n+1}]| - |[u^{n}]|)s_1^{n+1}ds + \kappa \int_I u_1^{n+1}|[e^{n}]|s_1^{n+1}ds \\
&\quad -\kappa \int_I e_1^{n+1}|[e^{n}]|s_1^{n+1}ds.
\end{aligned}$$

In order to treat the five terms above, apply the same arguments for F_2 and subtract the result from F_1. Let $F_1 - F_2 = F_{12,1} + F_{12,2} + F_{12,3} + F_{12,4} + F_{12,5}$, defined as follows.

$$\begin{aligned}
F_{12,1} &= \kappa \int_I (e_1^{n+1} - e_1^{n})|[u^{n+1}]|s_1^{n+1}ds + \kappa \int_I e_1^{n}(|[u^{n+1}]| - |[u^{n}]|)s_1^{n+1}ds \quad (2.3.9) \\
&= \kappa\Delta t \int_I |[u^{n+1}]||s_1^{n+1}|^2 ds + \kappa\Delta t \int_I e_1^{n}\frac{|[u^{n+1}]| - |[u^{n}]|}{\Delta t}s_1^{n+1}ds \\
&\quad +\kappa\Delta t \int_I \frac{\eta_1^{n+1} - \eta_1^{n}}{\Delta t}|[u^{n+1}]|s_1^{n+1}ds
\end{aligned}$$

The term $\kappa \int_I \Delta t|[u^{n+1}]||s_1^{n+1}|^2 ds$ is non-negative and it stays in the left hand side. The Cauchy-Schwarz and Young's inequalities are used to bound the two remaining terms in the right hand side of (2.3.9).

The term

$$F_{12,2} = \kappa \int_I u_1^{n+1}(|[u^{n+1}]| - |[u^n]|)s_1^{n+1}ds - \kappa \int_I u_1^n(|[u^n]| - |[u^{n-1}]|)s_1^{n+1}ds$$
$$= \kappa \int_I \Delta t \frac{u_1^{n+1} - u_1^n}{\Delta t}(|[u^{n+1}]| - |[u^n]|)s_1^{n+1}ds$$
$$+\kappa \int_I u_1^n(|[u^{n+1}]| - 2|[u^n]| + |[u^{n-1}]|)s_1^{n+1}ds$$

is bounded by using Assumption 2.2.1 for the second integral in the right hand side and then applying the Cauchy-Schwarz and Young's inequalities.

Similarly, the Cauchy-Schwarz and Young's inequalities are used to derive the $O(H^2 + H\Delta t + \Delta t^2)$ bounds for $F_{12,3}, F_{12,4}, F_{12,5}$ - see [23] for details.

The following notation is used to simplify the computations below.

$$a = |[\hat{u}^n]|^{1/2}|[\hat{u}^{n-1}]|^{1/2} - \frac{1}{2}(|[\hat{u}^n]| + |[\hat{u}^{n-1}]|),$$
$$a_p = |[\hat{u}^{n-1}]|^{1/2}|[\hat{u}^{n-2}]|^{1/2} - \frac{1}{2}(|[\hat{u}^{n-1}]| + |[\hat{u}^{n-2}]|).$$

We now proceed with the bounds on the remainder of the interface terms (see [23] for the missing details).

$$\kappa \int_I \hat{u}_2^n |[\hat{u}^n]|^{1/2} |[\hat{u}^{n-1}]|^{1/2} s_1^{n+1} ds - \kappa \int_I u_2^{n+1} |[u^{n+1}]| s_1^{n+1} ds$$
$$-(\kappa \int_I \hat{u}_2^{n-1} |[\hat{u}^{n-1}]|^{1/2} |[\hat{u}^{n-2}]|^{1/2} s_1^{n+1} ds - \kappa \int_I u_2^n |[u^n]| s_1^{n+1} ds) =$$
$$\kappa \int_I \hat{u}_2^n (|[\hat{u}^n]|^{1/2} |[\hat{u}^{n-1}]|^{1/2} - \frac{1}{2}(|[\hat{u}^n]| + |[\hat{u}^{n-1}]|)) s_1^{n+1} ds$$
$$-\kappa \int_I \hat{u}_2^{n-1} (|[\hat{u}^{n-1}]|^{1/2} |[\hat{u}^{n-2}]|^{1/2} - \frac{1}{2}(|[\hat{u}^{n-1}]| + |[\hat{u}^{n-2}]|)) s_1^{n+1} ds$$
$$-\kappa \int_I e_2^n |[u^{n+1}]| s_1^{n+1} ds + \kappa \int_I e_2^{n-1} |[u^n]| s_1^{n+1} ds$$
$$+\kappa \int_I \hat{u}_2^n (\frac{|[\hat{u}^n]| + |[\hat{u}^{n-1}]|}{2} - |[u^{n+1}]|) s_1^{n+1} ds$$
$$-\kappa \int_I \hat{u}_2^{n-1} (\frac{|[\hat{u}^{n-1}]| + |[\hat{u}^{n-2}]|}{2} - |[u^n]|) s_1^{n+1} ds$$

Denote

$$I_1 = \kappa \int_I \hat{u}_2^n a s_1^{n+1} ds - \kappa \int_I \hat{u}_2^{n-1} a_p s_1^{n+1} ds$$
$$I_2 = -\kappa \int_I e_2^n |[u^{n+1}]| s_1^{n+1} ds + \kappa \int_I e_2^{n-1} |[u^n]| s_1^{n+1} ds$$
$$I_3 = \kappa \int_I \hat{u}_2^n (\frac{|[\hat{u}^n]| + |[\hat{u}^{n-1}]|}{2} - |[u^{n+1}]|) s_1^{n+1} ds$$
$$-\kappa \int_I \hat{u}_2^{n-1} (\frac{|[\hat{u}^{n-1}]| + |[\hat{u}^{n-2}]|}{2} - |[u^n]|) s_1^{n+1} ds$$

.

The integrals in I_1 are treated as follows.

$$I_1 = \kappa \int_I \hat{u}_2^n a s_1^{n+1} ds - \kappa \int_I \hat{u}_2^{n-1} a_p s_1^{n+1} ds$$
$$= \kappa \int_I \hat{u}_2^n a s_1^{n+1} ds - \kappa \int_I u_2^n a s_1^{n+1} ds + \kappa \int_I u_2^n a s_1^{n+1} ds$$
$$-\kappa \int_I u_2^{n-1} a s_1^{n+1} ds + \kappa \int_I u_2^{n-1} a_p s_1^{n+1} ds - \kappa \int_I u_2^n a_p s_1^{n+1} ds$$
$$+\kappa \int_I u_2^{n-1} a s_1^{n+1} ds - \kappa \int_I \hat{u}_2^{n-1} a_p s_1^{n+1} ds$$

Denoting $x = |[\hat{u}^n]|^{1/2}$ and $y = |[\hat{u}^{n-1}]|^{1/2}$, we write

$$|a| = |xy - \frac{1}{2}(x^2+y^2)| = |-\frac{1}{2}(-2xy+x^2+y^2)| = |-\frac{1}{2}(x-y)^2| \quad (2.3.10)$$
$$\leq \frac{1}{2}|x-y|(x+y) = \frac{1}{2}|x^2-y^2| = \frac{1}{2}|[\hat{u}^n - \hat{u}^{n-1}]|$$

Then

$$|a| \leq \frac{1}{2}|[\hat{u}^n - \hat{u}^{n-1}]| \leq \frac{1}{2}|[e^n - e^{n-1}] - [u^n - u^{n-1}]|$$
$$\leq \frac{1}{2}|[\phi^n - \phi^{n-1}]| + \frac{1}{2}|[\eta^n - \eta^{n-1}]| + \frac{\Delta t}{2}\left|\left[\frac{u^n - u^{n-1}}{\Delta t}\right]\right|$$
$$\leq \frac{1}{2}\Delta t|s_1^n| + \frac{1}{2}\Delta t|s_2^n| + \frac{1}{2}\Delta t\left|\left[\frac{\eta^n - \eta^{n-1}}{\Delta t}\right]\right| + \frac{1}{2}\Delta t\left|\left[\frac{u^n - u^{n-1}}{\Delta t}\right]\right|$$

Since a is bounded, we can bound each line in I_1:

$$\kappa\int_I \hat{u}_2^n a s_1^{n+1} ds - \kappa\int_I u_2^n a s_1^{n+1} ds$$
$$\leq C\kappa\int_I |e_2^n|\Delta t\left[|s_1^n| + |s_1^n| + \left|\frac{\eta^n - \eta^{n-1}}{\Delta t}\right| + \left|[\frac{u^n - u^{n-1}}{\Delta t}]\right|\right]|s_1^{n+1}|ds$$

$$\kappa\int_I u_2^n a s_1^{n+1} ds - \kappa\int_I u_2^{n-1} a s_1^{n+1} ds \leq C\kappa\int_I \Delta t^2\left|\frac{u_2^n - u_2^{n-1}}{\Delta t}\right||a||s_1^{n+1}|ds$$

$$\kappa\int_I u_2^{n-1} a_p s_1^{n+1} ds - \kappa\int_I \hat{u}_2^{n-1} a_p s_1^{n+1} ds \leq C\kappa\int_I |e_2^{n-1}|\Delta t|a||s_1^{n+1}|ds$$

Instead of trying to show the second order of smallness of $|a - a_p|$, we will show that a (and therefore a_p) is small enough. Each of the last two terms in I_1, is bounded using Assumption 2.2.1, as follows.

$$|\kappa \int_I u_2^n (|[\hat{u}^n]|^{1/2} - |[\hat{u}^{n-1}]|^{1/2})^2 s_1^{n+1} ds|$$
$$\leq \kappa \int_I (u_2^n/\alpha)|[u^n]|(|[\hat{u}^n]|^{1/2} - |[\hat{u}^{n-1}]|^{1/2})^2 |s_1^{n+1}| ds = A$$

$$|[u^n]|(|[\hat{u}^n]|^{1/2} - |[\hat{u}^{n-1}]|^{1/2})^2 = \frac{1}{4}\Bigg[4|[u^n]| - (|[\hat{u}^n]|^{1/2} + |[\hat{u}^{n-1}]|^{1/2})^2$$
$$+ (|[\hat{u}^n]|^{1/2} + |[\hat{u}^{n-1}]|^{1/2})^2\Bigg](|[\hat{u}^n]|^{1/2} - |[\hat{u}^{n-1}]|^{1/2})^2$$
$$= \frac{1}{4}\Bigg[4|[u^n]| - 2|[\hat{u}^n]| - 2|[\hat{u}^{n-1}]| + (|[\hat{u}^n]|^{1/2} - |[\hat{u}^{n-1}]|^{1/2})^2$$
$$+ (|[\hat{u}^n]|^{1/2} + |[\hat{u}^{n-1}]|^{1/2})^2\Bigg](|[\hat{u}^n]|^{1/2} - |[\hat{u}^{n-1}]|^{1/2})^2$$
$$= \frac{1}{4}\Bigg[2(|[u^n]| - |[\hat{u}^n]|) + 2(|[u^n]| - |[u^{n-1}]|)$$
$$+ 2(|[u^{n-1}]| - |[\hat{u}^{n-1}]|)\Bigg](|[\hat{u}^n]|^{1/2} - |[\hat{u}^{n-1}]|^{1/2})^2$$
$$+ \frac{1}{4}(|[\hat{u}^n]|^{1/2} - |[\hat{u}^{n-1}]|^{1/2})^4 + \frac{1}{4}(|[\hat{u}^n]| - |[\hat{u}^{n-1}]|)^2$$

Thus,

$$A \leq \kappa \int_I \frac{1}{\alpha}|u_2^n||s_1^{n+1}|\Bigg[\Bigg(\Delta t\left|\left[\frac{u^n - u^{n-1}}{\Delta t}\right]\right| + |[\eta^n]| + |[\phi^n]| + |[\eta^{n-1}]|$$
$$+ |[\phi^{n-1}]|\Bigg)\Bigg[\Delta t\left|\left[\frac{u^n - u^{n-1}}{\Delta t}\right]\right| + \Delta t\left|\left[\frac{\eta^n - \eta^{n-1}}{\Delta t}\right]\right| + \Delta t|[s^n]|\Bigg]$$
$$+ \Delta t^2\left|\left[\frac{u^n - u^{n-1}}{\Delta t}\right]\right|^2 + \Delta t^2\left|\left[\frac{\eta^n - \eta^{n-1}}{\Delta t}\right]\right|^2 + \Delta t^2|[s^n]|^2\Bigg] ds. \quad (2.3.11)$$

We will now show how to bound some of the terms in the right hand side of (2.3.11); see [23] for more details.

$$\kappa \int_I \frac{1}{\alpha}|u_2^n||s_1^{n+1}|\Delta t^2 \left|\left[\frac{\eta^n-\eta^{n-1}}{\Delta t}\right]\right|^2 ds \leq C\Delta t^2\|\nabla s_1^{n+1}\| \left\|\left[\frac{\nabla\eta^n-\nabla\eta^{n-1}}{\Delta t}\right]\right\|^2$$
$$\leq \epsilon(\nu_1+H_1)\Delta t\|\nabla s_1^{n+1}\|^2 + C\Delta t^2\Delta t \left\|\left[\frac{\nabla\eta^n-\nabla\eta^{n-1}}{\Delta t}\right]\right\|^4 \tag{2.3.12}$$

The next term is bounded in two different ways, depending on the relationship between the mesh diameter and the time step.

$$\begin{aligned}\kappa \int_I \frac{1}{\alpha}|u_2^n||s_1^{n+1}||\phi_1^n|\Delta t|s_1^n|ds &\leq C\Delta t\|\phi_1^n\|^{1/2}\|\nabla\phi_1^n\|^{1/2}\|\nabla s_1^n\|\|\nabla s_1^{n+1}\| \\ &\leq \epsilon(\nu_1+H_1)\Delta t\|\nabla s_1^{n+1}\|^2 + \frac{C}{\nu_1+H_1}\Delta t\|\phi_1^n\|\|\nabla\phi_1^n\|\|\nabla s_1^n\|^2\end{aligned} \tag{2.3.13}$$

$$\leq \begin{cases} \epsilon(\nu_1+H_1)\Delta t\|\nabla s_1^{n+1}\|^2 + \frac{C}{\nu_1+H_1}\Delta t h^{-1}(h^2+\Delta t^2)\|\nabla s_1^n\|^2 & \text{if } \Delta t < h \\ \epsilon(\nu_1+H_1)\Delta t\|\nabla s_1^{n+1}\|^2 + \frac{C}{\nu_1+H_1}(h+\Delta t)\Delta t^{1/2}(h+\Delta t)\|\nabla s_1^n\|^2 & \\ \leq \epsilon(\nu_1+H_1)\Delta t\|\nabla s_1^{n+1}\|^2 + \frac{C}{\nu_1+H_1}\Delta t^{3/2}\Delta t\|\nabla s_1^n\|^2 & \text{if } h < \Delta t \end{cases}$$

Given, that $max(h,\Delta t) \leq \frac{\epsilon(\nu_1+H_1)^2}{C}$, the terms in the right-hand side of (2.3.13) are small enough to either be subsumed in the left-hand side, or to provide the necessary accuracy.

The remainder of the terms in (2.3.11) are bounded, using the Cauchy-Schwarz and Young's inequalities, similar to (2.3.12)-(2.3.13); see [23].

Add and subtract $\kappa\int e_2^n|[u^n]|s_1^{n+1}ds$ for I_2 and
$\kappa\int \hat{u}_2^n(\frac{|[\hat{u}^{n-1}]|+|[\hat{u}^{n-2}]|}{2} - |[u^n]|)s_1^{n+1}ds$ for I_3. The goal, as usual, is to get the

second order of smallness in each of the interface terms; for most of them, applying the Cauchy-Schwarz and Young's inequalities is straightforward. The only problematic term is the one remaining from I_3:

$$\kappa \int_I u_2^n \left(|[\hat{\mathbf{u}}^n]| - |[\hat{\mathbf{u}}^{n-1}]| - |[\mathbf{u}^n]| + |[\mathbf{u}^{n-1}]| \right) s_1^{n+1} ds \tag{2.3.14}$$

The second order of smallness for the interface term (2.3.14) is achieved as follows. Notice that here lies the reason for us restricting the proof to the $2-D$ problems; the rest of the proof of this theorem (and all other theorems in this Chapter) is also valid in $3-D$.

$$\begin{aligned} &|[\hat{\mathbf{u}}^n]| - |[\hat{\mathbf{u}}^{n-1}]| - |[\mathbf{u}^n]| + |[\mathbf{u}^{n-1}]| \\ &= \left((|[\hat{\mathbf{u}}^n]|^{\frac{1}{2}} - |[\mathbf{u}^{n-1}]|^{\frac{1}{2}})^2 - (|[\mathbf{u}^n]|^{\frac{1}{2}} - |[\hat{\mathbf{u}}^{n-1}]|^{\frac{1}{2}})^2 \right) \\ &+2 \left(|[\hat{\mathbf{u}}^n]|^{\frac{1}{2}} |[\mathbf{u}^{n-1}]|^{\frac{1}{2}} - |[\mathbf{u}^n]|^{\frac{1}{2}} |[\hat{\mathbf{u}}^{n-1}]|^{\frac{1}{2}} \right) = G + 2L. \end{aligned} \tag{2.3.15}$$

The second order of smallness of G follows from an argument given in (2.3.11). With $h + \Delta t \leq C\alpha$, we have

$$[\hat{\mathbf{u}}^n] = [\mathbf{u}^n] - [\mathbf{e}^n] \Rightarrow |[\hat{\mathbf{u}}^n]| \geq |[\mathbf{u}^n]| - |[\mathbf{e}^n]| \geq \frac{\alpha}{2}.$$

Then,

$$\begin{aligned} |L| &\leq \frac{1}{\alpha} |L| \left(|[\hat{\mathbf{u}}^n]|^{\frac{1}{2}} |[\mathbf{u}^{n-1}]|^{\frac{1}{2}} + |[\mathbf{u}^n]|^{\frac{1}{2}} |[\hat{\mathbf{u}}^{n-1}]|^{\frac{1}{2}} \right) \\ &\leq \frac{1}{\alpha} |[\hat{\mathbf{u}}^n]| |[\mathbf{u}^{n-1}]| - |[\mathbf{u}^n]| |[\hat{\mathbf{u}}^{n-1}]|| = \frac{1}{\alpha} |D|. \end{aligned} \tag{2.3.16}$$

At the same time,

$$|[\hat{\mathbf{u}}^n][\mathbf{u}^{n-1}] - [\mathbf{u}^n][\hat{\mathbf{u}}^{n-1}]| = |[\mathbf{u}^n][\mathbf{u}^{n-1}] - [\mathbf{e}^n][\mathbf{u}^{n-1}] - [\mathbf{u}^n][\mathbf{u}^{n-1}] \quad (2.3.17)$$
$$+[\mathbf{u}^n][\mathbf{e}^{n-1}]| \leq |[\mathbf{e}^n]|\Delta t|\frac{\mathbf{u}^n - \mathbf{u}^{n-1}}{\Delta t}| + |\mathbf{u}^n||[\mathbf{e}^n] - [\mathbf{e}^{n-1}]|.$$

In $2-D$: for any $i,j = 1,2$, $\hat{u}_i \cdot n = u_j \cdot n = 0$ on I, therefore $\hat{u}_i || u_j$ on I.

Thus, in $2-D$

$$|[\hat{\mathbf{u}}^n]||[\mathbf{u}^{n-1}]| = |[\hat{\mathbf{u}}^n][\mathbf{u}^{n-1}]| \text{ and } |[\mathbf{u}^n]||[\hat{\mathbf{u}}^{n-1}]| = |[\mathbf{u}^n][\hat{\mathbf{u}}^{n-1}]|.$$

Putting it together, it follows from (2.3.15)-(2.3.17) that

$$\begin{aligned}|L| \leq \frac{1}{\alpha}|D| &\leq \frac{1}{\alpha}|[\hat{\mathbf{u}}^n]||[\mathbf{u}^{n-1}] - [\mathbf{u}^n]||[\hat{\mathbf{u}}^{n-1}]| \\ &\leq \frac{1}{\alpha}\Bigg[\Delta t|[\mathbf{e}^n]||\frac{[\mathbf{u}^n] - [\mathbf{u}^{n-1}]}{\Delta t}| + \Delta t|[\mathbf{u}^n]||\frac{[\eta^n] - [\eta^{n-1}]}{\Delta t}| \\ &\qquad + \Delta t|[\mathbf{u}^n]||[s^n]|\Bigg]. \quad (2.3.18)\end{aligned}$$

The last term in (2.3.18) will be dealt with by using the Gronwall's lemma, and the rest of the terms are $O(\Delta t(h + \Delta t))$.

Combining all the bounds together leads to

$$\begin{aligned}\frac{\|s_1^{n+1}\|^2 - \|s_1^n\|^2}{2} + (\nu_1 + H_1)\Delta t\|\nabla s_1^{n+1}\|^2 &\leq \epsilon\Delta t(\nu_1 + H_1)\|\nabla s_1^{n+1}\|^2 \\ + \frac{d\Delta t}{4\epsilon(\nu_1 + H_1)}\inf_{q_1 \in Q_1^h}\|\frac{p_1^{n+1} - p_1^n}{\Delta t} - q_1\|^2 &+ \frac{\Delta t H_1^2}{4\epsilon(\nu_1 + H_1)}C^2_{\nabla u_{1t}} \\ + \frac{\Delta t}{4\epsilon(\nu_1 + H_1)}\|\frac{\rho_1^{n+1} - \rho_1^n}{\Delta t}\|^2_{-1}&\end{aligned}$$

$$+\frac{\Delta tC_{PF}}{4\epsilon(\nu_1+H_1)}\|\frac{\eta_1^{n+1}-2\eta_1^n+\eta_1^{n-1}}{\Delta t^2}\|_{-1}^2$$
$$+\frac{\Delta t(\nu_1+H_1)}{4\epsilon}\|\nabla(\frac{\eta_1^{n+1}-\eta_1^n}{\Delta t})\|^2$$
$$+\frac{C_{\nabla u_{1t}}^2\Delta t}{4\epsilon(\nu_1+H_1)}\|\nabla\phi_1^{n+1}\|^2+\frac{C_{\nabla u_{1t}}^2\Delta t}{4\epsilon(\nu_1+H_1)}\|\nabla\eta_1^{n+1}\|^2$$
$$+\frac{C_{\nabla u_1}^2\Delta t}{4\epsilon(\nu_1+H_1)}\|\nabla(\frac{\eta_1^{n+1}-\eta_1^n}{\Delta t})\|^2+\Delta t(\frac{C_{\nabla u_{1t}}^2}{2}+\frac{C_{u_1}^2}{16\epsilon(\nu_1+H_1)})\|s_1^{n+1}\|^2$$
$$+\frac{4\Delta t}{\epsilon^3(\nu_1+H_1)^3}\|\nabla\phi_1^{n+1}\|^4\|s_1^{n+1}\|^2+\frac{4\Delta t}{\epsilon^3(\nu_1+H_1)^3}\|\nabla\eta_1^{n+1}\|^4\|s_1^{n+1}\|^2$$
$$+\frac{\Delta t}{4\epsilon(\nu_1+H_1)}\|\nabla\eta_1^{n+1}\|^2\|\nabla(\frac{\eta_1^{n+1}-\eta_1^n}{\Delta t})\|^2$$
$$+\frac{\Delta t}{4\epsilon(\nu_1+H_1)}\|\nabla\phi_1^{n+1}\|^2\|\nabla(\frac{\eta_1^{n+1}-\eta_1^n}{\Delta t})\|^2$$
$$+C\frac{\kappa^2}{(\nu_1+H_1)}\Delta t\|\nabla e_1^n\|^2+\frac{C\kappa^2}{(\nu_1+H_1)}\Delta t\|\nabla(\frac{\eta_1^{n+1}-\eta_1^n}{\Delta t})\|^2$$
$$+\frac{C\kappa^2}{(\nu_1+H_1)}\Delta t\Delta t^2+C\kappa\Delta t^2\|\nabla s_1^{n+1}\|^2$$
$$+\frac{C\kappa^2}{(\nu_1+H_1)}\Delta t\Delta t^2\|\nabla(\frac{\eta_1^{n+1}-\eta_1^n}{\Delta t})\|^2$$
$$+\frac{C\kappa^2}{(\nu_1+H_1)}\Delta t\Delta t^2\|\nabla\eta_1^n\|^2+\frac{C\kappa^2}{(\nu_1+H_1)}\Delta t\|s_1^{n+1}\|^2$$
$$+\epsilon\Delta t(\nu_1+H_1)\|\nabla s_1^n\|^2+\epsilon\Delta t(\nu_1+H_1)\|\nabla s_2^n\|^2$$
$$+\frac{C\kappa^2}{(\nu_1+H_1)}\Delta t\|s_1^n\|^2+\frac{C\kappa^2}{(\nu_1+H_1)}\Delta t\|s_2^n\|^2$$
$$+\frac{C\kappa}{(\nu_1+H_1)^3}\Delta t\|\nabla e_1^n\|^4\|s_1^{n+1}\|^2$$
$$+\frac{C\kappa}{(\nu_1+H_1)^3}\Delta t\|\nabla e_2^n\|^4\|s_1^{n+1}\|^2$$
$$+\frac{C\kappa^2}{(\nu_1+H_1)}\Delta t\|\nabla e_1^n\|^2\|\nabla(\frac{\eta_1^{n+1}-\eta_1^n}{\Delta t})\|^2$$
$$+\frac{C\kappa^2}{(\nu_1+H_1)}\Delta t\|\nabla e_2^n\|^2\|\nabla(\frac{\eta_1^{n+1}-\eta_1^n}{\Delta t})\|^2$$
$$+\frac{C\kappa^2}{(\nu_1+H_1)}\Delta t\|\nabla e_1^n\|^2\|[\nabla(\frac{\eta_1^n-\eta_1^{n-1}}{\Delta t})]\|^2$$

$$
\begin{aligned}
&+\frac{C\kappa^2}{(\nu_1+H_1)^2}\Delta t\|e_1^n\|\|\nabla e_1^n\|\|\nabla s_1^n\|^2(\nu_1+H_1)\\
&+\frac{C\kappa^2}{(\nu_1+H_1)^2}\Delta t\|e_2^n\|\|\nabla e_2^n\|\|\nabla s_1^n\|^2(\nu_1+H_1)\\
&+\frac{C\kappa^2}{(\nu_1+H_1)^2}\Delta t\|e_2^n\|\|\nabla e_2^n\|\|\nabla s_2^n\|^2(\nu_1+H_1)+\frac{C_{\nabla u_t}^2\kappa^2}{(\nu_1+H_1)}\Delta t\|\nabla e_2^n\|^2\\
&+\frac{C\kappa^2}{(\nu_1+H_1)^2}\Delta t\|e_2^{n-1}\|\|\nabla e_2^{n-1}\|\|\nabla s_1^n\|^2(\nu_1+H_1)\\
&+\frac{C\kappa^2}{(\nu_1+H_1)^2}\Delta t\|e_2^{n-1}\|\|\nabla e_2^{n-1}\|\|\nabla s_2^n\|^2(\nu_1+H_1)+\frac{C_{\nabla u_t}^2\kappa^2}{(\nu_1+H_1)}\Delta t\|\nabla e_2^{n-1}\|^2\\
&+\frac{C_{\nabla u_{2t}}^2\kappa^2}{4\epsilon(\nu_1+H_1)}\Delta t\Delta t^2\|\nabla s_1^n\|^2+\frac{C_{\nabla u_{2t}}^2\kappa^2}{4\epsilon(\nu_1+H_1)}\Delta t\Delta t^2\|\nabla s_2^n\|^2\\
&+\frac{C_{\nabla u_{2t}}^2\kappa^2}{4\epsilon(\nu_1+H_1)}\Delta t\Delta t^2\|\nabla(\frac{[\eta^n-\eta^{n-1}]}{\Delta t})\|^2+\frac{C_{\nabla u_{2t}}^2\kappa^2}{4\epsilon(\nu_1+H_1)}\Delta t\Delta t^2C_{\nabla u_t}^2\\
&+C\Delta t\Delta t^2\|\nabla(\frac{[\eta^n-\eta^{n-1}]}{\Delta t})\|^4+\frac{C}{(\nu_1+H_1)}\Delta t\|\phi_1^n\|\|\nabla\phi_1^n\|\|\nabla s_1^n\|^2\\
&+\frac{C}{\nu_1+H_1}\Delta t\|\nabla\phi_1^n\|^2+\frac{C}{\epsilon(\nu_1+H_1)}\Delta t^2\Delta t\|\nabla[s^n]\|^4\\
&+\frac{C\kappa}{\epsilon(\nu_1+H_1)}\Delta t\|\nabla[s^n]\|^2\|\nabla[\eta^n]\|^2
\end{aligned}
$$

Summing over the time levels, multiplying both sides by 2, letting appropriate ϵ and using the modified Gronwall's lemma gives

$$\|s_1^{n+1}\|^2+(\nu_1+H_1)\Delta t\sum_{j=1}^{n}\|\nabla s_1^{n+1}\|^2\le C\left(\|s_1^2\|^2+O(h^{2m}+(\Delta t)^2+H^2)\right)$$

In order to be able to finish the proof using the discrete Gronwall's lemma, we will need the following bound

$$\|s_i^2\|^2+\Delta t\|\nabla s_i^1\|^2+\Delta t\|\nabla s_i^2\|^2\le C(h^2+(\Delta t)^2)$$

Notice that the method requires two initial conditions, so that we are given $\hat{u}_i^0$ and $\hat{u}_i^1$, $i=1,2$. Then we can take $\tilde{u_i}^0$ and $\tilde{u_i}^1$ to be the L^2 projections of $\hat{u}_i^0$

and $\hat{u}_i^1$, respectively, onto X^h. The details of the calculations are shown in [23]; one should notice that here lies the necessity for the Assumption 2.2.2. In the end, we obtain

$$\|s_1^2\|^2 + (\nu_1 + H_1)\Delta t\|\nabla s_1^2\|^2 \leq C(\Delta t^2 + h^{2m-2}).$$

For $2 \leq m$, we get

$$\|s_1^2\|^2 + (\nu_1 + H_1)\Delta t\|\nabla s_1^2\|^2 \leq C(\Delta t^2 + h^2).$$

Terms in domain 2 are treated in exactly the same way. After adding the inequalities for domains 1 and 2 , use the discrete Gronwall's lemma and the triangle inequality, we obtain for $e_j^i = u_j^i - \hat{u}_j^i$ $(j = 1, 2)$:

$$\|\frac{\mathbf{e}^{n+1} - \mathbf{e}^n}{\Delta t}\|^2 + (\nu_1 + H_1)\Delta t \sum_{j=1}^{n} \|\nabla \left(\frac{e_1^{j+1} - e_1^j}{\Delta t} \right)\|^2$$

$$+(\nu_2 + H_2)\Delta t \sum_{j=1}^{n} \|\nabla \left(\frac{e_2^{j+1} - e_2^j}{\Delta t} \right)\|^2 \leq C\left(h^2 + (\Delta t)^2 + H_1^2 + H_2^2\right). \blacksquare$$

□

We now proceed to show the stability and increased accuracy of the correction step approximation cu. The left hand sides of the equations satisfied by u and cu are the same, so parts of the proofs of stability and accuracy of the defect step approximation can be reused here.

Theorem 2.3.4 (Stability of Correction Step of DDC)**.** *Let* $\tilde{\mathbf{u}}^{\mathbf{n+1}} \in \mathbf{X^h}$ *satisfy (2.2.15) for each* $n \in \left\{0, 1, 2, \cdots, \frac{T}{\Delta t} - 1\right\}$*. Then* $\exists C > 0$ *independent of* h, Δt *such that* $\tilde{\mathbf{u}}^{n+1}$ *satisfies:*

$$\left\|\tilde{u}_1^{n+1}\right\|^2+\left\|\tilde{u}_2^{n+1}\right\|^2+(\nu_1+H_1)\Delta t\sum_{k=1}^{n+1}\left\|\nabla\tilde{u}_1^k\right\|^2+(\nu_1+H_2)\Delta t\sum_{k=1}^{n+1}\left\|\nabla\tilde{u}_2^k\right\|^2$$
$$+\kappa\,\Delta t\int_I\left|\tilde{u}_1^{n+1}|[\tilde{\mathbf{u}}^n]|^{1/2}-\tilde{u}_2^n|[\tilde{\mathbf{u}}^{n-1}]|^{1/2}\right|^2ds$$
$$+\kappa\,\Delta t\int_I\left|\tilde{u}_2^{n+1}|[\tilde{\mathbf{u}}^n]|^{1/2}-\tilde{u}_1^n|[\tilde{\mathbf{u}}^{n-1}]|^{1/2}\right|^2ds$$
$$\leq\frac{C\Delta t}{\nu_1+H_1}\sum_{j=1}^{n}\Bigg[\|\nabla e_1^{j+1}\|^2+\|e_2^j\|\|\nabla e_2^j\|\|\nabla e_i^j\|^2$$
$$+\|\nabla e_i^{j+1}\|^2+\|e_1^{j+1}\|\|\nabla e_1^{j+1}\|\|\nabla e_i^j\|^2+\|e_1^j\|\|\nabla e_1^j\|\|\nabla e_i^j\|^2+\|\nabla e_2^j\|^2\Bigg]$$
$$+\frac{\Delta t}{14(\nu_1+H_1)}\sum_{j=1}^{n}(\|\nabla e_2^j\|^2+\|e_2^j\|\|\nabla e_2^j\|\|\nabla e_i^j\|^2)$$
$$+\frac{8\Delta t(\nu_1+H_1)}{19}\sum_{j=1}^{n}\left\{\Delta t^2\|\nabla(\frac{e_1^{j+1}-e_1^j}{\Delta t})\|^2+\Delta t^2C^2_{\nabla\hat{u}_t})\right\}$$
$$+\frac{8\Delta t(\nu_1+H_1)}{19}\sum_{j=1}^{n}\Bigg[\Delta t\|\nabla\hat{u}_1^{j+1}\|^2\Delta t\|\nabla(\frac{e_1^{j+1}-e_1^j}{\Delta t})\|^2$$
$$+\Delta t\|\nabla\hat{u}_1^{j+1}\|^2\Delta tC^2_{\nabla\hat{u}_{1t}}+\Delta t\|\nabla\hat{u}_1^j\|^2\Delta t\|\nabla(\frac{e_1^{j+1}-e_1^j}{\Delta t})\|^2$$
$$+\Delta t\|\nabla\hat{u}_1^j\|^2\Delta tC^2_{\nabla\hat{u}_{1t}}\Bigg]$$
$$+\frac{19\Delta t}{(\nu_1+H_1)}\sum_{j=1}^{n}\left[H_1^2\|\nabla\hat{u}_1^{j+1}\|^2+\|\frac{f_1^{j+1}+f_1^j}{2}\|^2_{-1}\right]$$
$$+\frac{\Delta tC_{\nabla u^{n+1}}}{\nu_1+H_1}\sum_{j=1}^{n}\left[1+\kappa\|\nabla e_i^{j+1}\|^2\right]$$
$$+\Delta tC\sum_{j=1}^{n}(\|e_1^{j+1}\|^{1/2}\|\nabla e_1^{j+1}\|^{1/2}+\|e_2^{j+1}\|^{1/2}\|\nabla e_2^{j+1}\|^{1/2})\|\nabla e_i^{j+1}\|^2 \quad (2.3.19)$$

Proof. Choosing $v_1=\tilde{u}_1^{n+1}$ in (2.2.15) gives

$$\left(\frac{\tilde{u}_1^{n+1}-\tilde{u}_1^n}{\Delta t},\tilde{u}_1^{n+1}\right)+(\nu_1+H_1)\left(\nabla\tilde{u}_1^{n+1},\nabla\tilde{u}_1^{n+1}\right)$$
$$-\kappa\int_I\tilde{u}_2^n|[\tilde{u}^n]|^{1/2}|[\tilde{u}^{n-1}]|^{1/2}\tilde{u}_1^{n+1}ds-(\tilde{p}_1^{n+1},\nabla\cdot\tilde{u}_1^{n+1})$$
$$+\kappa\int_I|[\tilde{u}^n]|\tilde{u}_1^{n+1}\tilde{u}_1^{n+1}ds+c_1\left(\tilde{u}_1^{n+1};\tilde{u}_1^{n+1},\tilde{u}_1^{n+1}\right)=\left(\frac{f_1^{n+1}+f_1^n}{2},\tilde{u}_1^{n+1}\right)$$
$$+\frac{\Delta t(\nu_1+H_1)}{2}\left(\nabla(\frac{\hat{u}_1^{n+1}-\hat{u}_1^n}{\Delta t}),\nabla\tilde{u}_1^{n+1}\right)-\frac{1}{2}c_1(\hat{u}_1^n;\hat{u}_1^n,\tilde{u}_1^{n+1})$$
$$+\frac{\kappa}{2}\Delta t\int_I|[\hat{u}^n]|(\frac{\hat{u}_1^{n+1}-\hat{u}_1^n}{\Delta t})\tilde{u}_1^{n+1}ds-\frac{\kappa}{2}\Delta t\int_I\hat{u}_1^{n+1}(\frac{|[\hat{u}^{n+1}]|-|[\hat{u}^n]|}{\Delta t})\tilde{u}_1^{n+1}ds$$
$$+H_1\left(\nabla(\frac{\hat{u}_1^{n+1}+\hat{u}_1^n}{2}),\nabla\tilde{u}_1^{n+1}\right)+\frac{1}{2}c_1(\hat{u}_1^{n+1};\hat{u}_1^{n+1},\tilde{u}_1^{n+1})$$
$$-\kappa\int_I\hat{u}_2^n|[\hat{u}^n]|^{1/2}|[\hat{u}^{n-1}]|^{1/2}\tilde{u}_1^{n+1}ds+\frac{\kappa}{2}\int_I|[\hat{u}^{n+1}]|\hat{u}_2^{n+1}\tilde{u}_1^{n+1}ds$$
$$+\frac{\kappa}{2}\int_I|[\hat{u}^n]|\hat{u}_2^n\tilde{u}_1^{n+1}ds-\left(\frac{\hat{p}_1^{n+1}-\hat{p}_1^n}{2},\nabla\cdot\tilde{u}_1^{n+1}\right),\ \forall v_1\in X_{1,h}.\quad(2.3.20)$$

We will be applying the Cauchy-Schwarz inequality and Young's inequality to subsume all the $\hat{u}_1$-terms, leading to the telescoping series in the left hand side of (2.3.20) - in exactly the same way the stability of the defect step was proven in [21].

The nonlinear terms in the right hand side are treated as follows.

$$\frac{1}{2}c_1(\hat{u}_1^{n+1};\hat{u}_1^{n+1},\tilde{u}_1^{n+1})-\frac{1}{2}c_1(\hat{u}_1^n;\hat{u}_1^n,\tilde{u}_1^{n+1})$$
$$=\frac{1}{2}c_1(\hat{u}_1^{n+1};\hat{u}_1^{n+1},\tilde{u}_1^{n+1})-\frac{1}{2}c_1(\hat{u}_1^n;\hat{u}_1^n,\tilde{u}_1^{n+1})$$
$$+\frac{1}{2}c_1(\hat{u}_1^{n+1};\hat{u}_1^n,\tilde{u}_1^{n+1})-\frac{1}{2}c_1(\hat{u}_1^{n+1};\hat{u}_1^n,\tilde{u}_1^{n+1})$$
$$=\frac{\Delta t}{2}c_1(\hat{u}_1^{n+1};\frac{\hat{u}_1^{n+1}-\hat{u}_1^n}{\Delta t},\tilde{u}_1^{n+1})+\frac{\Delta t}{2}c_1(\frac{\hat{u}_1^{n+1}-\hat{u}_1^n}{\Delta t};\hat{u}_1^n,\tilde{u}_1^{n+1})$$
$$=A+B$$

$$A \leq \frac{\Delta t}{2}\|\nabla \hat{u}_1^{n+1}\| \left\|\nabla\left(\frac{\hat{u}_1^{n+1}-\hat{u}_1^n}{\Delta t}\right)\right\| \|\nabla \tilde{u}_1^{n+1}\|$$

$$\leq \epsilon(\nu_1+H_1)\|\nabla \tilde{u}_1^{n+1}\|^2 + \frac{\Delta t^2}{16\epsilon(\nu_1+H_1)}\|\nabla \hat{u}_1^{n+1}\|^2 \left\|\nabla\left(\frac{\hat{u}_1^{n+1}-\hat{u}_1^n}{\Delta t}\right)\right\|^2$$

$$\leq \epsilon(\nu_1+H_1)\|\nabla \tilde{u}_1^{n+1}\|^2 + \frac{2\Delta t}{16\epsilon(\nu_1+H_1)}\|\nabla \hat{u}_1^{n+1}\|^2 \Delta t \left\|\nabla\left(\frac{e_1^{n+1}-e_1^n}{\Delta t}\right)\right\|^2$$

$$+\frac{2\Delta t}{16\epsilon(\nu_1+H_1)}\|\nabla \hat{u}_1^{n+1}\|^2 \Delta t C^2_{\nabla \hat{u}_{1t}}$$

Similarly,

$$B \leq \epsilon(\nu_1+H_1)\|\nabla \tilde{u}_1^{n+1}\|^2 + \frac{2\Delta t}{16\epsilon(\nu_1+H_1)}\|\nabla \hat{u}_1^{n}\|^2 \Delta t \left\|\nabla\left(\frac{e_1^{n+1}-e_1^n}{\Delta t}\right)\right\|^2$$

$$+ \frac{2\Delta t}{16\epsilon(\nu_1+H_1)}\|\nabla \hat{u}_1^{n+1}\|^2 \Delta t C^2_{\nabla \hat{u}_{1t}}.$$

Note that $\Delta t\|\nabla \hat{u}_1^n\|^2 \leq \Delta t \sum_{i=1}^n \|\nabla \hat{u}_1^i\|^2$ and the stability bound for the defect step approximation can be utilized. The two interface terms on the left hand side of (2.3.20) are treated in the same way as in the stability proof in [21] .

Replacing $\hat{u}_i$ with $u_i - e_i$ leads to

$$\frac{\kappa}{2}\int_I |[\hat{u}^{n+1}]|(\hat{u}_2^{n+1}-\hat{u}_1^{n+1})\tilde{u}_1^{n+1}ds$$

$$= \frac{\kappa}{2}\int_I |[\hat{u}^{n+1}]|(u_2^{n+1}-u_1^{n+1})\tilde{u}_1^{n+1}ds - \frac{\kappa}{2}\int_I |[\hat{u}^{n+1}]|(e_2^{n+1}-e_1^{n+1})\tilde{u}_1^{n+1}ds$$

Repeating this replacement and applying the Cauchy-Schwarz and Young's in-

equalities, we obtain

$$\begin{aligned}
&\frac{\kappa}{2}\int_I |[\hat{u}^{n+1}]|(\hat{u}_2^{n+1}-\hat{u}_1^{n+1})\tilde{u}_1^{n+1}ds \\
&\leq \frac{\kappa C_{\nabla u^{n+1}}}{2(\nu_1+H_1)}+\frac{3\epsilon(\nu_1+H_1)}{2}\|\nabla\tilde{u}_1^{n+1}\|^2+\frac{C}{(\nu_1+H_1)}(\|\nabla e_1^{n+1}\|^2+\|\nabla e_2^{n+1}\|^2) \\
&\qquad \frac{\kappa C_{\nabla u^{n+1}}}{2(\nu_1+H_1)}(\|\nabla e_1^{n+1}\|^2+\|\nabla e_2^{n+1}\|^2)+\frac{\epsilon(\nu_1+H_1)}{2}\|\nabla\tilde{u}_1^{n+1}\|^2 \\
&\quad + C(\|e_1^{n+1}\|^{1/2}\|\nabla e_1^{n+1}\|^{1/2}+\|e_2^{n+1}\|^{1/2}\|\nabla e_2^{n+1}\|^{1/2})(\|\nabla e_1^{n+1}\|^2+\|\nabla e_2^{n+1}\|^2)
\end{aligned}$$

Next, we bound the interface term $W=\kappa\int_I \hat{u}_1^{n+1}|[\hat{u}^n]|\tilde{u}_1^{n+1}ds$.

$$W=\kappa\int_I u_1^{n+1}|[\hat{u}^n]|\tilde{u}_1^{n+1}ds-\kappa\int_I e_1^{n+1}|[\hat{u}^n]|\tilde{u}_1^{n+1}ds$$

Since $|a-b|\leq|a|+|b|$, $\|\nabla[\hat{u}^n]\|\leq\|\nabla\hat{u}_1^n\|+\|\nabla\hat{u}_2^n\|$. Thus,

$$\begin{aligned}
W\leq{}& \frac{C_{\nabla u^{n+1}}}{(\nu_1+H_1)}(\|\nabla\hat{u}_1^n\|^2+\|\nabla\hat{u}_2^n\|^2)+\epsilon(\nu_1+H_1)\|\nabla\tilde{u}_1^{n+1}\|^2 \\
&+C\|e_1^{n+1}\|^{1/2}\|\nabla e_1^{n+1}\|^{1/2}\|\nabla e_1^n\|\|\nabla\tilde{u}_1^{n+1}\| \\
&+C\|e_1^{n+1}\|^{1/2}\|\nabla e_1^{n+1}\|^{1/2}\|\nabla e_2^n\|\|\nabla\tilde{u}_1^{n+1}\| \\
&+C\|e_1^{n+1}\|^{1/2}\|\nabla e_1^{n+1}\|^{1/2}\|\nabla[u]^n\|\|\nabla\tilde{u}_1^{n+1}\|
\end{aligned} \tag{2.3.21}$$

The last three summands in the right hand side of (2.3.21) are bounded by

$$\begin{aligned}
&C\|e_1^{n+1}\|^{1/2}\|\nabla e_1^{n+1}\|^{1/2}\|\nabla[u]^n\|\|\nabla\tilde{u}_1^{n+1}\| \\
&\qquad\qquad \leq \frac{C}{(\nu_1+H_1)}\|\nabla e_1^{n+1}\|^2+\epsilon(\nu_1+H_1)\|\nabla\tilde{u}_1^{n+1}\|^2,
\end{aligned}$$

and

$$C\|e_1^{n+1}\|^{1/2}\|\nabla e_1^{n+1}\|^{1/2}\|\nabla e_1^n\|\|\nabla \tilde{u}_1^{n+1}\| \tag{2.3.22}$$

$$+C\|e_1^{n+1}\|^{1/2}\|\nabla e_1^{n+1}\|^{1/2}\|\nabla e_2^n\|\|\nabla \tilde{u}_1^{n+1}\|$$

$$\leq 2\epsilon(\nu_1+H_1)\|\nabla \tilde{u}_1^{n+1}\|^2$$

$$+\frac{C}{(\nu_1+H_1)}\|e_1^{n+1}\|\|\nabla e_1^{n+1}\|(\|\nabla e_1^n\|^2+\|\nabla e_2^n\|^2).$$

In order to bound the last summand in the right hand side of (2.3.22), choose one of the two options below, depending on the relationship between the mesh diameter and the time step. Both of these upper bounds are of the required order of smallness.

$$\begin{cases} \frac{C}{(\nu_1+H_1)}\frac{1}{h}(h^2+\Delta t^2)(\|\nabla e_1^n\|^2+\|\nabla e_2^n\|^2) & \text{if } \Delta t < h \\ \frac{C}{(\nu_1+H_1)}[\Delta t(\|\nabla e_1^n\|^4+\|\nabla e_2^n\|^4)+\Delta t\|\nabla e_1^{n+1}\|^2] & \text{if } h < \Delta t \end{cases}$$

The terms $\frac{\kappa}{2}\int_I \hat{u}_1^n|[\hat{u}^n]|\tilde{u}_1^{n+1}ds$ and $\kappa\int_I \hat{u}_2^n|[\hat{u}^n]|\tilde{u}_1^{n+1}ds$ are bounded in the same way as the term W.

Since $|[\hat{u}^n]|^{1/2}|[\hat{u}^{n-1}]|^{1/2} \leq \frac{|[\hat{u}^n]|+|[\hat{u}^{n-1}]|}{2}$, we get

$$\kappa\int_I |\hat{u}_2^n||[\hat{u}^n]|^{1/2}|[\hat{u}^{n-1}]|^{1/2}|\tilde{u}_1^{n+1}|ds$$

$$= \frac{\kappa}{2}\int_I |\hat{u}_2^n||[\hat{u}^n]||\tilde{u}_1^{n+1}|ds + \frac{\kappa}{2}\int_I |\hat{u}_2^n||[\hat{u}^{n-1}]||\tilde{u}_1^{n+1}|ds$$

$$= I + II$$

Both the I and II terms are bounded similar to the bound on W. Terms in domain 2 are treated in exactly the same way and then the inequalities for domains 1 and 2 are added together. Finally, choosing $\epsilon = \frac{1}{38}$ allow us to subsume

the $\nabla\tilde{u}_i$-terms in the LHS. Multiplying through by $2\Delta t$ and summing over the time levels gives us the desired result. ■ □

We now have all the intermediate results that are needed for proving the accuracy of the correction step solution $\tilde{\mathbf{u}}$.

Theorem 2.3.5. *(Accuracy of Correction Step) Let the assumptions of Theorems 2.3.2 and* 2.3.3 *be satisfied. Then* $\exists C > 0$ *independent of* h, Δt *such that for any* $n \in \{0, 1, 2, \cdots, M-1 = \frac{T}{\Delta t} - 1\}$, *the solution* $\tilde{u}_i^{n+1}$ *of (2.2.15) satisfies*

$$\begin{aligned} \|\mathbf{u}^{n+1} - \tilde{\mathbf{u}}^{n+1}\|^2 + (\nu + H_1)\Delta t \sum_{j=1}^{n+1} \|\nabla(u_1^j - \tilde{u}_1^j)\|^2 \\ + (\nu + H_2)\Delta t \sum_{j=1}^{n+1} \|\nabla(u_2^j - \tilde{u}_2^j)\|^2 \\ \leq C\left(h^4 + h^2\Delta t^2 + H_1^4 + H_1^2\Delta t^2 + H_2^4 + H_2^2\Delta t^2 + (\Delta t)^4\right) \end{aligned} \tag{2.3.23}$$

Proof. First, sum (2.3.5) at time levels t_n and t_{n+1} and divide by 2, to obtain in Ω_1:

$$\left(\frac{u_1^{n+1}-u_1^n}{\Delta t},v_1\right)+(\nu_1+H_1)(\nabla(\frac{u_1^{n+1}+u_1^n}{2}),\nabla v_1)+\frac{1}{2}c_1(u_1^{n+1};u_1^{n+1},v_1)$$
$$+\frac{1}{2}c_1(u_1^n;u_1^n,v_1)-\left(\frac{p_1^{n+1}+p_1^n}{2},\nabla\cdot v_1\right)+\frac{\kappa}{2}\int_I|[u^{n+1}]|(u_1^{n+1}-u_2^{n+1})v_1ds$$
$$+\frac{\kappa}{2}\int_I|[u^n]|(u_1^n-u_2^n)v_1ds=\left(\frac{f_1^{n+1}+f_1^n}{2},v_1\right)$$
$$+H_1\left(\nabla\left(\frac{u_1^{n+1}+u_1^n}{2}\right),\nabla v_1\right)-\left(\frac{u_{1,t}^{n+1}+u_{1,t}^n}{2},v_1\right)+\left(\frac{u_1^{n+1}-u_1^n}{\Delta t},v_1\right) \tag{2.3.24}$$

For the $O(\Delta t^2)$-term introduce the notation $\frac{u_i^{n+1}-u_i^n}{\Delta t}-\frac{u_{i,t}^{n+1}+u_{i,t}^n}{2}\equiv\gamma_i^{n+1}$. Subtract the correction step equation (2.2.15) from (2.3.24). Denoting $ce_i^{n+1}=u_i(t_{n+1})-\tilde{u}_i^{n+1}, i=1,2$, we obtain

$$\left(\frac{ce_1^{n+1}-ce_1^n}{\Delta t},v_1\right)+(\nu_1+H_1)(\nabla ce_1^{n+1},\nabla v_1)+c_1(u_1^{n+1};u_1^{n+1},v_1)$$
$$-\frac{1}{2}c_1(u_1^{n+1};u_1^{n+1},v_1)-c_1(\tilde{u}_1^{n+1};\tilde{u}_1^{n+1},v_1)+\frac{1}{2}c_1(u_1^n;u_1^n,v_1)$$
$$+\frac{1}{2}c_1(\hat{u}_1^{n+1};\hat{u}_1^{n+1},v_1)-\frac{1}{2}c_1(\hat{u}_1^n;\hat{u}_1^n,v_1)$$
$$-\left(p_1^{n+1}-\tilde{p}_1^{n+1},\nabla\cdot v_1\right)+\frac{\kappa}{2}\int_I(u_1^{n+1}-u_2^{n+1})|[u^{n+1}]|v_1ds$$
$$-\kappa\int_I\tilde{u}_1^{n+1}|[\tilde{u}^n]|v_1ds+\kappa\int_I\tilde{u}_2^n|[\tilde{u}^n]|^{1/2}|[\tilde{u}^{n-1}]|^{1/2}v_1ds$$
$$+\frac{\kappa}{2}\int_I(u_1^n-u_2^n)|[u^n]|v_1ds=\frac{\Delta t(\nu_1+H_1)}{2}\left(\nabla(\frac{e_1^{n+1}-e_1^n}{\Delta t}),\nabla v_1\right)$$
$$+\frac{H_1\Delta t}{2}\left(\nabla(\frac{u_1^{n+1}-u_1^n}{\Delta t}),\nabla v_1\right)+H_1(\nabla e_1^{n+1},\nabla v_1)+(\gamma_1^{n+1},v_1)$$
$$+\frac{\Delta t}{2}\left(\frac{p_1^{n+1}-p_1^n}{\Delta t}-\frac{\hat{p}_1^{n+1}-\hat{p}_1^n}{\Delta t},\nabla\cdot v_1\right)$$
$$+\kappa\int_I\hat{u}_2^n|[\hat{u}^n]|^{1/2}|[\hat{u}^{n-1}]|^{1/2}v_1ds-\kappa\int_I\hat{u}_1^{n+1}|[\hat{u}^n]|v_1ds+\frac{\kappa}{2}\int_I\hat{u}_1^{n+1}|[\hat{u}^{n+1}]|v_1ds$$
$$+\frac{\kappa}{2}\int_I\hat{u}_1^n|[\hat{u}^n]|v_1ds-\frac{\kappa}{2}\int_I\hat{u}_2^{n+1}|[\hat{u}^{n+1}]|v_1ds-\frac{\kappa}{2}\int_I\hat{u}_2^n|[\hat{u}^n]|v_1ds \quad (2.3.25)$$

Similarly to the error decomposition in the case of the defect approximation, decompose $ce_1^{n+1}=u_1^{n+1}-\tilde{u}_1^{n+1}=\phi_1^{n+1}-\eta_1^{n+1},\phi_1\in X_{1,h}$. We now choose $v_1=\phi_1^{n+1}\in X_{1,h}$ in (2.3.25).

Notice that after applying the Cauchy-Schwarz and Young's inequalities, the first five terms in the right hand side will provide the expected second order of smallness, $O(\Delta t(h+H_1+\Delta t))$. This follows from the results of Theorems 2.3.2 and 2.3.3.

We now briefly introduce the approach to treating the twelve interface terms of (2.3.25). After the proper pairing, the proof follows similarly to the treatment of the interface terms in Theorem 2.3.3.

Combine $-\frac{\kappa}{2}\int_I u_1^{n+1}|[u^{n+1}]|\phi_1^{n+1}ds$ and $-\frac{\kappa}{2}\int_I u_1^{n}|[u^{n}]|\phi_1^{n+1}ds$ with half of $\kappa\int_I \tilde{u}_1^{n+1}|[\tilde{u}^{n}]|\phi_1^{n+1}ds$ term for each.

Similarly, pair $\frac{\kappa}{2}\int_I u_2^{n+1}|[u^{n+1}]|\phi_1^{n+1}ds$ and $\frac{\kappa}{2}\int_I u_2^{n}|[u^{n}]|\phi_1^{n+1}ds$ with half of $-\kappa\int_I \tilde{u}_2^{n}|[\tilde{u}^{n}]|^{1/2}|[\tilde{u}^{n-1}]|^{1/2}\phi_1^{n+1}ds$ term for each.

Also, add and subtract $I \equiv \kappa\int_I[u^{n+1}]|[u^{n+1}]|\phi_1^{n+1}ds$ from the rest of the interface terms.

Pair up I with $-\kappa\int_I \hat{u}_1^{n+1}|[\hat{u}^{n}]|\phi_1^{n+1}ds$ and $\kappa\int_I \hat{u}_2^{n}|[\hat{u}^{n}]|^{1/2}|[\hat{u}^{n-1}]|^{1/2}\phi_1^{n+1}ds$. Combine $-I$ with the remainder of the interface terms. Then follow the proof of Theorem 2.3.3 to obtain the corresponding bounds.

The nonlinear terms are treated as follows.

$$
\begin{aligned}
&c_1(u_1^{n+1};u_1^{n+1},\phi_1^{n+1}) - c_1(\tilde{u}_1^{n+1};\tilde{u}_1^{n+1},\phi_1^{n+1}) - \frac{1}{2}c_1(u_1^{n+1};u_1^{n+1},\phi_1^{n+1})\\
&\quad+\frac{1}{2}c_1(\hat{u}_1^{n+1};\hat{u}_1^{n+1},\phi_1^{n+1}) + \frac{1}{2}c_1(u_1^{n};u_1^{n},\phi_1^{n+1}) - \frac{1}{2}c_1(\hat{u}_1^{n};\hat{u}_1^{n},\phi_1^{n+1})\\
&= c_1(u_1^{n+1};ce_1^{n+1},\phi_1^{n+1}) + c_1(ce_1^{n+1};\tilde{u}_1^{n+1},\phi_1^{n+1}) - \frac{1}{2}c_1(u_1^{n+1};e_1^{n+1},\phi_1^{n+1})\\
&\quad-\frac{1}{2}c_1(e_1^{n+1};\hat{u}_1^{n+1},\phi_1^{n+1}) + \frac{1}{2}c_1(u_1^{n};e_1^{n},\phi_1^{n+1}) + \frac{1}{2}c_1(e_1^{n};\hat{u}_1^{n},\phi_1^{n+1})
\end{aligned}
$$

Adding and subtracting more nonlinear terms and writing $ce_1^{n+1} = \eta_1^{n+1} - \phi_1^{n+1}$ we get

$$
\begin{aligned}
&-c_1(u_1^{n+1};\phi_1^{n+1},\phi_1^{n+1}) + c_1(u_1^{n+1};\eta_1^{n+1},\phi_1^{n+1}) - c_1(\phi_1^{n+1};\tilde{u}_1^{n+1},\phi_1^{n+1})\\
&\quad+c_1(\eta_1^{n+1};\tilde{u}_1^{n+1},\phi_1^{n+1}) + \frac{\Delta t}{2}c_1(\frac{u_1^{n+1}-u_1^{n}}{\Delta t};e_1^{n},\phi_1^{n+1})\\
&+\frac{\Delta t}{2}c_1(u_1^{n+1};\frac{e_1^{n+1}-e_1^{n}}{\Delta t},\phi_1^{n+1}) + \frac{\Delta t}{2}c_1(e_1^{n+1};\frac{u_1^{n+1}-u_1^{n}}{\Delta t},\phi_1^{n+1})\\
&-\frac{\Delta t}{2}c_1(e_1^{n+1};\frac{e_1^{n+1}-e_1^{n}}{\Delta t},\phi_1^{n+1}) + \frac{\Delta t}{2}c_1(\frac{e_1^{n+1}-e_1^{n}}{\Delta t};\hat{u}_1^{n},\phi_1^{n+1}).
\end{aligned}
$$

The first of these terms is identically zero; the third term is treated by using the sharper bound (2.2.11) and then it is subsumed using the Gronwall's lemma. The remainder of the nonlinear terms provide the necessary second order of smallness. Terms in domain 2 are treated in exactly the same way. Finally, summing over $i = 1, 2$ and using the Gronwall's lemma completes the proof. ■ □

2.4 Computational Testing

We use a manufactured solution test to illustrate the theoretical findings of this chapter. An exact solution in the domain $\Omega = \Omega_1 \cup \Omega_2$ with $\Omega_1 = [0,1] \times [0,1]$ and $\Omega_2 = [0,1] \times [0,-1]$ is given by

$$
\begin{aligned}
u_{1,1} &= a\nu_1 e^{-t} x^2 (1-x)^2 (1+y) + a e^{-t/2} x(1-x)\nu_1/\sqrt{\kappa a} \\
u_{1,2} &= a\nu_1 e^{-t} xy(2+y)(1-x)(2x-1) + a e^{-t/2} y(2x-1)\nu_1/\sqrt{\kappa a} \\
u_{2,1} &= a\nu_1 e^{-t} x^2 (1-x)^2 (1+\frac{\nu_1}{\nu_2} y) \\
u_{2,2} &= a\nu_1 e^{-t} xy(1-x)(2x-1)(2+\frac{\nu_1}{\nu_2} y),
\end{aligned}
$$

where $u_{i,j} : \Omega_i \to R, \forall i, j = 1, 2$. Parameters are chosen as follows: $a = 1$, $\nu_1 = 0.5$, $\nu_2 = 0.1$, $\kappa = 1$ and the final time $T = 1$. The solution has a vortex region in the lower subdomain.

Pressures in both domains are set to zero (for simplicity only, not a requirement), and the right hand side forcing terms, initial and boundary values are calculated accordingly. For simplicity, we have used the true solution for two initial values. Instead, one could use one step of the Geometric Averaging Method as a starting method to find the second initial value. In order to compute the

convergence rates easily, we have chosen the mesh size(h), time step(Δt), and both artificial viscosities (H_i) equal to $1/N$, where N is the number of mesh points on per unit line segment. Taylor-Hood elements, piecewise quadratic polynomials for the velocity and piecewise linear polynomials for the pressure, have been used in these computations.

As seen in Table (2.1) and Table (2.2), the convergence rates of the artificial viscosity (AV) approximation (2.2.14) in both the $||.||_{L^2(0,T;L^2(\Omega))}$ and $||.||_{L^2(0,T;H^1(\Omega))}$ norms are 1, whereas those of the correction step (CS) approximation (2.2.15) in both norms are 2. These results are consistent with the theory developed in this chapter. We note that the correct convergence rates require not just the improvement of the time accuracy, but also the reduction of artificial viscosity effects on the solution. In terms of qualitative assessment, consider Figure (2.1) and Figure (2.2). It can be clearly seen that the computed solution successfully captures all the structures of the true solution, including the vortex in the second domain. Beyond the theory, we note that the correction step improves the accuracy of the computed solution even for large values of the time step, mesh and viscosity values outside of the asymptotic regime. This is important for atmosphere-ocean applications, since discretization parameters for these simulations are not expected to lie in the asymptotic regime.

2.5 Summary and future work

A method was proposed to reduce time-consistency errors and artificial viscosity effects in computational simulations for a model of two coupled fluids. Our

N	$\|\| u - \hat{u} \|\|_{L^2(0,T;L^2(\Omega))}$	rate	$\|\| u - \hat{u} \|\|_{L^2(0,T;H^1(\Omega))}$	rate
2	1.4798e-002	-	7.3869e-002	-
4	9.4941e-003	0.64	6.8654e-002	0.10
8	5.5097e-003	0.78	4.9680e-002	0.46
16	2.9407e-003	0.90	2.9957e-002	0.72
32	1.5262e-003	0.94	1.5786e-002	0.92
64	7.9193e-004	0.94	7.7512e-003	1.02
128	4.0867e-004	0.95	3.7515e-003	1.04

Table 2.1: AV approximation $\hat{u}$.

N	$\|\| u - \tilde{u} \|\|_{L^2(0,T;L^2(\Omega))}$	rate	$\|\| u - \tilde{u} \|\|_{L^2(0,T;H^1(\Omega))}$	rate
2	1.0087e-002	-	6.0656e-002	-
4	5.1671e-003	0.96	4.2536e-002	0.51
8	2.3203e-003	1.15	2.3754e-002	0.84
16	8.7794e-004	1.40	1.0149e-002	1.22
32	2.8166e-004	1.64	3.3514e-003	1.60
64	8.1197e-005	1.79	9.2868e-004	1.85
128	2.2172e-005	1.87	2.3908e-004	1.96

Table 2.2: CS approximation $\tilde{u}$.

model was chosen to roughly represent the numerical viscosity (or diffusion) and flux coupling techniques used in many atmosphere-ocean interaction (AOI)

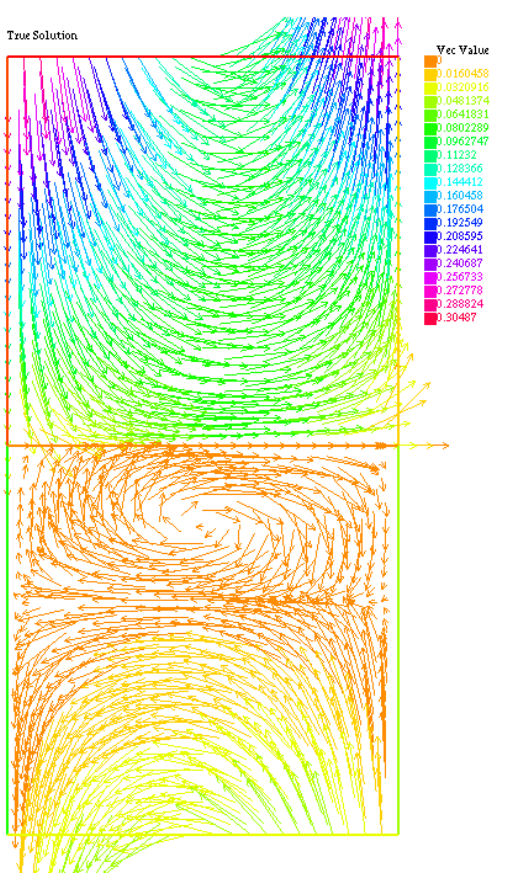

Figure 2.1: True Solution

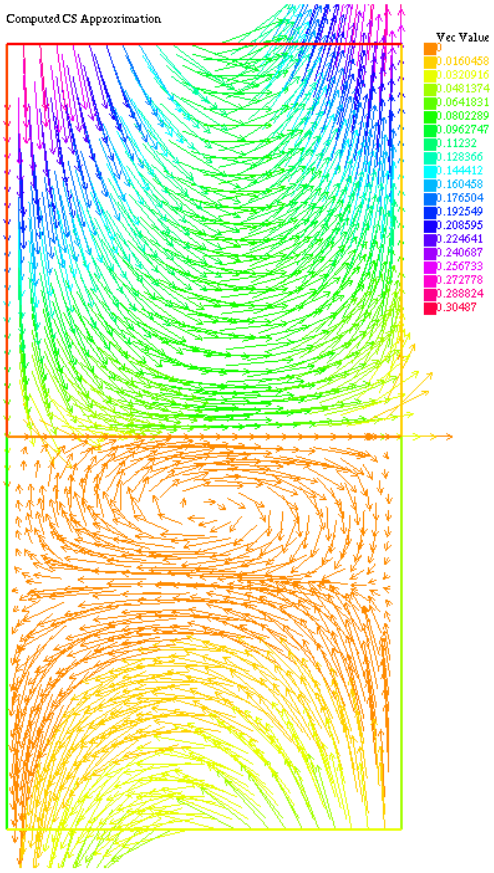

Figure 2.2: Computed Solution

simulations. The point of the simplified model has been to illustrate the general algorithmic approach, but also to provide a rigorous numerical analysis and testing to illustrate the theory, which would have been too cumbersome for the full physics and numerics of an application code. We believe that our analysis helps to begin filling in gaps in the literature; few examples of numerical analysis exist that seek to address the AOI coupling problem (see [30, 21, 32, 38, 46]).

The formal, global consistency in time was improved using deferred correction. The deferred correction approach allowed the lower-order numerics to be

employed for a predictor-type calculation, which was then modified to create a corrector step with a formal increase in the order of accuracy in time. This improvement applied to the global time stepping method, but in particular the coupling consistency was lifted to second order, which would typically be of first order in practice. Defect correction was applied to mitigate artificial viscosity effects, which we demonstrated could be implemented as a slight modification to the deferred correction step. We subsequently proved the unconditional stability and optimal convergence of the method, as well as the formal reduction of numerical viscosity effects.

A numerical example was provided to illustrate the theory. A manufactured solution was derived for the coupled fluid model, so that errors could be computed explicitly as time step and artificial viscosity parameters were varied. In this way, the predictions of the theory were demonstrated clearly. That is, the second-order convergence rate was verified as the time step was decreased, as well as the improved accuracy using defect correction to reduce the artificial viscosity effects. Beyond the theory, a significant improvement was observed for the largest values of time step and artificial viscosity parameters. This indicates the possibility of a benefit in application, where solutions are marginally resolved due to turbulent behavior and a wide range of scales.

In this chapter we have provided an initial step toward numerical improvements for AOI simulations, but some important issues remain to be considered in future work. One is the extension of the methodology to account for the existence of additional physics, more complex geometry and different numerical methods encountered in application codes. We have explained in Sections 2.1.1-

2.1.2 that the combined DDC approach may, in principle, be applied to a broad class of numerical methods. In this regard, the most important extension will be to consider smaller time steps in the "atmosphere" fluid regime and incorporate a more general class of flux coupling methods, such as in [33, 32]. This extension will illuminate another benefit of the DDC approach: improvement of time consistency within each fluid regime individually, not just for the coupling (as has been emphasized in this chapter).

Another issue for future study is that new algorithmic approaches for AOI are not practical unless they can be integrated into existing code structures. We believe the implementation would be reasonable, since one may leverage the existing code structure used for the base (predictor) step to a considerable degree for the corrector calculation. Roughly speaking, this is because the corrector step is equivalent to a second predictor step with additional source terms and an algebraic change in the flux calculations.

Finally, code efficiency must be addressed, but this cannot be determined until testing is performed using an application-level code. We have hope that the DDC approach would lead to an improvement in efficiency because of the significant improvement in accuracy observed in our test using parameter choices outside of the regime of asymptotic convergence. The cost of the DDC method is around 3 to 4 times that of the base method; to achieve the same accuracy with the base method alone (by decreasing the time step size, for example) may cost much more than a factor of 3 to 4. Furthermore, reducing artificial viscosity effects in current, coupled AOI simulations is not as simple as just reducing parameter values. The defect correction approach may provide an efficient way

to reduce these effects.

Chapter 3

Note On the Usage of Grad-Div Stabilization for the Penalty-Projection Algorithm in Magnetohydrodynamics

3.1 Introduction

Magnetically conducting fluids are ubiquitous in real-life applications from different areas, including astrophysics, geophysics, engineering, cooling of nuclear reactors, sea water propulsion, etc. When the fluid is electrically conducting, the flow is affected by Lorentz forces, leading to a coupled system of magnetohydrodynamics (MHD) equations for the velocity and magnetic fields. A large body of literature is dedicated to MHD flows, both from the experimental and

theoretical perspective - see, e.g., [57, 58, 59, 62, 61, 60].

The difficulties in resolving MHD flows are well documented: when common discretization techniques are used, the resulting linear systems often require prohibitively small time steps, otherwise demonstrating the unstable and non-physical behavior of the solutions. Similar difficulties exist for modeling non-conducting fluid flows via the Navier-Stokes equations. The family of splitting methods is one of the known techniques for resolving incompressible fluid flows in an efficient way. These methods originated in the sixties from the work of Chorin [50] and Temam [63], followed by Kim and Moin [54] and Brown *et al.* [49]. This approach is known as fractional step method, penalty-projection or pressure-correction method. The latter name was introduced to separate this idea from the alternative, known as the velocity-correction approach; see [47], page 323, for a short survey of these approaches.

Based on the idea of applying the penalty-projection technique to MHD flows, a method was presented in [48] (see Algorithm 3.2.1 below), that efficiently resolves MHD flows. The method is based on the stable decoupling procedure of [51], and it also utilizes the penalty-projection method (see, e.g., [52] for some recent results for penalty-projection methods for incompressible flows). The Scott-Vogelius finite element pair (see, e.g., [53]) and grad-div stabilization technique (see, e.g., [55]) are used for stabilization in the fully discrete version of the model. The method is proven to be first order accurate in the grad-div parameter γ: as this parameter increases (while the mesh diameter h and the time step Δt are fixed), the solution converges to a solution given by the IMEX method of [51]. In turn, that solution is within $O(h^2+\Delta t)$ from the true solution,

when the (P_2, P_1^{disc}) Scott-Vogelius pair is used.

However, if one tries to apply the penalty-projection method of [48] with the routinely used Taylor-Hood finite element spaces, the method fails. In this chapter we demonstrate numerically this blow-up of solutions, and we propose a simple modification of the method, which allows for the usage of Taylor-Hood finite elements and results in an optimally convergent approximation.

The formulation of MHD in Elsasser variables, [56], seeks to find v, w, q, r, that satisfy

$$v_t + w \cdot \nabla v - (\tilde{B}_0 \cdot \nabla)v + \nabla q - \frac{\nu + \nu_m}{2}\Delta v - \frac{\nu - \nu_m}{2}\Delta w = f_1, \qquad (3.1.1)$$

$$\nabla \cdot v = 0, \qquad (3.1.2)$$

$$w_t + v \cdot \nabla w + (\tilde{B}_0 \cdot \nabla)w + \nabla r - \frac{\nu + \nu_m}{2}\Delta w - \frac{\nu - \nu_m}{2}\Delta v = f_2, \qquad (3.1.3)$$

$$\nabla \cdot w = 0. \qquad (3.1.4)$$

In order to consider a fully discrete, decoupled penalty-projection method for solving (3.1.1), some notation will be introduced in the next section. The method of [48] will then be considered on the much more common Taylor-Hood pair of finite element spaces (one for v, w and one for q, r), and a treatment will be provided for the demonstrated blow-up of the solutions. Section 3.3 gives the results of numerical tests, which show that the modified version of the method converges, where the existing method has failed.

3.2 Algorithms

The following spaces are used for the penalty-projection approach to MHD in the spatial domain $\Omega \subset R^d, d = 2, 3$.

$$X := H_0^1(\Omega), Q := L_0^2(\Omega), Y := \{v \in H^1(\Omega), v \cdot n = 0 \text{ on } \partial\Omega\}.$$

Notice that the additional velocity space Y, needed for the splitting, differs from the space X only in the boundary conditions: for the functions in Y these are only imposed in the normal direction.

Denote the usual L^2 norm and inner product by $\|\cdot\|$ and $(\cdot, \cdot)$. Introduce also the space of divergence-free functions $V := \{v \in X : (\nabla \cdot v, q) = 0, \forall q \in Q\}$.

The finite element approximation begins by selecting conforming finite element spaces $X^h \subset X, Q^h \subset Q$ satisfying the usual discrete inf-sup condition. In this chapter, we use the Taylor-Hood velocity-pressure pair (P_2, P_1) of piecewise polynomials.

Denote the space of discretely divergence free functions V^h by:

$$V^h := \{v^h \in X^h : (q^h, \nabla \cdot v^h) = 0, \forall\ q^h \in Q^h\}.$$

Note, that, contrary to the case of Scott-Vogelius finite elements, for the Taylor-Hood choice of X^h, Q^h the functions in V^h are not necessarily divergence-free pointwise.

Define the skew symmetric trilinear form

$$b^*(u, v, w) := \frac{1}{2}(u \cdot \nabla v, w) - \frac{1}{2}(u \cdot \nabla w, v), \tag{3.2.1}$$

Finally, define $Y^h = (P_2)^d \cap Y$ - additional discrete velocity space, where the boundary condition is only enforced in the normal direction. The scheme for solving (3.1.1) reads

Algorithm 3.2.1. *(Grad-div stabilized penalty-projection scheme of [48])*

Let $f_1, f_2 \in L^\infty(0,T;H^{-1}(\Omega))$, stabilization parameter $\gamma > 0$ and time step $\Delta t > 0$ and end time $T > 0$ be given. Set $M = T/\Delta t$ and start with $\tilde{v}^0 = v(0)$, $\tilde{w}^0 = w(0) \in H^2 \cup V$. For all $n = 0, 1, ..., M-1$, compute $\hat{v}_h^{n+1}, \hat{w}_h^{n+1}, \hat{p}_h^{n+1}, \hat{q}_h^{n+1}$ via:

Step 1: Find $\hat{v}_h^{n+1} \in X_h$ satisfying for all $\chi_h \in X_h$,

$$\begin{aligned}\left(\frac{\hat{v}_h^{n+1} - \tilde{v}_h^n}{\Delta t}, \chi_h \right) + b^*(\hat{w}_h^n, \hat{v}_h^{n+1}, \chi_h) - (\tilde{B}_0(t^{n+1}) \cdot \nabla \hat{v}_h^{n+1}, \chi_h) \\ + \frac{\nu + \nu_m}{2}(\nabla \hat{v}_h^{n+1}, \nabla \chi_h) + \frac{\nu - \nu_m}{2}(\nabla \hat{w}_h^n, \nabla \chi_h) \\ + \gamma(\nabla \cdot \hat{v}_h^{n+1}, \nabla \cdot \chi_h) = (f_1(t^{n+1}), \chi_h).\end{aligned} \tag{3.2.2}$$

Step 2: Find $(\tilde{v}_h^{n+1}, \hat{q}_h^{n+1}) \in (Y_h \times Q_h)$ satisfying for all $(v_h, q_h) \in (Y_h \times Q_h)$,

$$\begin{aligned}\left(\frac{\tilde{v}_h^{n+1} - \hat{v}_h^{n+1}}{\Delta t}, v_h \right) - (\hat{q}_h^{n+1}, \nabla \cdot v_h) = 0, \\ (\nabla \cdot \tilde{v}_h^{n+1}, q_h) = 0.\end{aligned} \tag{3.2.3}$$

Step 3: Compute $\tilde{w}_h^{n+1} \in X_h$ for all $l_h \in X_h$,

$$\begin{aligned}\left(\frac{\hat{w}_h^{n+1} - \tilde{w}_h^n}{\Delta t}, l_h \right) + b^*(\hat{v}_h^n, \hat{w}_h^{n+1}, l_h) + (\tilde{B}_0(t^{n+1}) \cdot \nabla \hat{w}_h^{n+1}, l_h) \\ + \frac{\nu + \nu_m}{2}(\nabla \hat{w}_h^{n+1}, \nabla l_h) + \frac{\nu - \nu_m}{2}(\nabla \hat{v}_h^n, \nabla l_h) \\ + \gamma(\nabla \cdot \hat{w}_h^{n+1}, \nabla \cdot l_h) = (f_2(t^{n+1}), l_h).\end{aligned} \tag{3.2.4}$$

Step 4: Find $(\tilde{w}_h^{n+1}, \hat{\lambda}_h^{n+1}) \in (Y_h \times Q_h)$ satisfying for all $(s_h, r_h) \in (Y_h \times Q_h)$,

$$\left(\frac{\tilde{w}_h^{n+1} - \hat{w}_h^{n+1}}{\Delta t}, s_h \right) - (\hat{\lambda}_h^{n+1}, \nabla \cdot s_h) = 0,$$
$$(\nabla \cdot \tilde{w}_h^{n+1}, r_h) = 0. \tag{3.2.5}$$

This penalty-projection method was investigated with the use of Scott-Vogelius finite element spaces, and it was shown to converge to the "conservative" solution of [51] as the stabilization parameter γ is increased (while h and Δt are kept fixed). The question of convergence to a known true solution of (3.1.1) is still open, when γ stays fixed and the mesh size and time step are being refined. Moreover, the main advantage of penalty-projection is the improved computational efficiency, and yet this scheme has not been investigated in a setting where the Scott-Vogelius elements are replaced with a less sophisticated (and less computationally challenging) choice. To that end, we employ the Taylor-Hood finite elements and we show that the method fails, as h and Δt are refined (see next section). We propose the following simple change, adding the grad-div stabilization to steps 2 and 4 of the algorithm.

Algorithm 3.2.2. *(Penalty-projection with grad-div stabilization in pressure equation)*

Let $f_1, f_2 \in L^\infty(0,T;H^{-1}(\Omega))$ *, stabilization parameter* $\gamma > 0$ *and time step* $\Delta t > 0$ *and end time* $T > 0$ *be given. Set* $M = T/\Delta t$ *and start with* $\tilde{v}^0 = v(0)$, $\tilde{w}^0 = w(0) \in H^2 \cup V$*. For all* $n = 0, 1, ..., M-1$*, compute* $\hat{v}_h^{n+1}, \hat{w}_h^{n+1}, \hat{p}_h^{n+1}, \hat{q}_h^{n+1}$ *via:*

Step 1: Find $\hat{v}_h^{n+1} \in X_h$ *satisfying for all* $\chi_h \in X_h$,

$$\begin{aligned}\left(\frac{\hat{v}_h^{n+1} - \tilde{v}_h^n}{\Delta t}, \chi_h \right) + b^*(\hat{w}_h^n, \hat{v}_h^{n+1}, \chi_h) - (\tilde{B}_0(t^{n+1}) \cdot \nabla \hat{v}_h^{n+1}, \chi_h) \\ + \frac{\nu + \nu_m}{2}(\nabla \hat{v}_h^{n+1}, \nabla \chi_h) + \frac{\nu - \nu_m}{2}(\nabla \hat{w}_h^n, \nabla \chi_h) \\ + \gamma(\nabla \cdot \hat{v}_h^{n+1}, \nabla \cdot \chi_h) = (f_1(t^{n+1}), \chi_h).\end{aligned} \tag{3.2.6}$$

Step 2: Find $(\tilde{v}_h^{n+1}, \hat{q}_h^{n+1}) \in (Y_h \times Q_h)$ *satisfying for all* $(v_h, q_h) \in (Y_h \times Q_h)$,

$$\begin{aligned}\left(\frac{\tilde{v}_h^{n+1} - \hat{v}_h^{n+1}}{\Delta t}, v_h \right) - (\hat{q}_h^{n+1}, \nabla \cdot v_h) + \gamma(\nabla \cdot \tilde{v}_h^{n+1}, \nabla \cdot v_h) = 0, \\ (\nabla \cdot \tilde{v}_h^{n+1}, q_h) = 0.\end{aligned} \tag{3.2.7}$$

Step 3: Compute $\tilde{w}_h^{n+1} \in X_h$ *for all* $l_h \in X_h$,

$$\begin{aligned}\left(\frac{\hat{w}_h^{n+1} - \tilde{w}_h^n}{\Delta t}, l_h \right) + b^*(\hat{v}_h^n, \hat{w}_h^{n+1}, l_h) + (\tilde{B}_0(t^{n+1}) \cdot \nabla \hat{w}_h^{n+1}, l_h) \\ + \frac{\nu + \nu_m}{2}(\nabla \hat{w}_h^{n+1}, \nabla l_h) + \frac{\nu - \nu_m}{2}(\nabla \hat{v}_h^n, \nabla l_h) \\ + \gamma(\nabla \cdot \hat{w}_h^{n+1}, \nabla \cdot l_h) = (f_2(t^{n+1}), l_h).\end{aligned} \tag{3.2.8}$$

Step 4: Find $(\tilde{w}_h^{n+1}, \hat{\lambda}_h^{n+1}) \in (Y_h \times Q_h)$ *satisfying for all* $(s_h, r_h) \in (Y_h \times Q_h)$,

$$\begin{aligned}\left(\frac{\tilde{w}_h^{n+1} - \hat{w}_h^{n+1}}{\Delta t}, s_h \right) - (\hat{\lambda}_h^{n+1}, \nabla \cdot s_h) + \gamma(\nabla \cdot \tilde{w}_h^{n+1}, \nabla \cdot s_h) = 0, \\ (\nabla \cdot \tilde{w}_h^{n+1}, r_h) = 0.\end{aligned} \tag{3.2.9}$$

We will show in Section 3.3 that this new algorithm converges to the true solution at the optimal rate.

3.3 Computational Testing

In order to show the difference in Algorithms 3.2.1 and 3.2.2, we consider the test problem from Section 5.1 of [48]. Choose the final time $T = 1$, introduce $\nu = 1, \nu_m = 0.5$ (to avoid unnecessary cancellation of terms), take $\gamma = 10^5$ and let $\Delta t = h = \frac{1}{N}$. Tables 3.3 and 3.4 show that the refinement of both the mesh and the time step eventually leads to a non-physical blow-up of the solution. Taylor-Hood pair of finite element spaces (piecewise quadratic polynomials for velocity and piecewise linears for the pressure) is used, via the FreeFEM software, in all the numerical tests of this chapter.

Applying Algorithm 3.2.2 to the same test problem leads to a first order accurate approximation of v, w - see Tables 3.1 and 3.2. This agrees with the theoretical findings of [48], as the first order accuracy in time is expected.

N	$\|\| v - v^h \|\|_{L^2(0,T;L^2(\Omega))}$	rate	$\|\| v - v^h \|\|_{L^2(0,T;H^1(\Omega))}$	rate
2	0.0017261	-	0.0240934	-
4	0.00163595	0.077	0.0220761	0.12
8	0.000819784	0.99	0.00759246	1.53
16	0.000423041	0.95	0.00361052	1.07
32	0.000214447	0.98	0.00172608	1.06
64	0.000107897	0.99	0.000858492	1.00

Table 3.1: Algorithm 3.2.2. Accuracy of v^h. $\Delta t = h = \frac{1}{N}$.

Finally, in order to prove the second order spatial accuracy of the solution,

N	$\| w - w^h \|_{L^2(0,T;L^2(\Omega))}$	rate	$\| w - w^h \|_{L^2(0,T;H^1(\Omega))}$	rate
2	0.00266961	-	0.0372761	-
4	0.00170584	0.64	0.0271122	0.45
8	0.000828133	1.04	0.00832559	1.70
16	0.000422762	0.97	0.00373864	1.15
32	0.000214283	0.98	0.00173525	1.10
64	0.000107804	0.99	0.000848726	1.03

Table 3.2: Algorithm 3.2.2. Accuracy of w^h. $\Delta t = h = \frac{1}{N}$.

obtained by Algorithm 3.2.2, we take $\Delta t = h^2$ in the test problem considered above. Tables 3.5 and 3.6 verify the claimed (and optimal) quadratic convergence rate.

3.4 Summary and future work

A method was presented in [48], that aims at approximating the MHD flows in an efficient way; the two key ingredients were the stable decoupling of the MHD system and the usage of the penalty-projection technique. The method showed good results when the Scott-Vogelius finite elements were used. However, we showed in this chapter, that if one tries to use the more common (and, most importantly, less computationally challenging) pair of Taylor-Hood finite elements - the method of [48] fails. We demonstrated numerically that the solution fails, and we showed a simple and effective way of resolving the issue. By adding

two more grad-div stabilization terms, we obtained a method that resolves the MHD flows in a more efficient way: it combines the penalty-projection technique with the computationally attractive choice of Taylor-Hood finite element spaces. We showed numerically that this modified approach is stable and accurate, with optimal convergence rate.

N	$\| v - v^h \|_{L^2(0,T;L^2(\Omega))}$	rate	$\| v - v^h \|_{L^2(0,T;H^1(\Omega))}$	rate
2	0.0017261	-	0.0240934	-
4	0.00163595	0.077	0.0220761	0.12
8	0.000819793	0.99	0.00759253	1.53
16	0.000423053	0.95	0.00361062	1.07
32	986444	–31.11	1.04093e+0 7	–31.42
64	3.29793e+11	– 18.35	3.03772e+13	– 21.47

Table 3.3: Algorithm 3.2.1. Accuracy of v^h. $\Delta t = h = \frac{1}{N}$.

N	$\| w - w^h \|_{L^2(0,T;L^2(\Omega))}$	rate	$\| w - w^h \|_{L^2(0,T;H^1(\Omega))}$	rate
2	0.00266958	-	0.0372761	-
4	0.00170589	0.64	0.0271129	0.45
8	0.000828166	1.04	0.00832582	1.70
16	0.000422804	0.96	0.00373889	1.15
32	6.47278e+11	--50.44	5.50982e+13	--53.71
64	4.28696e+14	–9.37	6.15723e+16	--10.12

Table 3.4: Algorithm 3.2.1. Accuracy of w^h. $\Delta t = h = \frac{1}{N}$.

N	$\| v - v^h \|_{L^2(0,T;L^2(\Omega))}$	rate	$\| v - v^h \|_{L^2(0,T;H^1(\Omega))}$	rate
2	0.00157575	-	0.0219946	-
4	0.00107462	0.55	0.0187298	0.23
8	0.000139787	2.94	0.00393326	2.25
16	3.1187e-05	2.16	0.00131798	1.57
32	7.02949e-06	2.14	0.000289867	2.18

Table 3.5: Algorithm 3.2.2. Accuracy of v^h. $\Delta t = h^2 = \frac{1}{N^2}$.

N	$\|\| w - w^h \|\|_{L^2(0,T;L^2(\Omega))}$	rate	$\|\| w - w^h \|\|_{L^2(0,T;H^1(\Omega))}$	rate
2	0.00251314	-	0.0350914	-
4	0.00120641	1.05	0.024198	0.53
8	0.000164786	2.87	0.00528656	2.19
16	3.35303e-05	2.29	0.00175146	1.59
32	7.44182e-06	2.17	0.000462205	1.92

Table 3.6: Algorithm 3.2.2. Accuracy of w^h. $\Delta t = h^2 = \frac{1}{N^2}$.

Chapter 4

A Second order Decoupled Penalty Projection Method based on Deferred Correction for MHD in Elsässer variable

4.1 Introduction

We consider an efficient numerical approximation for the magnetohydrodynamic (MHD) system, given in a convex domain $\Omega \times (0, T]$ by

$$u_t + (u \cdot \nabla)u - s(B \cdot \nabla)B - \nu\Delta u + \nabla p = f, \tag{4.1.1}$$

$$\nabla \cdot u = 0, \tag{4.1.2}$$

$$B_t + (u \cdot \nabla)B - (B \cdot \nabla)u - \nu_m \Delta B + \nabla\lambda = \nabla \times g, \tag{4.1.3}$$

$$\nabla \cdot B = 0, \tag{4.1.4}$$

with appropriate initial and boundary conditions. Here u is the velocity of fluid, p is the modified pressure, B is the magnetic field, λ is a Lagrange multiplier (dummy variable) corresponding to the solenoidal constraint on the magnetic field, f and $\nabla\times g$ are body forces, s is the coupling number, ν is the kinematic viscosity and ν_m is the magnetic diffusivity.

It is known that solving MHD systems arising from various important applications, including geophysics [76, 80], process metallurgy, astrophysics [64, 68, 71], can be very challenging. Significant progress has been made in recent years (see e.g. [67, 77, 81] and references therein). However, due to the coupling between the velocity and the magnetic field, solving the fully coupled system can be very difficult for many problems. Because of this reason, to obtain unconditionally stable uncoupled algorithms, an excellent idea was pioneered by [51]. It is shown that the stable algorithm can be achieved by writing the system (4.1.1)-(4.1.2) in Elsässer variables [56]. The Elsässer fields are defined by $v =: u + \sqrt{s}B$, $w =: u - \sqrt{s}B$, $f_1 =: f + \sqrt{s}(\nabla \times g)$, $f_2 =: f - \sqrt{s}(\nabla \times g)$, $q =: p + \sqrt{s}\lambda$ and $r =: p - \sqrt{s}\lambda$. These decompositions modify (4.1.1)-(4.1.2) to

$$v_t + w \cdot \nabla v - (\tilde{B}_0 \cdot \nabla)v + \nabla q - \frac{\nu + \nu_m}{2}\Delta v - \frac{\nu - \nu_m}{2}\Delta w = f_1, \qquad (4.1.5)$$

$$\nabla \cdot v = 0, \qquad (4.1.6)$$

$$w_t + v \cdot \nabla w + (\tilde{B}_0 \cdot \nabla)w + \nabla \lambda - \frac{\nu + \nu_m}{2}\Delta w - \frac{\nu - \nu_m}{2}\Delta v = f_2, \qquad (4.1.7)$$

$$\nabla \cdot w = 0. \qquad (4.1.8)$$

The main goal of this chapter consists in proposing and studying numerically an efficient second order accurate fully uncoupled approximation of (4.1.5)-(4.1.8) based on the decoupled penalty-projection method. A numerical anal-

ysis of the penalty-projection method with the DC method will be presented to achieve second order accuracy. The numerical studies include the Taylor-Hood finite element pair augmented with the grad-div stabilization term in the algorithm to improve mass conservation in solutions.

The time discretization we used here is the DC principle used for solving ODEs and PDEs by using the method of lines. The main advantage of the DC method is that high-order approximations to the solution of the differential equations can be constructed based on a simple low-order method by a process of iterated corrections.

First proposal of the classical DC method dates back to [10] and of spectral DC methods to [8]. In [17], a semi implicit spectral DC method was presented for ODEs which uses the Picard integral equation and discretization of it. This enables to use the non-stiff terms explicitly and the stiff terms implicitly. Some related works to the different types of DC method include [22] and [69] where the DDC is studied for Navier Stokes equations and two-domain convection-dominated convection-diffusion problem, respectively. We refer to reader for the survey article [82] for other approaches.

There are a number of papers analyzing the MHD system in Elsässer variables. Theoretical analyses of (4.1.5)-(4.1.8) for the first and second order schemes in a semi discrete setting, originally were performed in [78] and [51], respectively. In [51], unconditionally stable IMEX type uncoupling discretization is introduced and high order accurate method augmented with the DC method of [51] is studied in a semi discrete setting in the work of [83]. The fully discrete unconditionally stable scheme of MHD system in Elsässer variables has

been considered in [74] with appropriate choices ν and ν_m.

On the other hand, it was observed that the penalty-projection method yields more efficient solution with very little sacrifice of accuracy (see e.g. [52, 55]), subsequently, [48] suggests a grad-div stabilized penalty projection scheme for (4.1.5)-(4.1.8) for extra efficiency and it was shown that if one uses the Scott-Vogelius finite element pair (see, e.g., [53]), the equivalency of the penalty projection scheme and the fully coupled solutions can be obtained as a first order for large penalty parameter, γ. Additionally, it was observed that Taylor-Hood finite elements suffering from poor mass conservation are a popular choice on a much wider set of problems, [72, 79]. To avoid poor mass conservation on them, the grad-div stabilization is studied in [66]. In addition, as it was recently presented in [70], with the modification of the grad-div penalty projection algorithm of [48] for (4.1.5)-(4.1.8), the Taylor-Hood pair with grad-div stabilization leads to a first order accuracy while the existing method would fail on the Taylor-Hood element. These two observations are some of the motivations of the current chapter. Thus, in this study, we use the Taylor-Hood finite element pair with grad-div stabilized penalty projection scheme for (4.1.5)-(4.1.8) to improve accuracy and mass conservation properties.

The rest of the chapter is organized as follows. In order to consider a fully discrete, decoupled penalty-projection method and DC method for solving (4.1.5)-(4.1.8), some notation and algorithms will be presented in Section 2. The method of [48] will then be considered for the Taylor-Hood pair of finite element spaces. After the introduction of the DC algorithm used for the second order accuracy in Section 2, the stability of the correction step has been established based on

some assumptions. Numerical experiments are presented in Section 4 to verify theoretical results and a summary finishes the chapter.

4.2 Deferred Correction Algorithm

In this section, the studied algorithms are described in detail. We first summarize some notations. The L^2 norm and inner product are denoted by $\|\cdot\|$ and $(\cdot,\cdot)$, respectively. Let $\Omega \subset R^d, (d = 2, 3)$ be a convex polygonal or polyhedral domain. The following spaces are used for the penalty-projection algorithm of (4.1.5)-(4.1.8) in Ω:

$$X := H_0^1(\Omega),\ Q := L_0^2(\Omega),\ Y := \{v \in H^1(\Omega), v \cdot n = 0 \text{ on } \partial\Omega\}.$$

Notice that the additional velocity space Y, needed for the splitting, differs from the space X only in the boundary conditions: the functions in Y are only imposed in the normal direction. We also introduce the space of divergence-free functions

$$V := \{v \in X : (\nabla \cdot v, q) = 0, \forall q \in Q\}.$$

Define the skew symmetric trilinear form

$$b^*(u, v, w) := \frac{1}{2}(u \cdot \nabla v, w) - \frac{1}{2}(u \cdot \nabla w, v). \tag{4.2.1}$$

Through the analysis, we use the following bounds for the skew symmetric form (4.2.1), (see [73], for the proof);

$$b^*(u, v, w) \leq C(\Omega)\sqrt{\|u\|\|\nabla u\|}\|\nabla v\|\|\nabla w\| \tag{4.2.2}$$

$$b^*(u, v, w) \leq C(\Omega)\|\nabla u\|\|\nabla v\|\|\nabla w\|. \tag{4.2.3}$$

To consider finite element formulation of the problem, let $X^h \subset X, Q^h \subset Q$ be two finite element spaces corresponding to a family of regular conforming partition of the domain Ω. Furthermore we assume the existence of a finite element space $Y^h = (P_2)^d \cap Y$ with $X^h \subset Y^h$. In this chapter, we will consider the well known Taylor-Hood finite element pair (P_2, P_1) of piecewise polynomials, which fulfills the discrete inf-sup condition and has optimal approximation properties, see [73]. The space of discretely divergence free functions V^h is given by:

$$V^h := \{v^h \in X^h : (q^h, \nabla \cdot v^h) = 0, \forall\ q^h \in Q^h\}.$$

Note that, contrary to the case of Scott-Vogelius finite elements, for the Taylor-Hood choice of (X^h, Q^h) the functions in V^h are not necessarily divergence-free pointwise. Thus, in general, approximations obtained by using Scott-Vogelius has strong (pointwise) mass conservation property but poor mass conservation property in the case of using Taylor-Hood elements, (see e.g. [66]). Because of this reason, the use of Taylor-Hood finite elements introduces an extra error when using penalty projection method, thus the formulation in [48] does not work without the simple fix of [70]. Thus, by adding the grad-div stabilization terms to pressure equations for both Elsässer fields, we showed that the DC method also works for the Taylor-Hood elements for large γ. As it is shown below, this combination greatly increases efficiency and accuracy.

We now present the DC discretization of (4.1.5)-(4.1.8) combined with the penalty projection method of [48] by using the Taylor-Hood finite elements. The method consists of the first step of the algorithm of [48] followed by the algorithm for correction step.

Algorithm 4.2.1. *(Penalty-projection with grad-div stabilization in pressure equation for the first step)*

Let $f_1, f_2 \in L^\infty(0,T;H^{-1}(\Omega))$ *, stabilization parameter* $\gamma > 0$ *and time step* $\Delta t > 0$ *and end time* $T > 0$ *be given. Set* $M = T/\Delta t$*,* $t^n = n\Delta t$ *and start with* $\tilde{v}^0 = v(0)$*,* $\tilde{w}^0 = w(0) \in H^2 \cup V$*. For all* $n = 0, 1, ..., M-1$*, we compute the approximations* $\hat{v}_h^{n+1}, \hat{w}_h^{n+1}, \hat{p}_h^{n+1}, \hat{q}_h^{n+1}$ *via:*

Step 1: Find $\hat{v}_h^{n+1} \in X_h$ *satisfying for all* $\chi_h \in X_h$*,*

$$\begin{aligned}\left(\frac{\hat{v}_h^{n+1} - \tilde{v}_h^n}{\Delta t}, \chi_h \right) + b^*(\hat{w}_h^n, \hat{v}_h^{n+1}, \chi_h) - (\tilde{B}_0(t^{n+1}) \cdot \nabla \hat{v}_h^{n+1}, \chi_h) \\ + \frac{\nu + \nu_m}{2}(\nabla \hat{v}_h^{n+1}, \nabla \chi_h) + \frac{\nu - \nu_m}{2}(\nabla \hat{w}_h^n, \nabla \chi_h) \\ + \gamma(\nabla \cdot \hat{v}_h^{n+1}, \nabla \cdot \chi_h) = (f_1(t^{n+1}), \chi_h).\end{aligned} \tag{4.2.4}$$

Step 2: Find $(\tilde{v}_h^{n+1}, \hat{q}_h^{n+1}) \in (Y_h \times Q_h)$ *satisfying for all* $(v_h, q_h) \in (Y_h \times Q_h)$*,*

$$\begin{aligned}\left(\frac{\tilde{v}_h^{n+1} - \hat{v}_h^{n+1}}{\Delta t}, v_h \right) - (\hat{q}_h^{n+1}, \nabla \cdot v_h) + \gamma(\nabla \cdot \tilde{v}_h^{n+1}, \nabla \cdot v_h) = 0, \\ (\nabla \cdot \tilde{v}_h^{n+1}, q_h) = 0.\end{aligned} \tag{4.2.5}$$

Step 3: Compute $\tilde{w}_h^{n+1} \in X_h$ *for all* $l_h \in X_h$*,*

$$\begin{aligned}\left(\frac{\hat{w}_h^{n+1} - \tilde{w}_h^n}{\Delta t}, l_h \right) + b^*(\hat{v}_h^n, \hat{w}_h^{n+1}, l_h) + (\tilde{B}_0(t^{n+1}) \cdot \nabla \hat{w}_h^{n+1}, l_h) \\ + \frac{\nu + \nu_m}{2}(\nabla \hat{w}_h^{n+1}, \nabla l_h) + \frac{\nu - \nu_m}{2}(\nabla \hat{v}_h^n, \nabla l_h) \\ + \gamma(\nabla \cdot \hat{w}_h^{n+1}, \nabla \cdot l_h) = (f_2(t^{n+1}), l_h).\end{aligned} \tag{4.2.6}$$

Step 4: Find $(\tilde{w}_h^{n+1}, \hat{\lambda}_h^{n+1}) \in (Y_h \times Q_h)$ *satisfying for all* $(s_h, r_h) \in (Y_h \times Q_h)$*,*

$$\left(\frac{\tilde{w}_h^{n+1} - \hat{w}_h^{n+1}}{\Delta t}, s_h \right) - (\hat{\lambda}_h^{n+1}, \nabla \cdot s_h) + \gamma(\nabla \cdot \tilde{w}_h^{n+1}, \nabla \cdot s_h) = 0,$$
$$(\nabla \cdot \tilde{w}_h^{n+1}, r_h) = 0. \tag{4.2.7}$$

Note that Algorithm 4.2.1 includes grad-div stabilization terms in Step 2 and Step 4, to be able to use the Taylor Hood finite element pair. The work of [48] differs from the current chapter because it uses the Scott-Vogelius finite element pair and it has first accuracy in time. We now introduce the DC algorithm for Algorithm 4.2.1.

Algorithm 4.2.2. *(Penalty-projection with grad-div stabilization in pressure equation for the correction step)*

By using the same notation above, we start with $\widetilde{cv}^0 = cv(0)$, $\widetilde{cw}^0 = cw(0) \in H^2 \cup V$. *For all* $n = 0, 1, ..., M-1$, *compute* $\widehat{cv}_h^{n+1}, \widehat{cw}_h^{n+1}, \widehat{cp}_h^{n+1}, \widehat{cq}_h^{n+1}$ *via:*
Step 1: Find $\widehat{cv}_h^{n+1} \in X_h$ *satisfying for all* $\chi c_h \in X_h$,

$$\begin{aligned}
&\left(\frac{\widehat{cv}_h^{n+1} - \widetilde{cv}_h^n}{\Delta t}, \chi c_h \right) + \frac{\nu - \nu_m}{2}(\nabla \widehat{cw}_h^n, \nabla \chi c_h) + b^*(\widehat{cw}_h^n, \widehat{cv}_h^{n+1}, \chi c_h) \\
&-(\tilde{B}_0(t^{n+1}) \cdot \nabla \widehat{cv}_h^{n+1}, \chi c_h) + \frac{\nu + \nu_m}{2}(\nabla \widehat{cv}_h^{n+1}, \nabla \chi c_h) + \gamma(\nabla \cdot \widehat{cv}_h^{n+1}, \nabla \cdot \chi c_h) \\
&-\frac{\nu - \nu_m}{2}(\nabla \hat{w}_h^n, \nabla \chi c_h) - b^*(\hat{w}_h^n, \hat{v}_h^{n+1}, \chi c_h) + (\tilde{B}_0(t^{n+1}) \cdot \nabla \hat{v}_h^{n+1}, \chi c_h) \\
&-\frac{\nu + \nu_m}{2}(\nabla \hat{v}_h^{n+1}, \nabla \chi c_h) - \gamma(\nabla \cdot \hat{v}_h^{n+1}, \nabla \cdot \chi c_h) + \gamma(\nabla \cdot (\frac{\hat{v}_h^{n+1} + \hat{v}_h^n}{2}), \nabla \cdot \chi c_h) \\
&+\frac{\nu + \nu_m}{2}(\nabla (\frac{\hat{v}_h^{n+1} + \hat{v}_h^n}{2}), \nabla \chi c_h) - (\frac{\tilde{B}_0(t^{n+1}) \cdot \nabla \hat{v}_h^{n+1} + \tilde{B}_0(t^n) \cdot \nabla \hat{v}_h^n}{2}, \chi c_h) \\
&+\frac{b^*(\hat{w}_h^{n+1}, \hat{v}_h^{n+1}, \chi c_h) + b^*(\hat{w}_h^n, \hat{v}_h^n, \chi c_h)}{2} \\
&+\frac{\nu - \nu_m}{2}(\nabla (\frac{\hat{w}_h^{n+1} + \hat{w}_h^n}{2}), \nabla \chi c_h) = (\frac{f_1(t^{n+1}) + f_1(t^n)}{2}, \chi c_h).
\end{aligned} \tag{4.2.8}$$

Step 2: Find $(\widetilde{cv}_h^{n+1}, \widehat{cq}_h^{n+1}) \in (Y_h \times Q_h)$ *satisfying for all* $(vc_h, qc_h) \in (Y_h \times Q_h)$,

$$\left(\frac{\widetilde{cv}_h^{n+1} - \widehat{cv}_h^{n+1}}{\Delta t}, vc_h \right) - (\widehat{cq}_h^{n+1}, \nabla \cdot vc_h) + (\hat{q}_h^{n+1}, \nabla \cdot vc_h) - (\frac{\hat{q}_h^{n+1} + \hat{q}_h^n}{2}, \nabla \cdot vc_h)$$
$$+\gamma(\nabla \cdot \widetilde{cv}_h^{n+1}, \nabla \cdot vc_h) - \gamma(\nabla \cdot \tilde{v}_h^{n+1}, \nabla \cdot vc_h) + \gamma(\nabla \cdot (\frac{\tilde{v}_h^{n+1} + \tilde{v}_h^n}{2}), \nabla \cdot vc_h) = 0, \tag{4.2.9}$$

$$(\nabla \cdot \widetilde{cv}_h^{n+1}, qc_h) = 0. \tag{4.2.10}$$

Step 3: Compute $\widetilde{cw}_h^{n+1} \in X_h$ *for all* $lc_h \in X_h$,

$$\left(\frac{\widehat{cw}_h^{n+1} - \widetilde{cw}_h^n}{\Delta t}, lc_h \right) + \frac{\nu - \nu_m}{2}(\nabla \widehat{cv}_h^n, \nabla lc_h) + b^*(\widehat{cv}_h^n, \widehat{cw}_h^{n+1}, lc_h)$$
$$+(\tilde{B}_0(t^{n+1}) \cdot \nabla \widehat{cw}_h^{n+1}, lc_h) + \frac{\nu + \nu_m}{2}(\nabla \widehat{cw}_h^{n+1}, \nabla lc_h) + \gamma(\nabla \cdot \widehat{cw}_h^{n+1}, \nabla \cdot lc_h)$$
$$-\frac{\nu - \nu_m}{2}(\nabla \hat{v}_h^n, \nabla lc_h) - b^*(\hat{v}_h^n, \hat{w}_h^{n+1}, lc_h) - (\tilde{B}_0(t^{n+1}) \cdot \nabla \hat{w}_h^{n+1}, lc_h)$$
$$-\frac{\nu + \nu_m}{2}(\nabla \hat{w}_h^{n+1}, \nabla lc_h) - \gamma(\nabla \cdot \hat{w}_h^{n+1}, \nabla \cdot lc_h) + \gamma(\nabla \cdot (\frac{\hat{w}_h^{n+1} + \hat{w}_h^n}{2}), \nabla \cdot lc_h)$$
$$+\frac{\nu + \nu_m}{2}(\nabla (\frac{\hat{w}_h^{n+1} + \hat{w}_h^n}{2}), \nabla lc_h)$$
$$+(\frac{\tilde{B}_0(t^{n+1}) \cdot \nabla \hat{w}_h^{n+1} + \tilde{B}_0(t^n) \cdot \nabla \hat{w}_h^n}{2}, lc_h) + \frac{b^*(\hat{v}_h^{n+1}, \hat{w}_h^{n+1}, lc_h) + b^*(\hat{v}_h^n, \hat{w}_h^n, lc_h)}{2}$$
$$+\frac{\nu - \nu_m}{2}(\nabla (\frac{\hat{v}_h^{n+1} + \hat{v}_h^n}{2}), \nabla lc_h) = (\frac{f_2(t^{n+1}) + f_2(t^n)}{2}, lc_h). \tag{4.2.11}$$

Step 4: Find $(\widetilde{cw}_h^{n+1}, \widehat{c\lambda}_h^{n+1}) \in (Y_h \times Q_h)$ *satisfying for all* $(sc_h, rc_h) \in (Y_h \times Q_h)$,

$$\left(\frac{\widetilde{cw}_h^{n+1} - \widehat{cw}_h^{n+1}}{\Delta t}, sc_h \right) - (\widehat{c\lambda}_h^{n+1}, \nabla \cdot sc_h) + (\hat{\lambda}_h^{n+1}, \nabla \cdot sc_h)$$
$$-(\frac{\hat{\lambda}_h^{n+1} + \hat{\lambda}_h^n}{2}, \nabla \cdot sc_h) + \gamma(\nabla \cdot \widetilde{cw}_h^{n+1}, \nabla \cdot sc_h) - \gamma(\nabla \cdot \tilde{w}_h^{n+1}, \nabla \cdot sc_h) \quad (4.2.12)$$
$$+\gamma(\nabla \cdot (\frac{\tilde{w}_h^{n+1} + \tilde{w}_h^n}{2}), \nabla \cdot sc_h) = 0,$$

$$(\nabla \cdot \widetilde{cw}_h^{n+1}, rc_h) = 0. \quad (4.2.13)$$

Remark 4.2.1. *We note that since the grad-div stabilized penalty projection scheme of the solution of Algorithm 2.1 and Algorithm 2.2 converges to divergence-free solution of it as $\gamma \to \infty$, (see [48]), as it is shown in Section 4, a larger choice of γ will be used for the validity of the numerical scheme.*

4.3 Stability

The unconditional stability of Algorithm 4.2.1 is well-studied and is known to have unique solutions under some regularity assumptions on data, [48]. Based on these results, we make the following assumptions on the solutions of Algorithm 4.2.1.

Assumption 4.3.1. *Assume that, there exists a constant $\tilde{C}$ independent from $\Delta t, h$ and γ such that, the solutions of Algorithm 4.2.1 satisfy*

$$\max_{0 \le n \le M-1} (\|\hat{v}_h^n\|^2 + \|\hat{w}_h^n\|^2) \le \tilde{C} \quad (4.3.1)$$

$$\max_{0 \le n \le M-1} (\|\nabla \hat{v}_h^n\|^2 + \|\nabla \hat{w}_h^n\|^2) \le \tilde{C} \quad (4.3.2)$$

$$\max_{0 \le n \le M-1} \gamma(\|\nabla \cdot \hat{v}_h^n\|^2 + \|\nabla \cdot \hat{w}_h^n\|^2) \le \tilde{C} \quad (4.3.3)$$

where the constant $\tilde{C} > 0$ depends only on problem data.

Assumption 4.3.2. *The solution of Algorithm 4.2.1 satisfies*

$$\begin{aligned} \left\|e^{n+1}\right\|^2 &\leq O(\Delta t^2 + h^2) \\ \Delta t \sum_{i=1}^{N} \left\|\nabla e^i\right\|^2 &\leq O(\Delta t^2 + h^2) \end{aligned} \tag{4.3.4}$$

for $e = w - \hat{w}$

$$\begin{aligned} \left\|\eta^{n+1}\right\|^2 &\leq O(\Delta t^2 + h^2) \\ \Delta t \sum_{i=1}^{N} \left\|\nabla \eta^i\right\|^2 &\leq O(\Delta t^2 + h^2) \end{aligned} \tag{4.3.5}$$

for $\eta = v - \hat{v}$ and

$$\tilde{B}_0 \in L^\infty(0, T; \Omega), \tag{4.3.6}$$

where w and v are solutions of (4.1.5)-(4.1.8).

We now prove the stability of the correction step approximation of Algorithm 4.2.2.

Theorem 4.3.1 (Stability of Correction Step)**.** *Let $\widehat{cv}_h^{n+1}$, $\widehat{cw}_h^{n+1}$, $\widetilde{cv}_h^{n+1}$ and $\widetilde{cw}_h^{n+1} \in X^h$ satisfy Algorithm 4.2.2 for each $n \in \left\{0, 1, 2, \cdots, \frac{T}{\Delta t} - 1\right\}$. Then*

there exists a $C > 0$ independent of Δt, h such that $\widehat{cv}_h^{n+1}$ and $\widehat{cw}_h^{n+1}$ satisfy:

$$\left\|\widehat{cv}_h^{n+1}\right\|^2 + \left\|\widehat{cw}_h^{n+1}\right\|^2 + \Delta t\frac{(\nu+\nu_m)}{2}\sum_{j=1}^{n+1}(\left\|\nabla\widehat{cv}_h^j\right\|^2 + \left\|\nabla\widehat{cw}_h^j\right\|^2)$$
$$+ \Delta t\gamma\sum_{j=1}^{n+1}(\left\|\nabla\cdot\widehat{cv}_h^j\right\|^2 + \left\|\nabla\cdot\widehat{cw}_h^j\right\|^2) \leq \|\widehat{cv}_h^0\|^2 + \|\widehat{cw}_h^0\|^2$$
$$+ \left(\frac{3(\nu-\nu_m)^2\Delta t}{2(\nu+\nu_m)} + \frac{6C^2\Delta t}{(\nu+\nu_m)} + \frac{3(\nu+\nu_m)\Delta t}{2}\right)\left[\sum_{j=1}^{n}\left\|\nabla\hat{w}_h^j\right\|^2\right.$$
$$\left. + \sum_{j=1}^{n+1}\left\|\nabla\hat{w}_h^j\right\|^2)\right]$$
$$+ \left(\frac{3(\nu-\nu_m)^2\Delta t}{2(\nu+\nu_m)} + \frac{6C^2\Delta t}{(\nu+\nu_m)} + \frac{3(\nu+\nu_m)\Delta t}{2}\right)\left[\sum_{j=1}^{n}\left\|\nabla\hat{v}_h^j\right\|^2\right.$$
$$\left. + \sum_{j=1}^{n+1}\left\|\nabla\hat{v}_h^j\right\|^2)\right]$$
$$+ \frac{6\Delta t}{(\nu+\nu_m)}\sum_{j=1}^{n}(\left\|e^{j+1}\right\| + \left\|e^j\right\|)(\left\|\nabla e^{j+1}\right\| + \left\|\nabla e^j\right\|)[\left\|\nabla\hat{v}_h^{j+1}\right\|^2 + \left\|\nabla\hat{v}_h^j\right\|^2]$$
$$+ \frac{6\Delta t}{(\nu+\nu_m)}\sum_{j=1}^{n}(\left\|\eta^{j+1}\right\| + \left\|\eta^j\right\|)(\left\|\nabla\eta^{j+1}\right\| + \left\|\nabla\eta^j\right\|)[\left\|\nabla\hat{w}_h^{j+1}\right\|^2 + \left\|\nabla\hat{w}_h^j\right\|^2]$$
$$+ \frac{\gamma\Delta t}{2}\left(\sum_{j=1}^{n+1}\left\|\nabla\cdot\hat{v}_h^j\right\|^2 + \sum_{j=1}^{n}\left\|\nabla\cdot\hat{v}_h^j\right\|^2\right)$$
$$+ \frac{\gamma\Delta t}{2}\left(\sum_{j=1}^{n+1}\left\|\nabla\cdot\hat{w}_h^j\right\|^2 + \sum_{j=1}^{n}\left\|\nabla\cdot\hat{w}_h^j\right\|^2\right)$$
$$+ \frac{6\Delta t C_1}{(\nu+\nu_m)}\sum_{j=1}^{n+1}|\tilde{B}_0(t^j)|(\left\|\nabla\hat{v}_h^j\right\|^2 + \left\|\nabla\hat{w}_h^j\right\|^2)$$
$$+ \frac{6\Delta t C_1}{(\nu+\nu_m)}\sum_{j=1}^{n}|\tilde{B}_0(t^j)|(\left\|\nabla\hat{v}_h^j\right\|^2$$
$$+ \left\|\nabla\hat{w}_h^j\right\|^2) + \frac{24\Delta t}{(\nu+\nu_m)}\sum_{j=1}^{n}\left(\left\|\frac{f_1^{j+1}+f_1^j}{2}\right\|_*^2 + \left\|\frac{f_2^{j+1}+f_2^j}{2}\right\|_*^2\right). \quad (4.3.7)$$

Remark 4.3.1. *Note that from Assumption 4.3.1 and Assumption 4.3.2, it follows that the right hand side of (4.3.7) is bounded by the data.*

Proof. The proof of the stability starts with the choices $\chi c_h = \widehat{cv}_h^{n+1}$ in (4.2.8) and $lc_h = \widehat{cw}_h^{n+1}$ in (4.2.11). Along with the polarization identity, one obtains

$$\begin{aligned}
&\frac{1}{2\Delta t}(\left\|\widehat{cv}_h^{n+1}\right\|^2 - \|\widetilde{cv}_h^n\|^2 + \left\|\widehat{cv}_h^{n+1} - \widehat{cv}_h^n\right\|^2) + \frac{\nu+\nu_m}{2}\left\|\nabla\widehat{cv}_h^{n+1}\right\|^2 + \gamma\left\|\nabla\cdot\widehat{cv}_h^{n+1}\right\|^2 \\
&= -\frac{\nu-\nu_m}{2}(\nabla\widehat{cw}_h^n, \nabla\widehat{cv}_h^{n+1}) + \frac{\nu-\nu_m}{2}(\nabla\hat{w}_h^n, \nabla\widehat{cv}_h^{n+1}) + b^*(\hat{w}_h^n, \hat{v}_h^{n+1}, \widehat{cv}_h^{n+1}) \\
&-(\tilde{B}_0(t^{n+1})\cdot\nabla\hat{v}_h^{n+1}, \widehat{cv}_h^{n+1}) + \frac{\nu+\nu_m}{2}(\nabla\hat{v}_h^{n+1}, \nabla\widehat{cv}_h^{n+1}) + \gamma(\nabla\cdot\hat{v}_h^{n+1}, \nabla\cdot\widehat{cv}_h^{n+1}) \\
&+(\frac{f_1(t^{n+1})+f_1(t^n)}{2}, \widehat{cv}_h^{n+1}) - \gamma(\nabla\cdot(\frac{\hat{v}_h^{n+1}+\hat{v}_h^n}{2}), \nabla\cdot\widehat{cv}_h^{n+1}) \\
&-\frac{\nu+\nu_m}{2}(\nabla(\frac{\hat{v}_h^{n+1}+\hat{v}_h^n}{2}), \nabla\widehat{cv}_h^{n+1}) + (\frac{\tilde{B}_0(t^{n+1})\cdot\nabla\hat{v}_h^{n+1} + \tilde{B}_0(t^n)\cdot\nabla\hat{v}_h^n}{2}, \widehat{cv}_h^{n+1}) \\
&-\frac{b^*(\hat{w}_h^{n+1}, \hat{v}_h^{n+1}, \widehat{cv}_h^{n+1}) + b^*(\hat{w}_h^n, \hat{v}_h^n, \widehat{cv}_h^{n+1})}{2} - \frac{\nu-\nu_m}{2}(\nabla(\frac{\hat{w}_h^{n+1}+\hat{w}_h^n}{2}), \nabla\widehat{cv}_h^{n+1}),
\end{aligned} \tag{4.3.8}$$

and

$$\begin{aligned}
&\frac{1}{2\Delta t}(\left\|\widehat{cw}_h^{n+1}\right\|^2 - \|\widehat{cw}_h^n\|^2 + \left\|\widehat{cw}_h^{n+1} - \widehat{cw}_h^n\right\|^2) + \frac{\nu+\nu_m}{2}\left\|\nabla\widehat{cw}_h^{n+1}\right\|^2 \\
&+\gamma\left\|\nabla\cdot\widehat{cw}_h^{n+1}\right\|^2 = -\frac{\nu-\nu_m}{2}(\nabla\widehat{cv}_h^n, \nabla\widehat{cw}_h^{n+1}) + \frac{\nu-\nu_m}{2}(\nabla\hat{v}_h^n, \nabla\widehat{cw}_h^{n+1}) \\
&+b^*(\hat{v}_h^n, \hat{w}_h^{n+1}, \widehat{cw}_h^{n+1}) + (\tilde{B}_0(t^{n+1})\cdot\nabla\hat{w}_h^{n+1}, \widehat{cw}_h^{n+1}) + \frac{\nu+\nu_m}{2}(\nabla\hat{w}_h^{n+1}, \nabla\widehat{cw}_h^{n+1}) \\
&+\gamma(\nabla\cdot\hat{w}_h^{n+1}, \nabla\cdot\widehat{cw}_h^{n+1}) + (\frac{f_2(t^{n+1})+f_2(t^n)}{2}, \widehat{cw}_h^{n+1}) \\
&-\gamma(\nabla\cdot(\frac{\hat{w}_h^{n+1}+\hat{w}_h^n}{2}), \nabla\cdot\widehat{cw}_h^{n+1}) - \frac{\nu+\nu_m}{2}(\nabla(\frac{\hat{w}_h^{n+1}+\hat{w}_h^n}{2}), \nabla\widehat{cw}_h^{n+1}) \\
&-(\frac{\tilde{B}_0(t^{n+1})\cdot\nabla\hat{w}_h^{n+1} + \tilde{B}_0(t^n)\cdot\nabla\hat{w}_h^n}{2}, \widehat{cw}_h^{n+1}) \\
&-\frac{b^*(\hat{v}_h^{n+1}, \hat{w}_h^{n+1}, \widehat{cw}_h^{n+1}) + b^*(\hat{v}_h^n, \hat{w}_h^n, \widehat{cw}_h^{n+1})}{2} \\
&-\frac{\nu-\nu_m}{2}(\nabla(\frac{\hat{v}_h^{n+1}+\hat{v}_h^n}{2}), \nabla\widehat{cw}_h^{n+1}),
\end{aligned} \tag{4.3.9}$$

where we have used

$$b^*(\widehat{cw}_h^n, \widehat{cv}_h^{n+1}, \widehat{cv}_h^{n+1}) = 0$$
$$(\tilde{B}_0(t^{n+1}) \cdot \nabla \widehat{cv}_h^{n+1}, \widehat{cv}_h^{n+1}) = 0$$
$$b^*(\widehat{cv}_h^n, \widehat{cw}_h^{n+1}, \widehat{cw}_h^{n+1}) = 0$$
$$(\tilde{B}_0(t^{n+1}) \cdot \nabla \widehat{cw}_h^{n+1}, \widehat{cw}_h^{n+1}) = 0,$$

following from (4.2.1). Since the right hand sides of (4.3.8) and (4.3.9) are similar, it is enough to bound only the right hand side of (4.3.8).

The first term is bounded by the Cauchy-Schwarz inequality and Young's inequality:

$$-\frac{\nu-\nu_m}{2}(\nabla \widehat{cw}_h^n, \nabla \widehat{cv}_h^{n+1}) \le \frac{\epsilon(\nu+\nu_m)}{2}\left\|\nabla \widehat{cv}_h^{n+1}\right\|^2 + \frac{(\nu-\nu_m)^2}{8\epsilon(\nu+\nu_m)}\|\nabla \widehat{cw}_h^n\|^2. \tag{4.3.10}$$

Similarly, for the second and last terms of the right hand side of (4.3.8) one also gets

$$\begin{aligned} &\frac{\nu-\nu_m}{2}(\nabla \hat{w}_h^n, \nabla \widehat{cv}_h^{n+1}) - \frac{\nu-\nu_m}{2}(\nabla(\frac{\hat{w}_h^{n+1}+\hat{w}_h^n}{2}), \nabla \widehat{cv}_h^{n+1}) \\ &\le \epsilon(\nu+\nu_m)\left\|\nabla \widehat{cv}_h^{n+1}\right\|^2 + \frac{(\nu-\nu_m)^2}{32\epsilon(\nu+\nu_m)}\|\nabla \hat{w}_h^n\|^2 + \frac{(\nu-\nu_m)^2}{32\epsilon(\nu+\nu_m)}\left\|\nabla \hat{w}_h^{n+1}\right\|^2. \end{aligned} \tag{4.3.11}$$

To bound nonlinear terms in (4.3.8), we first rewrite them as:

$$\begin{aligned} &b^*(\hat{w}_h^n, \hat{v}_h^{n+1}, \widehat{cv}_h^{n+1}) - \frac{b^*(\hat{w}_h^{n+1}, \hat{v}_h^{n+1}, \widehat{cv}_h^{n+1}) + b^*(\hat{w}_h^n, \hat{v}_h^n, \widehat{cv}_h^{n+1})}{2} \\ &= \frac{1}{2}b^*(\hat{w}_h^n - \hat{w}_h^{n+1}, \hat{v}_h^{n+1}, \widehat{cv}_h^{n+1}) + \frac{1}{2}b^*(\hat{w}_h^n, \hat{v_h}^{n+1} - \hat{v}_h^n, \widehat{cv}_h^{n+1}). \end{aligned} \tag{4.3.12}$$

To estimate the first term in the right hand side of (4.3.12), decompose $\hat{w}_h^{n+1} - \hat{w}_h^n = (e^{n+1} - e^n) - (w^{n+1} - w^n)$ and use the bounds (4.2.2)-(4.2.3). Then,

application of the Cauchy-Schwarz and Young's inequalities yield

$$\begin{aligned}\frac{\Delta t}{2}\left\|\frac{e^{n+1}-e^n}{\Delta t}\right\|^{\frac{1}{2}}\left\|\nabla(\frac{e^{n+1}-e^n}{\Delta t})\right\|^{\frac{1}{2}}\|\nabla\hat{v}_h^{n+1}\|\|\nabla\widehat{c}v_h^{n+1}\| \\ +\frac{C}{2}\|\nabla\hat{v}_h^{n+1}\|\|\nabla\widehat{c}v_h^{n+1}\| \leq \epsilon(\nu+\nu_m)\|\nabla\widehat{c}v_h^{n+1}\|^2 \\ +\frac{1}{8\epsilon(\nu+\nu_m)}(\|e^{n+1}\|+\|e^n\|)(\|\nabla e^{n+1}\|+\|\nabla e^n\|)\|\nabla\hat{v}_h^{n+1}\|^2 \\ +\frac{C^2}{8\epsilon(\nu+\nu_m)}\|\nabla\hat{v}_h^{n+1}\|^2.\end{aligned} \tag{4.3.13}$$

There are two possible cases for bounding (4.3.13). We now examine each case:

Case 1. If $\Delta t < h$: For the second term in the right hand side of (4.3.13), using the inverse inequality ([65], p112): for any $\hat{v}_h \in X^h$

$$\|\nabla\hat{v}_h\| \leq Ch^{-1}\|\hat{v}_h\|, \tag{4.3.14}$$

Assumption 4.3.1 and Assumption 4.3.2, one gets

$$(\|e^{n+1}\|+\|e^n\|)\|\nabla\hat{v}_h\|^2 = O(h^{-1}). \tag{4.3.15}$$

We note that at the end of proof we will also multiply the error equation (4.3.8) by $2\Delta t$. Thus, by using Assumption 4.3.2 and $\Delta t < h$, one gets

$$\Delta t\sum_{i=1}^{N}\|\nabla e^i\| = O(h). \tag{4.3.16}$$

As a result of the combination of (4.3.15) and (4.3.16), one can conclude the boundedness of the second term in the right hand side of (4.3.13).

Case 2. If $\Delta t > h$: In this case, since

$$(\|e^{n+1}\|+\|e^n\|)\|\nabla\hat{v}_h^{n+1}\|^2 = O(\Delta t)\|\nabla\hat{v}_h^{n+1}\|^2 \tag{4.3.17}$$

is bounded via Assumption 4.3.1 and Assumption 4.3.2, we get

$$\frac{C\Delta t}{16\epsilon(\nu+\nu_m)}\sum_i\|\nabla e^i\|, \tag{4.3.18}$$

which is also bounded from Assumption 4.3.2. In a similar manner, for the second term in the right hand side of (4.3.12), with the help of decomposition where $\hat{v}_h^{n+1} - \hat{v}_h^n = (\eta^{n+1} - \eta^n) - (v^{n+1} - v^n)$, one obtains

$$\begin{aligned}
&\frac{\Delta t}{2}\|\nabla \hat{w}_h^n\|\big\|\nabla \widehat{cv}_h^{n+1}\|\Big\|\frac{\eta^{n+1}-\eta^n}{\Delta t}\Big\|^{\frac{1}{2}}\Big\|\nabla(\frac{\eta^{n+1}-\eta^n}{\Delta t})\Big\|^{\frac{1}{2}}\\
&\qquad + \frac{C}{2}\|\nabla \hat{w}_h^n\|\big\|\nabla \widehat{cv}_h^{n+1}\big\| \leq \epsilon(\nu+\nu_m)\big\|\nabla \widehat{cv}_h^{n+1}\big\|^2\\
&+\frac{1}{8\epsilon(\nu+\nu_m)}(\big\|\eta^{n+1}\big\| + \|\eta^n\|)(\big\|\nabla\eta^{n+1}\big\| + \|\nabla\eta^n\|)\|\nabla \hat{w}_h^n\|^2\\
&\qquad + \frac{C^2}{8\epsilon(\nu+\nu_m)}\|\nabla \hat{w}_h^n\|^2.
\end{aligned} \tag{4.3.19}$$

Then, arguing exactly as for (4.3.13) with assumptions (4.3.5), one concludes the bound for (4.3.19).

For the fourth term in the right hand side of (4.3.8), we use the Cauchy-Schwarz, Young's and Poincaré's inequalities:

$$\begin{aligned}
&-(\tilde{B}_0(t^{n+1})\cdot\nabla\hat{v}_h^{n+1}, \widehat{cv}_h^{n+1}) + (\frac{\tilde{B}_0(t^{n+1})\cdot\nabla\hat{v}_h^{n+1} + \tilde{B}_0(t^n)\cdot\nabla\hat{v}_h^n}{2}, \widehat{cv}_h^{n+1})\\
&\qquad = \frac{-1}{2}(\tilde{B}_0(t^{n+1})\cdot\nabla\hat{v}_h^{n+1}, \widehat{cv}_h^{n+1}) + \frac{1}{2}(\tilde{B}_0(t^n)\cdot\nabla\hat{v}_h^n, \widehat{cv}_h^{n+1})\\
&\qquad \leq \frac{1}{2}|\tilde{B}_0(t^{n+1})|\big\|\nabla\hat{v}_h^{n+1}\big\|\big\|\widehat{cv}_h^{n+1}\big\| + \frac{1}{2}|\tilde{B}_0(t^n)|\|\nabla\hat{v}_h^n\|\big\|\widehat{cv}_h^{n+1}\big\|\\
&\leq C_1\epsilon_1(\nu+\nu_m)\big\|\nabla\widehat{cv}_h^{n+1}\big\|^2 + \frac{1}{8C_1\epsilon_1(\nu+\nu_m)}|\tilde{B}_0(t^{n+1})|\big\|\nabla\hat{v}_h^{n+1}\big\|^2\\
&\qquad + \frac{1}{8C_1\epsilon_1(\nu+\nu_m)}|\tilde{B}_0(t^n)|\|\nabla\hat{v}_h^n\|^2.
\end{aligned} \tag{4.3.20}$$

One can conclude that (4.3.20) is also bounded from assumption (4.3.6). In the same way as for (4.3.10), the remaining terms in (4.3.8) are estimated by as follows:

$$\begin{aligned}
&\frac{\nu+\nu_m}{2}(\nabla\hat{v}_h^{n+1}, \nabla\widehat{cv}_h^{n+1}) - \frac{\nu+\nu_m}{2}(\nabla(\frac{\hat{v}_h^{n+1}+\hat{v}_h^n}{2}), \nabla\widehat{cv}_h^{n+1})\\
&\leq \epsilon(\nu+\nu_m)\big\|\nabla\widehat{cv}_h^{n+1}\big\|^2 + \frac{(\nu+\nu_m)}{32\epsilon}\big\|\nabla\hat{v}_h^{n+1}\big\|^2 + \frac{(\nu+\nu_m)}{32\epsilon}\|\nabla\hat{v}_h^n\|^2,
\end{aligned} \tag{4.3.21}$$

$$
\begin{aligned}
&(\frac{f_1(t^{n+1})+f_1(t^n)}{2}, \widehat{cv}_h^{n+1}) \\
&\leq \frac{\epsilon(\nu+\nu_m)}{2}\left\|\nabla \widehat{cv}_h^{n+1}\right\|^2 + \frac{1}{2\epsilon(\nu+\nu_m)}\left\|\frac{f_1(t^{n+1})+f_1(t^n)}{2}\right\|_*^2
\end{aligned} \tag{4.3.22}
$$

$$
\begin{aligned}
&\gamma(\nabla\cdot\hat{v}_h^{n+1}, \nabla\cdot\widehat{cv}_h^{n+1}) - \gamma(\nabla\cdot(\frac{\hat{v}_h^{n+1}+\hat{v}_h^n}{2}), \nabla\cdot\widehat{cv}_h^{n+1}) \\
&\leq 2\epsilon_2\gamma\left\|\nabla\cdot\widehat{cv}_h^{n+1}\right\|^2 + \frac{\gamma}{16\epsilon_2}\left\|\nabla\cdot\hat{v}_h^{n+1}\right\|^2 + \frac{\gamma}{16\epsilon_2}\|\nabla\cdot\hat{v}_h^n\|^2
\end{aligned} \tag{4.3.23}
$$

After putting all bounded terms in the right hand side of (4.3.8) and (4.3.9), we add them up. Then, dropping the non-negative terms in the right hand side of the resulting inequality and substituting all estimations along with $\epsilon = 1/24, \epsilon_1 = 1/4, C_1\epsilon_2 = 1/4$, and $(\nu+\nu_m)/2 \geq (\nu-\nu_m)^2/(8\epsilon(\nu+\nu_m))$ yields

$$
\begin{aligned}
&\frac{1}{2\Delta t}(\left\|\widehat{cv}_h^{n+1}\right\|^2 - \|\widetilde{cv}_h^n\|^2) + \frac{\nu+\nu_m}{4}\left\|\nabla\widehat{cv}_h^{n+1}\right\|^2 + \frac{\gamma}{2}\left\|\nabla\cdot\widehat{cv}_h^{n+1}\right\|^2 \\
&+\frac{1}{2\Delta t}(\left\|\widehat{cw}_h^{n+1}\right\|^2 - \|\widetilde{cw}_h^n\|^2) + \frac{\nu+\nu_m}{4}\left\|\nabla\widehat{cw}_h^{n+1}\right\|^2 + \frac{\gamma}{2}\left\|\nabla\cdot\widehat{cw}_h^{n+1}\right\|^2 \\
&\leq A + B,
\end{aligned} \tag{4.3.24}
$$

where

$$
\begin{aligned}
A = \Big[&\frac{3}{(\nu+\nu_m)}(\left\|e^{n+1}\right\| + \|e^n\|)(\left\|\nabla e^{n+1}\right\| + \|\nabla e^n\|) + \frac{3C^2}{(\nu+\nu_m)} \\
&+\frac{3}{(\nu+\nu_m)}|\tilde{B}_0(t^{n+1})| + \frac{3(\nu+\nu_m)}{4}\Big]\left\|\nabla\hat{v}_h^{n+1}\right\|^2 + \Big[\frac{3}{(\nu+\nu_m)}|\tilde{B}_0(t^n)| \\
&+\frac{3(\nu+\nu_m)}{4}\Big]\|\nabla\hat{v}_h^n\|^2 + \frac{3(\nu-\nu_m)^2}{4(\nu+\nu_m)}\left\|\nabla\hat{w}_h^{n+1}\right\|^2 + \Big[\frac{(3\nu-\nu_m)^2}{4(\nu+\nu_m)} + \frac{3C^2}{(\nu+\nu_m)} \\
&+\frac{3}{(\nu+\nu_m)}(\left\|\eta^{n+1}\right\| + \|\eta^n\|)(\left\|\nabla\eta^{n+1}\right\| + \|\nabla\eta^n\|)\Big]\|\nabla\hat{w}_h^n\|^2 \\
&+\frac{\gamma}{4}\left\|\nabla\cdot\hat{v}_h^{n+1}\right\|^2 + \frac{\gamma}{4}\|\nabla\cdot\hat{v}_h^n\|^2 + \frac{12}{2(\nu+\nu_m)}\left\|\frac{f_1(t^{n+1})+f_1(t^n)}{2}\right\|_*^2,
\end{aligned}
$$

and

$$B = \Big[\frac{3}{(\nu+\nu_m)}(\big\|\eta^{n+1}\big\| + \|\eta^n\|)(\big\|\nabla\eta^{n+1}\big\| + \|\nabla\eta^n\|) + \frac{3C^2}{(\nu+\nu_m)} + \frac{3}{(\nu+\nu_m)}|\tilde{B}_0(t^{n+1})| + \frac{3(\nu+\nu_m)}{4}\Big]\big\|\nabla\hat{w}_h^{n+1}\big\|^2 + \Big[\frac{3}{(\nu+\nu_m)}|\tilde{B}_0(t^n)| + \frac{3(\nu+\nu_m)}{4}\Big]\|\nabla\hat{w}_h^n\|^2 + \frac{3(\nu-\nu_m)^2}{4(\nu+\nu_m)}\big\|\nabla\hat{v}_h^{n+1}\big\|^2 + \Big[\frac{(3\nu-\nu_m)^2}{4(\nu+\nu_m)} + \frac{3C^2}{(\nu+\nu_m)} + \frac{3}{(\nu+\nu_m)}(\big\|e^{n+1}\big\| + \|e^n\|)(\big\|\nabla e^{n+1}\big\| + \|\nabla e^n\|)\Big]\|\nabla\hat{v}_h^n\|^2 + \frac{\gamma}{4}\big\|\nabla\cdot\hat{w}_h^{n+1}\big\|^2 + \frac{\gamma}{4}\|\nabla\cdot\hat{w}_h^n\|^2 + \frac{12}{2(\nu+\nu_m)}\Big\|\frac{f_2(t^{n+1})+f_2(t^n)}{2}\Big\|_*^2.$$

On the other hand, choosing $vc_h = \widetilde{cv}_h^{n+1}$ in (4.2.9) and $qc_h = \hat{q}_h^{n+1}$ in (4.2.10), applying the Cauchy-Schwarz and Young's inequalities results in

$$\big\|\widetilde{cv}_h^{n+1}\big\|^2 \leq \big\|\widehat{cv}_h^{n+1}\big\|^2 \tag{4.3.25}$$

Repeating exactly same arguments as above one can obtain the similar estimation for (4.3.9) e.g. for $\widehat{cw}_h$. Similarly, we choose $sc_h = \widetilde{cw}_h^{n+1}$ in (4.2.12) $rc_h = \hat{\lambda}_h^{n+1}$ in (4.2.13) so that

$$\big\|\widetilde{cw}_h^{n+1}\big\|^2 \leq \big\|\widehat{cw}_h^{n+1}\big\|^2 \tag{4.3.26}$$

In (4.3.24), adding the estimations for $\widehat{cv}_h$ using (4.3.25) and $\widehat{cw}_h$using (4.3.26), multiplying both sides by $2\Delta t$ and summing over time levels finishes the proof since the first approximation is unconditionally stable. □

Convergence analysis of Algorithm 4.2.1 in a fully discrete setting without a penalty-projection was performed in [48]. In addition, from Theorem 4.1 in [48], as $\gamma \to \infty$, penalty projection solutions have first order convergence to the

Algorithm 4.2.1 in a fully discrete setting without penalty-projection solution on a fixed mesh and time step. Thus, one can conclude first order convergence result for the solutions of Algorithm 4.2.1 as stated in (4.3.4)-(4.3.6). We now state second order convergence of solutions to Algorithm 4.2.2 to an Elsässer solution.

Theorem 4.3.2. *(Convergence of Correction Step) Assume (v, w, p) solves (4.1.5)-(4.1.8) and satisfying*

$$v, w \in L^\infty(0, T; H^m(\Omega)), \quad m = \max\{2, k+1\}$$

$$v_t, w_t \in L^\infty(0, T; H^{k+1}(\Omega))$$

$$v_{tt}, w_{tt} \in v, w \in L^\infty(0, T; L^2(\Omega))$$

Then the solution to Algorithm 4.2.2 converges to the true solution: for any $\Delta t > 0$,

$$\left\|v(T) - \widehat{cv}_h^M\right\| + \left\|w(T) - \widehat{cw}_h^M\right\|$$

$$+\frac{\nu\nu_m}{2(\nu+\nu_m)}\{\Delta t \sum_{n=1}^{M-1}(\|\nabla(v(t^n) - \widehat{cv}_h^n)\|^2 + \|\nabla(w(t^n) - \widehat{cw}_h^n)\|^2)\}^{\frac{1}{2}} \leq C(h^k + \Delta t^2)$$

Proof. Stability and accuracy results from [48] and [83] provide all the necessary details for the proof of this theorem. Thus, the technical proof of the convergence analysis can be established exactly in the same way. □

Remark 4.3.2. *From* (4.3.4)-(4.3.6) *and Theorem 4.3.2 under some regularity assumptions on true solution, by using the Taylor-Hood finite element, one can conclude*

$$\|v - \hat{v}_h\|_{2,2} + \|w - \hat{w}_h\|_{2,2} \leq C(\Delta t + h^2) \tag{4.3.27}$$

$$\|v - \hat{v}_h\|_{2,1} + \|w - \hat{w}_h\|_{2,1} \leq C(\Delta t + h^2) \tag{4.3.28}$$

for the solutions of Algorithm 4.2.1 and

$$\|v - \widehat{cv}\|_{2,2} + \|w - \widehat{cw}\|_{2,2} \leq C(\Delta t^2 + h^2) \tag{4.3.29}$$

$$\|v - \widehat{cv}\|_{2,1} + \|w - \widehat{cw}\|_{2,1} \leq C(\Delta t^2 + h^2) \tag{4.3.30}$$

for the solutions of Algorithm 4.2.2, where

$$\|\Phi\|_{2,2} := \|\Phi\|_{L^2(0,T;L^2(\Omega)^d)}$$

$$\|\Phi\|_{2,1} := \|\Phi\|_{L^2(0,T;H^1(\Omega)^d)}.$$

4.4 Computational Testing

In this section, we present two numerical experiments to test the proposed scheme and theory. The first example is for an analytical test problem with known solution. The second experiment is of more practical interest: it is a MHD channel flow over a forward and backward facing step. In all tests, the discretization of the problem is studied with the Taylor-Hood element pair. The computations are performed with the public license finite element software FreeFem++[75].

4.4.1 Convergence Rates

In this section, we present a numerical experiment for the verification of the expected convergence rates (4.3.27)-(4.3.30). We compare the proposed method with the penalty-projection method, which results in first order accuracy in time. In each case of the experiments, we also compare the results for with the $\gamma = 1$ and $\gamma = 10000$. To test the theoretically predicted convergence rates, we consider the solutions of Algorithm 4.2.1 and Algorithm 4.2.2 with $\Omega = [0, 1] \times [0, 1]$ and

with the prescribed solution

$$v = \begin{pmatrix} \cos y + (1+e^t)\sin y \\ \sin x + (1+e^t)\cos x \end{pmatrix},$$

$$w = \begin{pmatrix} \cos y - (1+e^t)\sin y \\ \sin x - (1+e^t)\cos x \end{pmatrix},$$

$$p = -\lambda = \sin(x+y).$$

In addition, the right hand side functions f_1 and f_2 are calculated from (4.1.5). For computations, we chose $\nu = 1$, $\nu_m = 0.5$, the final time $T = 1$ and $h = \Delta t = 1/M$. We compute the first step with Algorithm 4.2.1 and then use the results in Algorithm 4.2.2. We evaluate each error in $||.||_{L^2(0,T;L^2(\Omega))}$ and $||.||_{L^2(0,T;H^1(\Omega))}$ norms for each Elsässer variables.

The results are shown in Table 4.1-Table 4.4. We observe that for the large penalty parameter γ, a first order temporal convergence for the solutions of Algorithm 4.2.1 and a second order temporal convergence for the solutions of Algorithm 4.2.2 are obtained, as expected.

N	$\| v - \hat{v}_h \|_{L^2(0,T;L^2(\Omega))}$	rate	$\| v - \hat{v}_h \|_{L^2(0,T;H^1(\Omega))}$	rate
2	0.0017261	-	0.0240934	-
4	0.00163583	0.07	0.022075	0.12
8	0.000819807	0.99	0.00759258	1.53
16	0.00042305	0.95	0.00361056	1.07
32	0.000214446	0.98	0.00172605	1.06
64	0.000107892	0.99	0.000858431	1.00

Table 4.1: Algorithm 4.2.1. Accuracy of $\hat{v}_h$, for $\gamma = 100000$ and $\Delta t = h = \frac{1}{M}$.

N	$\| w - \hat{w}_h \|_{L^2(0,T;L^2(\Omega))}$	rate	$\| w - \hat{w}_h \|_{L^2(0,T;H^1(\Omega))}$	rate
2	0.00266961	-	0.0372761	-
4	0.00170579	0.64	0.027112	0.45
8	0.000828149	1.04	0.00832568	1.70
16	0.00042277	0.97	0.00373869	1.15
32	0.000214286	0.98	0.00173527	1.10
64	0.000107804	0.99	0.000848722	1.03

Table 4.2: Algorithm 4.2.1. Accuracy of $\hat{w}_h$, for $\gamma = 100000$ and $\Delta t = h = \frac{1}{M}$.

N	$\| v - \widehat{cv}_h \|_{L^2(0,T;L^2(\Omega))}$	rate	$\| v - \widehat{cv}_h \|_{L^2(0,T;H^1(\Omega))}$	rate
2	0.00172604	-	0.0240931	-
4	0.00123244	0.48	0.0213587	0.17
8	0.000174041	2.82	0.004284	2.31
16	4.398e-05	1.98	0.00139066	1.62
32	1.14404e-05	1.94	0.000304462	2.19
64	3.02593e-06	1.91	6.29791e-05	2.27

Table 4.3: Algorithm 4.2.2. Accuracy of $\widehat{cv}_h$, for $\gamma = 100000$ and $\Delta t = h = \frac{1}{M}$.

N	$\| w - \widehat{cw}_h \|_{L^2(0,T;L^2(\Omega))}$	rate	$\| w - \widehat{cw}_h \|_{L^2(0,T;H^1(\Omega))}$	rate
2	0.0026696	-	0.0372759	-
4	0.00137167	0.96	0.0273535	0.44
8	0.000197954	2.79	0.00570089	2.26
16	4.57471e-05	2.11	0.00183279	1.63
32	1.17158e-05	1.96	0.000476566	1.94
64	3.36945e-06	1.79	0.000111516	2.09

Table 4.4: Algorithm 4.2.2. Accuracy of $\widehat{cw}_h$, for $\gamma = 100000$ and $\Delta t = h = \frac{1}{M}$.

We also compute the solutions for $\gamma = 1$. While the tables above show expected convergence rate for the choice of large penalty parameter $\gamma = 100000$, as seen in Table 4.5-Table 4.8, the choice of $\gamma = 1$ significantly loses accuracy for both Algorithm 4.2.1 and Algorithm 4.2.2.

N	$\| v - \hat{v}_h \|_{L^2(0,T;L^2(\Omega))}$	rate	$\| v - \hat{v}_h \|_{L^2(0,T;H^1(\Omega))}$	rate
2	0.0538592	-	0.264343	-
4	0.0258353	1.05	0.136099	0.95
8	0.0136141	0.92	0.0749909	0.85
16	0.00747208	0.86	0.0431047	0.79
32	0.00389868	0.93	0.0242952	0.82
64	0.00181945	1.09	0.0128235	0.92

Table 4.5: Algorithm 4.2.1. Accuracy of $\hat{v}_h$, for $\gamma = 1$. $\Delta t = h = \frac{1}{M}$.

N	$\| w - \hat{w}_h \|_{L^2(0,T;L^2(\Omega))}$	rate	$\| w - \hat{w}_h \|_{L^2(0,T;H^1(\Omega))}$	rate
2	0.0707299	-	0.339429	-
4	0.0403039	0.81	0.194823	0.80
8	0.0330883	0.28	0.15507	0.32
16	0.0284572	0.21	0.132846	0.22
32	0.0223229	0.35	0.106202	0.32
64	0.0154592	0.53	0.0767291	0.46

Table 4.6: Algorithm 4.2.1. Accuracy of $\hat{w}_h$, for $\gamma = 1$. $\Delta t = h = \frac{1}{M}$.

N	$\| v - \widehat{cv}_h \|_{L^2(0,T;L^2(\Omega))}$	rate	$\| v - \widehat{cv}_h \|_{L^2(0,T;H^1(\Omega))}$	rate
2	0.0197291	-	0.114869	-
4	0.0109216	0.85	0.0633522	0.85
8	0.00740681	0.56	0.0434134	0.54
16	0.00494728	0.58	0.0304451	0.51
32	0.00294147	0.75	0.0196976	0.62
64	0.00149777	0.97	0.0113684	0.79

Table 4.7: Algorithm 4.2.2. Accuracy of $\widehat{cv}_h$, for $\gamma = 1$. $\Delta t = h = \frac{1}{M}$.

N	$\| w - \widehat{cw}_h \|_{L^2(0,T;L^2(\Omega))}$	rate	$\| w - \widehat{cw}_h \|_{L^2(0,T;H^1(\Omega))}$	rate
2	0.0474063	-	0.222608	-
4	0.0441578	0.10	0.202465	0.13
8	0.0385005	0.19	0.177266	0.19
16	0.0312935	0.29	0.145638	0.28
32	0.0234673	0.41	0.11166	0.38
64	0.0158558	0.56	0.078735	0.50

Table 4.8: Algorithm 4.2.2. Accuracy of $\widehat{cw}_h$, for $\gamma = 1$. $\Delta t = h = \frac{1}{M}$.

4.4.2 Channel flow over a step

The second experiment we consider is the channel flow in a 30×10 rectangular domain with a 1×1 step five units into the channel, in the presence of a magnetic

field. We chose $\nu = 0.001$, $\nu_m = 1$, $T = 40$ and $\Delta t = 0.025$. No slip boundary conditions are enforced for velocity components v and w, and $B =< 0, 1 >^T$ is used on the all walls and step. We also take $u =< y(10-y)/25, 0 >^T$ at the inlet and outlet. The initial conditions are chosen as $u =< y(10-y)/25, 0 >^T$ and $B = 0$. Numerical studies are performed for the penalty parameter $\gamma = 100000$. We are interested in studying evolution of the reattachment points of the recirculating vortices developing behind the step, for varying coupling numbers $s = 0$, $s = 0.01$ and $s = 0.05$

In Figure 4.1, we depict the streamlines over speed contours and corresponding magnetic field contours for each case. We clearly observe the eddy formation behind the step for each case. Due to the increasing effect of the magnetic field as s increases, the eddies tend to gather, shorten and seems steady. Thus, our solution captures the correct eddy structures behind the step and their detachment.

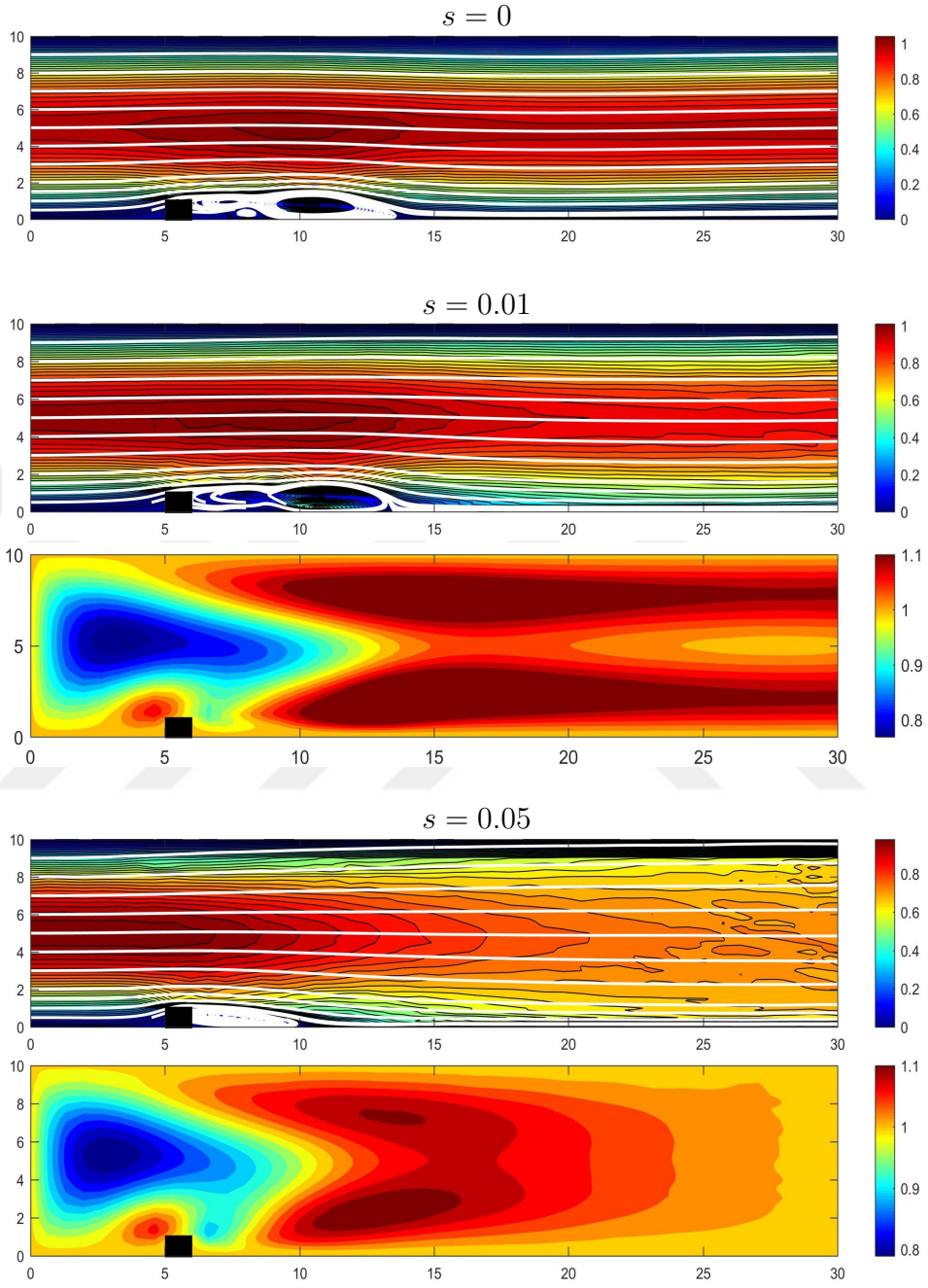

Figure 4.1: Plots of streamlines over speed contours and magnetic field contours for varying s

4.5 Summary and future work

This chapter studied an efficient second order penalty-projection DC method for the solutions of the MHD in Elsässer variables. The proposed algorithm uses the grad-div stabilized Taylor-Hood pair, which is a common choice of the finite element spaces, is used for large penalty parameter γ. In this way, the algorithm improves mass conservation in solutions. The stability analysis was performed for the correction step and expected converges rates are verified for the analytical test problem. Channel flow over a full step test problem was also presented in order to show the well performance of the method.

Chapter 5

Conclusion

Predictor-corrector methods are often considered to be too crude to tackle the stiff problems arising in fluid flow modeling. However, the author was able to show that both Defect and Deferred Correction methods can be useful, sometimes even invaluable, in a variety of CFD applications. It has been shown through a sequence of chapters.

In the first chapter, the DDC method for a fluid-fluid interaction problem (two convection-dominated convection-diffusion problems adjoined by an interface), which is a simplied version of the atmosphere-ocean coupling problem, was introduced. It is a partitioned time stepping method, yet it is of high order accuracy in both space and time. Also, it allows for the usage of the legacy codes (which is a common requirement when resolving flows in complex geometries), yet it can be applied to the problems with very small viscosity/diffusion coefficients. This is achieved by combining the defect correction technique for increased spatial accuracy (and for resolving the issue of high convection-to-

diffusion ratio) with the DC in time (which allows for the usage of the computationally attractive partitioned scheme, yet the time accuracy is increased beyond the usual result of partitioned methods being only first order accurate) into the DDC. The results are readily extendable to the higher order accuracy cases by adding more correction steps. Both the theoretical results and the numerical tests provided demonstrate that the computed solution is unconditionally stable and the accuracy in both space and time is improved after the correction step. This research was published in [69]; the author of this dissertation was responsible for the computational part of this publication.

In the second chapter, a method is proposed to improve two aspects of numerical simulations for a model of two fluids coupled across a flat interface. This problem is motivated by atmosphere-ocean interaction. A DC approach lifts the numerical order of accuracy formally from first order (very common in applications) to second order, in terms of the time interval of communication between the fluid code components. This is accomplished in a two-step predictor-corrector type method. In the second step, a further defect correction is included as well. The "defect" represents artificial diffusion used in the fluid solvers, which is often included to control numerical noise or to model subscale mixing processes. The addition of the defect correction adds only marginally to the expense, but in exchange may provide a significant reduction of overdiffusive effects. A full DDC algorithm is studied using finite elements in space, including an analysis of the stability and convergence. A computational example using a known (manufactured) solution illustrates the theoretical predictions. We observe a computational benefit in this example even for coarse time steps and over

a wide range of artificial viscosity values. Some discussion is provided regarding the possibility to generalize the approach for application codes. Briefly, legacy atmosphere and ocean codes may be used as-is over a coupling time interval for a predictor computation. The corrector step would then potentially be implemented as a straight-forward modification of the predictor step that leverages the existing code structure. This research was published in [23]; the author of this dissertation was responsible for the theoretical part of this publication.

In the third chapter, we propose a small modification of an recently presented algorithm for resolving magnetohydrodynamic (MHD) flows, that allowed for a stable decoupling of the system and used the penalty-projection method for extra efficiency. The algorithm relies on the choice of Scott-Vogelius finite elements to complement the grad-div stabilization. Our proposed modification allows for this algorithm to be used even with the less sophisticated (and more computationally attractive) Taylor-Hood pair of finite element spaces. We demonstrate numerically, that the new modification of the method is first order accurate in time (as expected by the theory), while the existing method would fail on the Taylor-Hood finite elements (the blow-up of the solution is demonstrated). This research was published in [70]; the author of this dissertation was responsible for the computational part of this publication.

In the fourth chapter, we study the DC method for the magnetohydrodynamics (MHD) system written in Elsässer variables. The proposed algorithm is based on the penalty projection with grad-div stabilized Taylor Hood solutions of the Elsässer formulation. In this way, second order accuracy of the method in time is obtained through the DC method with excellent mass conservation

properties. For the proposed method, stability is rigorously proven and numerical experiments are presented to verify the proposed scheme and theory. This research was published in [84]; the author of this dissertation was responsible for parts of both the theoretical and the computational parts of this publication.

References

[1] O. Axelsson and W. Layton, *Optimal interior estimates for the defect-correction, finite element approach to 2-D convection-diffusion problems*, ICMA report 88-116, Univ. of Pittsburgh (1988).

[2] W. Layton, H. K. Lee, J. Peterson, *A defect-correction method for the incompressible Navier–Stokes equations*, Applied Mathematics and Computation, Vol. 129, Issue 1 (2002), pp. 1-19.

[3] R.A. Adams and J.J.F. Fournier, *Sobolev Spaces*, vol. 140 of Pure and Applied Mathematics, Academic Press (2003).

[4] K. Böhmer, P. W. Hemker, H. J. Stetter, *The defect correction approach, in: K. Böhmer, H. J. Stetter (Eds.),Defect Correction Methods. Theory and Applications*, Springer Verlag (1984), pp. 1-32.

[5] D. Bresch and J. Koko, *Operator-Splitting and Lagrange Multiplier Domain Decomposition Methods for Numerical Simulation of Two Coupled Navier-Stokes Fluids*, Int. J. Appl. Math. Comput. Sci., Vol. 16, No. 4 (2006), pp. 419-429.

[6] E. Burman, Miguel A. Fernández, *Stabilization of explicit coupling in fluid-structure interaction involving fluid incompressibility*, Comput. Methods Appl. Mech. Engrg. 198 (2009), pp. 766-784.

[7] J. Connors, J. Howell and W. Layton, *Partitioned timestepping for a parabolic two domain problem*, SIAM Jour. Num. Anal., Vol. 47, No. 5 (2009).

[8] A. Dutt, L. Greengard, V. Rokhlin, *Spectral Deferred Correction Methods for Ordinary Differential Equations*, BIT 40 (2) (2000), pp. 241-266.

[9] V. J. Ervin, H. K. Lee, *Defect correction method for viscoelastic fluid flows at high Weissenberg number*, Numerical Methods for Partial Differential Equations, Volume 22, Issue 1 (2006), pp. 145 - 164.

[10] R. Frank, W. Ueberhuber, *Iterated Defect Correction for the Efficient Solution of Stiff Systems of Ordinary Differential Equations*, BIT 17 (1977), pp. 146-159.

[11] F. Hecht, A. LeHyaric and O. Pironneau, Freefem++ version 2.24-1 (2008), `http://www.freefem.org/ff++`.

[12] J. G. Heywood and R. Rannacher, *Finite-elements approximation of the nonstationary Navier-Stokes problem part IV: Error analysis for second-order discretization*, SIAM J. Numer. Anal., vol. 27(2) (1990), pp. 353-384.

[13] A. Labovsky, *A Defect Correction Method for the Evolutionary Convection Diffusion Problem with Increased Time Accuracy*, Computational Methods in Applied Mathematics, Vol. 9, No. 2 (2009), pp. 154-164.

[14] A. Labovsky, *A Defect Correction Method for the Time-Dependent Navier-Stokes Equations*, Numerical Methods for Partial Differential Equations, vol.25(1) (2008), pp.1-25.

[15] M. L. Minion, *Semi-Implicit Spectral Deferred Correction Methods for Ordinary Differential Equations*, Comm. Math. Sci. 1 (2003), 471-500.

[16] M. L. Minion, *Semi-Implicit Projection Methods for Incompressible Flow based on Spectral Deferred Corrections*, Appl. Numer. Math., 48(3-4) (2004), 369-387.

[17] M. L. Minion, *Semi-Implicit Projection Methods for Ordinary Differential Equations*, Comm. Math. Sci., 1(3) (2003), 471-500.

[18] A. Bourlioux, A. T. Layton, M. L. Minion, *High-Order Multi-Implicit Spectral Deferred Correction Methods for Problems of Reactive Flows*, Journal of Computational Physics, Vol. 189, No. 2 (2003), pp. 651-675.

[19] M. Gunzburger, A. Labovsky, *High Accuracy Method for Turbulent Flow Problems*, M3AS: Mathematical Models and Methods in Applied Sciences, vol. 22 (6) (2012).

[20] H. J. Stetter, *The defect correction principle and discretization methods*, *Numerische Mathematik*, vol. 29(4) (1978), pp. 425-443.

[21] J. Connors, J. Howell and W. Layton, *Decoupled time stepping methods for fluid-fluid interaction*, SIAM Jour. Num. Analysis, Vol. 50, No. 3 (2012), pp. 1297-1319.

[22] M. Aggul, A. Labovsky, *A High Accuracy Minimally Invasive Regularization Technique for Navier-Stokes Equations at High Reynolds Number*, Numerical Methods for Partial Differential Equations, vol. 33(3) (2017), pp. 814-839.

[23] M. Aggul, J. Connors, D. Erkmen, and A. Labovsky, *A Defect-Deferred Correction Method for Fluid-Fluid Interaction: Full Version*, Technical Report, Michigan Technological University (2017).

[24] G. P. Galdi, *An Introduction to the Mathematical Theory of the Navier-Stokes Equations, Springer Tracts in Natural Philosophy*, Volume I, Springer-Verlag, New York (1994).

[25] J.-W. Bao, J. M. Wilczak, J.-K. Choi and L. H. Kantha, *Numerical simulations of air-sea interaction under high wind conditions using a coupled model: A study fo hurricane development*, Monthly Weather Review, Vol. 128 (2000), pp. 2190-2210.

[26] G. Bellon, A. H. Sobel and J. Vialard, *Ocean-atmospere coupling in the monsoon intraseasonal oscillation: A simple model study*, Journal of Climate, Vol. 21 (2008), pp. 5254-5270.

[27] C. L. Brossier, V. Ducrocq and H. Giordani, *Effects of the air-sea coupling time frequency on the ocean response during Mediterranean intense events*, Ocean Dynamics, Vol. 59 (2009), pp. 539-549.

[28] F. O. Bryan, B. G. Kauffman, W. G. Large and P. R. Gent, *The NCAR CESM flux coupler*, Tech. Rept. NCAR/TN-424+STR, NCAR (1996).

[29] R. B. Neale, *et. al.*, *Description of the NCAR community atmosphere model (CAM 5.0)*, NCAR Tech. Note NCAR/TN-486+ STR (2010).

[30] J. Connors and B. Ganis, *Stability of algorithms for a two domain natural convection problem and observed model uncertainty*, Computational Geosciences, Vol. 15, No. 3 (2011), pp. 509-527.

[31] S. D. Nicholls and S. G. Decker, *Impact of coupling an ocean model to WRF nor'easter simulations*, Monthly Weather Review 143.12 (2015), pp. 4997-5016.

[32] F. Lemarié, E. Blayo and L. Debreu, *Analysis of ocean-atmosphere coupling algorithms: consistency and stability*, Procedia Computer Science, Vol. 51 (2015), pp. 2066-2075.

[33] F. Lemarié, P. Marchesiello, L. Debreu and E. Blayo, *Sensitivity of ocean-atmosphere coupled models to the coupling method: example of tropical cyclone Erica*, Doctoral dissertation, INRIA Grenoble; INRIA (2014).

[34] Randall, D.A., R.A. Wood, S. Bony, R. Colman, T. Fichefet, J. Fyfe, V. Kattsov, A. Pitman, J. Shukla, J. Srinivasan, R.J. Stouffer, A. Sumi and K.E. Taylor,*2007: Climate Models and Their Evaluation. In: Climate Change 2007: The Physical Science Basis. Contribution of Working Group I to the Fourth Assessment Report of the Intergovernmental Panel on Climate Change [Solomon, S., D. Qin, M. Manning, Z. Chen, M. Marquis, K.B. Averyt, M.Tignor and H.L. Miller (eds.)].* Cambridge University Press, Cambridge, United Kingdom and New York, NY, USA.

[35] M. Jochum, G. Danabasoglu, M. Holland, Y.-O. Kwon and W. G. Large, *Ocean viscosity and climate*, Journal of Geophysical Research, Vol. 113, C06017 (2008), pp. 1-24.

[36] Large, W.G., McWilliams, J.C. and Doney, S.C., *Oceanic vertical mixing: A review and a model with a nonlocal boundary layer*, Reviews of Geophysics, Vol. 32 (1994), pp. 363-403.

[37] J.-L. Lions, R. Temam and S. Wang, *Models of the coupled atmosphere and ocean (CAO I)*, Computational Mechanics Advances, Vol. 1 (1993), pp. 5-54.

[38] J.-L. Lions, R. Temam and S. Wang, *Numerical analysis of the coupled atmosphere ocean models (CAO II)*, Computational Mechanics Advances, Vol. 1 (1993), pp. 55-119.

[39] P. A. Mooney, D. O. Gill, F. J. Mulligan and C. L. Bruyère, *Hurrican simulation using different representations of atmosphere-ocean interaction: the case of Irene*, Atmospheric Science Letters, Vol. 17, No. 7 (2016), pp. 415-421.

[40] J. Nelson, R. He, J. C. Warner and J. Bane, *Air-sea interactions during strong winter extratropical storms*, Ocean Dynamics, Vol. 64, No. 9 (2014), pp. 1233-1246.

[41] N. Perlin, E. D. Skyllingstad, R. M. Samelson, P. L. Barbour, *Numerical simulation of air-sea coupling during coastal upwelling*, Journal of Physical Oceanography, Vol. 37 (2007), pp. 2081-2093.

[42] R. Smith, et. al., *The parallel ocean program (POP) reference manual*, Tech. Rep. LAUR-01853 141 (2010): 1-140.

[43] B. Wang and X. Xie, *Coupled modes of the warm pool climate system. Part 1: The role of air-sea interaction in maintaining Madden-Julian Oscillation*, Journal of Climate, Vol. 11 (1998), pp. 2116-2135.

[44] W. L. Washington and C. L. Parkinson, *An Introduction to Three-Dimensional Climate Modeling: Second Edition*, University Science Books, Sausalito, California (2005).

[45] R. M. Yablonsky, I. Ginis., *Limitation of one-dimensional ocean models for coupled hurricane–ocean model forecasts*, Monthly Weather Review 137.12 (2009): 4410-4419.

[46] Y. Zhang, Y. Hou and L. Shan, *Stability and convergence analysis of a decoupled algorithm for a fluid-fluid interaction problem*, SIAM Journal on Numerical Analysis, Vol. 54, No. 5 (2016), pp. 2833-2867.

[47] H. Aref and S. Balachandar *A first course in computational fluid dynamics*, Cambridge University Press (2018).

[48] M. Akbas, S. Kaya, M. Mohebujjaman, and L. Rebholz, *Numerical Analysis and Testing of a Fully Discrete, Decoupled Penalty-Projection Algorithm for MHD in Elsasser Variables*, IJNAM, vol 13(1) (2016), pp.90-113.

[49] D.L.Brown, R. Cortez, and M.L.Minion *Accurate projection methods for the incompressible Navier-Stokes equations*, J. Comp. Physics, 168(2) (2001), pp.464-499.

[50] A. J. Chorin, *Numerical solution of the Navier-Stokes equations*, Mathematics of Computation 22 (1968), pp. 745-762.

[51] C. Trenchea, *Unconditional stability of a partitioned IMEX method for magnetohydrodynamic flows*, Applied Mathematics Letters, vol. 27 (2014), pp. 97-100.

[52] M. Jobelin, C. Lapuerta, J.-C. Latche, Ph. Angot, and B. Piar, *A finite element penalty-projection method for incompressible flows.*, J. of Computational Physics, vol. 217 (2006), pp.502-518.

[53] S. Zhang *A new family of stable mixed finite elements for the 3d Stokes equations.*, Mathematics of Computation, vol. 74 (2005), pp.543-554.

[54] J. Kim and P. Moin, *Application of a fractional-step method to incompressible Navier-Stokes equations*, J. Comp. Physics, 59 (1985), pp. 308-323.

[55] A. Linke, M. Neilan, L. Rebholz, and N. Wilson *A connection between coupled and penalty projection timestepping schemes with FE spacial discretization for the Navier-Stokes equations.*, Journal of Numerical Mathematics, 25(4) (2017), pp. 229-248.

[56] W. M. Elsasser *The hydromagnetic equations.* Phys. Rev. (1950), 79:183.

[57] J.C.S. Meng, C.W. Henoch, and J.D. Hrubes, *Seawater electromagnetohydrodynamics: A new frontier*, Magnetohydrodynamics **30** (1994), 401–418.

[58] A. Tsinober, *MHD flow drag reduction*, Viscous Drag Reduction in Boundary Layers, (D.M. Busnell and J.N. Hefner, eds.), Progress in Astronautics and Aeronautics, vol. 123, American Institute of Astronautics and Aeronautics, Reston, VA, (1990), pp. 327–349.

[59] M.D. Gunzburger, A.J. Meir, and J. Peterson, *On the existence, uniqueness, and finite element approximation of solutions of the equations of stationary, incompressible magnetohydrodynamics*, Math. Comp. **56** (1991), no. 194, 523–563.

[60] A. Labovsky and C. Trenchea, *Approximate Deconvolution Models for Magnetohydrodynamics*, Numerical Functional Analysis and Optimization, 31(12) (2010), pp. 1362-1385.

[61] W. Layton, M. Sussman, and C. Trenchea, *Bounds on energy, magnetic helicity and cross helicity dissipation rates of approximate deconvolution models of turbulence for MHD flows*, Numer. Funct. Anal. Optim., 31:5 (2010), 577-595.

[62] M. Sermange and R. Temam, *Some mathematical questions related to the MHD equations*, Comm. Pure Appl. Math. **36** (1983), 635–664.

[63] R. Temam, *Sur l'approximation de la solution des Equations de Navier-Stokes par la methode des pas fractionnaires (II)*, Archive for Rational Mechanics and Analysis 33 (1969), pp. 377-385.

[64] J.D. Barrow, R. Maartens and C. G. Tsagas, *Cosmology with inhomogeneous magnetic fields*, Phys. Rep. 449 (2007), pp. 131-171.

[65] S. Brenner, L.R. Scott, *The Mathematical Theory of Finite Element Methods*, Springer-Verlag (2008).

[66] M. Case, V. Ervin, A. Linke and L. Rebholz, *A connection between Scott-Vogelius and grad-div stabilized Taylor-Hood FE approximations of the Navier-Stokes equations*, SIAM J. Numer. Anal., 49(4) (2011), pp. 1461-1481.

[67] M. Case, A. Labovsky, L. Rebholz and N. Wilson, *A high physical accuracy method for incompressible magnetohydrodynamics*, Int. J. Numer. Anal. Model., Series B., 1(2) (2010), pp. 217-236.

[68] E. Dormy and A. M. Soward, *Mathematical Aspects of Natural Dynamos*, CRC Press (2007).

[69] D. Erkmen and A. Labovsky, *Defect-deferred correction method for the two domain convection dominated convection diffusion problem*, J. Math Anal. Appl., 450(1) (2017), pp. 180-196.

[70] D. Erkmen and A. Labovsky, *Note on the usage of grad-div stabilization for the penalty-projection algorithm in magnetohydrodynamics*, Appl. Math. Comput., 349 (2019), pp. 48-52.

[71] B. Punsly, *Black Hole Gravitohydrodynamics. Astrophysics and Space Science Library*, vol. 355, Springer, Berlin, (2008).

[72] T. Gelhard, G. Lube, M.A. Olshanskii, and J.-H. Starcke, *Stabilized finite element schemes with LBB-stable elements for incompressible flows*, J. Comput. Appl. Math., 177 (2005), pp. 243-267.

[73] V. Girault and P.-A. Raviart, *Finite Element Methods for Navier-Stokes equations: Theory and Algorithms*, Springer-Verlag, New York (1986).

[74] T. Heister, M. Mohebujjaman and L. Rebholz, *Decoupled, unconditionally stable, higher order discretizations for MHD flow simulation*, J. Sci. Comput., 71(1) (2017), pp. 21-43.

[75] F. Hecht, *New development in FreeFem++*, J. Numer. Math., 20 (2012), pp. 251-265.

[76] Y. Q. Hu, X. C. Guo and C. Wang, *On the ionospheric and reconnection potentials of the Earth: Results from global MHD simulations*, J. Geophys. Res, 112, A07215 (2007).

[77] W. Layton, H. Tran and C. Trenchea, *Numerical analysis of two partitioned methods for uncoupling evolutionary MHD flows*, Numer. Methods Partial Differ. Equ., 30 (2014), pp. 1083-1101.

[78] Y. Li and C. Trenchea, *Partitioned second order method for magnetohydrodynamics in Elsässer variables*, Discrete Contin. Dyn - Ser. B., 23(7) (2018), pp. 2803-2823.

[79] M.A. Olshanskii, *A low order Galerkin finite element method for the Navier-Stokes equations of steady incompressible flow: A stabilization issue and iterative methods*, Comp. Meth. Appl. Mech. Eng., 191 (2002), pp. 5515-5536.

[80] A. Otto, *Three-dimensional magnetohydrodynamic simulations of processes at the Earth's magnetopause*, Geophys. Astrophys. Fluid Dyn., 62 (1991), pp. 69-72.

[81] Y. Rong and Y. Hou, *A partitioned second-order method for magnetohydrodynamic flows at small magnetic Reynolds numbers: partitioned second-order*

method for magnetohydrodynamic flows, Numer. Methods Partial Differ. Equ., 33(6) (2017), pp. 1966-1986.

[82] R. Skeel, *A theoretical framework for proving accuracy results for deferred corrections*, SIAM J. Numer. Anal., 19(1) (1981), pp. 171-196.

[83] N. Wilson, A. Labovsky and C. Trenchea, *High accuracy method for magnetohydrodynamics system in Elsässer variables*, Comput. Methods Appl. Math., 15(1) (2015), pp. 97-110.

[84] D. Erkmen, S. Kaya and A. Cibik, *A Second order Decoupled Penalty Projection Method based on Deferred Correction for MHD in Elsässer variable*, J. of Computational and Applied Math, Volume 371, 112694 (2020).